UNIVERSITY OF LIVERPOOL

Ketonisation of acetic acid on metal oxides catalysts

Thesis submitted in accordance with the requirements of the University of Liverpool for the degree of Doctor in Philosophy by

Safer Tale Almutairi

May 2020

Abstract

The ketonisation of acetic acid to acetone was studied in the gas phase using γ-Al_2O_3, TiO_2, ZrO_2 and CeO_2 as the catalysts in the temperature range of 180–350 °C and ambient pressure. Catalyst activity was found to increase in the order Al_2O_3 << TiO_2 < ZrO_2 < CeO_2. Catalyst resistance to deactivation increased in the order CeO_2 << ZrO_2 < TiO_2 in parallel with the amount of coke formed. TiO_2 (Degussa P25) and ZrO_2 were found to exhibit the best performance as represented by their activity and stability to deactivation. CeO_2 and ZrO_2 could be regenerated by air calcination to regain their activity.

Given the very good ketonisation performance of the TiO_2 and ZrO_2 pure oxides, it was interesting to test the performance of mixed oxide Ti-Zr catalysts in this reaction. All the mixed oxides were characterised by BET measurements as well as powder XRD. It was shown that TiO_2-ZrO_2 mixed oxides, prepared by sol-gel synthesis, are active catalysts in the ketonisation reaction of acetic acid to acetone at 300 ^oC. The 1:2 Ti-Zr catalyst showed the best acetic acid conversion, which exceeded the conversion over the pure TiO_2 and ZrO_2 oxides prepared by the sol-gel method. Although all of the catalysts showed varied performance in terms of conversion, all samples gave excellent selectivity to acetone of 98–100%. Overall, however, the sol-gel TiO_2, ZrO_2 and TiO_2-ZrO_2 catalysts had no advantages in activity and selectivity over the same catalysts prepared by the precipitation method. Moreover, mixed oxide TiO_2-ZrO_2 catalysts were considerably less active than the pure ZrO_2 prepared by the precipitation method.

Two mechanistically significant observations were made from our DRIFTS studies. First, facile exchange was found between the bidentate bridging acetate and co-adsorbed acetic acid on the oxide surfaces under mild conditions (130 ^oC) well below ketonisation temperatures. This demonstrates the lability of the surface bidentate bridging acetate species in the ketonisation system. This result shows that various types of surface acetate species are

equilibrated in the ketonisation system, which makes them kinetically indistinguishable. Second, at higher temperatures typical for acid ketonisation, in the absence of gas-phase acetic acid, we found that the adsorbed bidentate bridging acetate-d_3 species underwent H/D exchange with proton sites on oxide surfaces. This, for the first time, provides experimental evidence supporting the intermediacy of enolate species in the ketonisation of carboxylic acids.

Publications and presentations

1. S. T. Almutairi, E. F. Kozhevnikova, I. V. Kozhevnikov, *Ketonisation of acetic acid on metal oxides: Catalyst activity, stability and mechanistic insights, Applied Catalysis A, General*, 2018, **565**, 135-145.
2. S. T. Almutairi, E. F. Kozhevnikova, I. V. Kozhevnikov, *Poster Day, University of Liverpool*, Liverpool, UK 2018.
3. S. T. Almutairi, E. F. Kozhevnikova, I. V. Kozhevnikov, *The UK Catalysis Conference (UKCC2018)*, Loughborough, UK 2018.
4. S. T. Almutairi, E. F. Kozhevnikova, I. V. Kozhevnikov, *The 7th EuCheMS Chemistry Congress*, Liverpool, UK 2018.
5. S. T. Almutairi, E. F. Kozhevnikova, I. V. Kozhevnikov, *The UK Catalysis Conference (UKCC2019)*, Loughborough, UK 2019.

Acknowledgements

I would first like to express sincere thanks to my supervisor, Prof. Ivan V. Kozhevnikov, for his kind support and guidance throughout my PhD studies. His advice helped me achieve my goals, and he taught me many skills through his experience.

Many thanks are due to Dr. Elena F. Kozhevnikova for her kind assistance in conducting experiments and solving multiple technical issues in our group.

I would also like to thank all members of the technical support team in the Chemistry department and all members of my group at the University of Liverpool. Special thanks to Hanan Althikrallah, Maram Alqarni and Adam Dingle for their help with experiments.

Endless thanks and love go out my mother for her encouragement and support. I also wish to gratefully thank my brothers and sister for what they have done in helping me achieve my long-time goals.

Special thanks to my wife and children for standing by my side in my studies and in life. Without their help, I would not have successfully completed my work.

Finally, thanks are due to the Ministry of Education for their financial support and to the Saudi Cultural Bureau in London for their financial management.

Abbreviations

B	Brønsted acid site
BET	Brunauer, Emmett, Teller method
BJH	Barrett-Joyner-Halenda method
DRIFT	Diffuse reflectance infrared Fourier transform (spectroscopy)
DSC	Differential scanning calorimetry
FID	Flame ionisation detector
FTIR	Fourier transform infrared (spectroscopy)
GC	Gas chromatography
HOAc	Acetic acid
IR	Infrared
L	Lewis acid site
TGA	Thermogravimetric analysis
TOS	Time on stream
TPR	Temperature programmed reduction
XRD	X-ray diffraction

Contents

List of figures

List of Tables

List of schemes

Chapter 1: Introduction

1.1. The definition of catalysts

There are several ways to define a catalyst [1]. Usually it is defined as a chemical substance used to convert a reactant to products without being consumed in the reaction. The catalyst is not involved in the reaction stoichiometry, and therefore, does not change reaction equilibrium. Kirchhoff and Davy were the pioneers of catalysis, reporting catalytic reactions as early as 1812. Kirchhoff focused on acid catalysis in liquid phase, while Davy's research explored the gas-phase oxidation of alcohol in air over platinum [2]. The catalysts can take a solid, liquid or even gas form [3]. The liquid and solid forms are the most common of the three [2,4].

Catalysis plays a major role in the contemporary economy because it has many industrial uses in petrochemical, chemical, pharmaceutical and other industries. About 90% of petrochemical and chemical products are currently produced with the use of catalysts [1]. More recent catalyst uses include those in green chemistry [5–7], in production of renewable transportation fuels [8,9], in fuel cells [6,10–13] and in nanotechnology [14,15].

There are two main types of catalysis, namely, homogeneous and heterogeneous catalysis [16]. Homogeneous catalysis takes place when both the catalyst and the reactants are in the same, usually liquid, phase without a phase boundary. Heterogeneous catalysis occurs when the catalyst and reactants are in different phases separated by phase boundaries. Each type has advantages and disadvantages. Homogeneous catalysis generally occurs under milder reaction conditions, with almost all catalyst species being active, often with relatively high selectivity and easy reaction control. The disadvantages of homogeneous catalysis include difficult product separation and catalyst recovery, strong corrosion and expensive disposal of waste. In contrast, heterogeneous catalysis benefits from easy catalyst and product separation, less corrosion and elimination of waste. However, heterogeneously catalysed reactions are

more difficult to control, and often they suffer from mass and heat transport limitations (Table 1.1). Nevertheless, most of industrial chemical and petrochemical processes employ heterogeneous catalysis due to the ease of separation. Table 1.2 shows some industrial uses of heterogeneous catalysis commercialised between 1939 and 2000 [17,18].

Table 1.1. Comparison of homogeneous and heterogeneous catalysts.

HOMOGENEOUS CATALYSIS	HETEROGENEOUS CATALYSIS
Advantages	**Advantages**
Almost all catalyst species active Often higher selectivity Easier reaction control	Easy catalyst/product separation Less corrosion Elimination of waste
Disadvantages	**Disadvantages**
Difficult product separation and catalyst recovery Corrosion Expensive disposal of waste	More difficult process control Mass and heat transfer limitations

Since this research deals with catalysis by metal oxides, it should be noted that metal oxides make up a significant group of active catalytic materials, that are widely used in heterogeneous catalysis. Their behaviour can be categorised as redox, acid, base or amphoteric. Typically, metal oxides are solid materials, with their main properties relying on interactions between both their metal and inherent oxygen. Table 1.3 lists some examples of metal oxide catalysts.

Table 1.2. Historical uses of catalysis [16].

Year	Reaction/application	Catalyst
1939–1945	Dehydrogenation	Pt-Al_2O_4 Cr_2O_3-Al_2O_3
1946–1960	Oxidation of aromatics Hydrocracking Polymerisation	V_2O_5 Ni-aluminosilicate Ziegler–Natta
1961–1970	Low-pressure methanol synthesis Distillate dewaxing	Cu-ZnO-Al_2O_3 ZSM-5, mordenite
1971–1980	Automobile emission control	Pt-Rh-CeO_2 and Al_2O_3
1981–1985	Carbonylation Alkylation Esterification Selective catalytic reduction	Organic Rh complex Zeolite (ZSM-5) Ion-exchange resin V-Ti, Mo, W oxides
1986–2000	Environmental control Hydration Oxidation with H_2O_2 N_2O from nitric acid by catalytic destruction	Pt-Al_2O_3 Enzyme Ti-silicate Ti-silicate

Table 1.3. Examples of metal oxide catalysts and their uses [3].

Catalyst	Catalytic Process
$ZnCr_2O_4$, ZnO	Methanol synthesis (high pressure)
$ZnFe_2O_4$	Oxidative dehydrogenation
$Cu_xZn_{1-x}Cr_2O_4$, CuO	Methanol synthesis (low pressure)
$CuCr_2O_4$, CuO	Oxidation, hydrogenation
$Cr_xAl_{2-x}O_3$	Light alkane dehydrogenation

Catalysis is a phenomenon of enhancing chemical reactions by using a catalyst, a substance that possesses the ability to increase the rate of a chemical reaction without being consumed during the reaction. Figure 1.1 shows the potential energy diagram for a catalysed versus uncatalysed reaction. As seen, the catalyst offers a different pathway for the reaction that has a significantly lower activation energy.

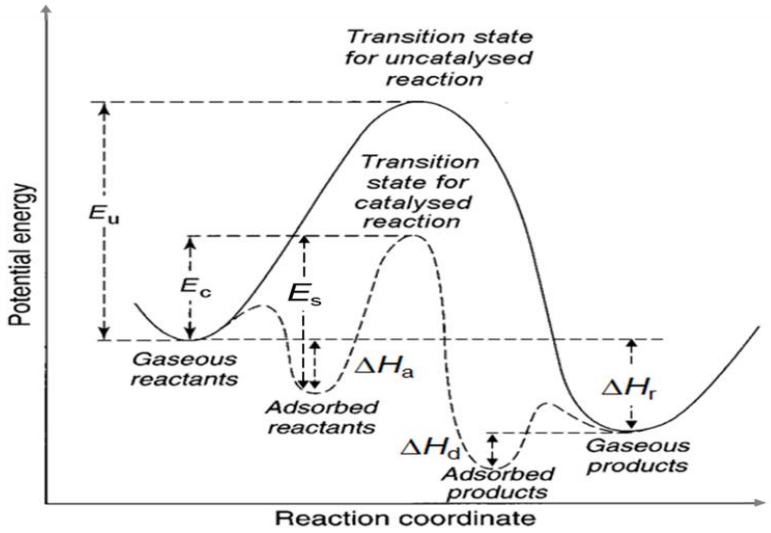

Figure 1.1. Potential energy diagram for a catalysed versus uncatalysed reaction. E_c is the activation energy of the catalysed reaction; E_u is the activation energy of the uncatalysed reaction; ΔH_r is the enthalpy of the reaction; ΔH_a is the enthalpy of reactant adsorption; and ΔH_d is the enthalpy of product desorption [2].

Therefore, the catalyst increases the rate of a chemical reaction to approach equilibrium (Figure 1.2) by providing a new, faster reaction pathway with a lower activation energy. The catalyst works by forming chemical bonds with reactants and is therefore specific to the chemical reaction. The catalyst does not change reaction equilibrium; only thermodynamically feasible reactions with Gibbs free energy $\Delta G < 0$ can be catalysed. If a reaction at certain conditions is strongly uphill in energy ($\Delta G >> 0$), it cannot be catalysed at these conditions as too unfavourable thermodynamically. However, the ΔG may be reduced to an appropriate level

by choosing different conditions (temperature and pressure). Thus if the reaction entropy is positive, $\Delta S > 0$, increasing temperature will decrease ΔG ($\Delta G = \Delta H - T\Delta S$) to make the reaction in question thermodynamically feasible.

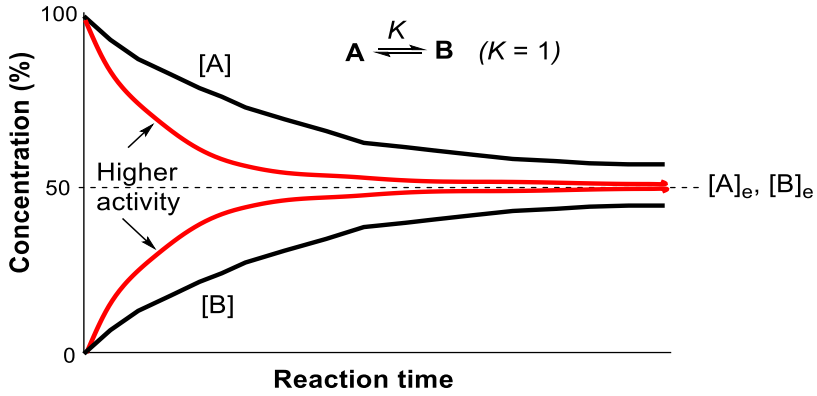

Figure 1.2. The catalyst accelerates the reaction to approach equilibrium ([A_e], [B_e]). A more active catalyst (red lines) reaches equilibrium faster, but does not change the equilibrium [19].

1.2. Catalyst activity, selectivity and lifetime

Catalyst activity can be defined as the rate of conversion of reactants to products under specified reaction conditions. The activity can be measured in terms of the amount of reactant consumed or the amount of product formed per unit time per catalyst weight or per catalyst volume. In heterogeneous catalysis, catalyst activity is often determined per catalyst surface area. More rigorously catalyst activity can be defined in terms of turnover frequency (TOF) as the number of molecules reacted or formed per unit time per single active site.

Catalyst selectivity is defined as catalyst activity to a particular reaction relative to all other reactions occurring in the system. In general, except for parallel reactions, the selectivity depends on reactant conversion, hence catalyst selectivities must be compared at the same conversion level.

Catalyst lifetime (long-term catalyst stability) is a period of time during which a set of reaction conditions (temperature, contact time, etc.) can be kept constant without loss of

catalytic activity and/or selectivity. The lifetime of catalysts varies very broadly from about 10 years for the synthesis of ammonia over iron catalyst down to a few seconds for the catalytic cracking of paraffins over HY zeolite. In the last case, the catalyst is continuously regenerated by burning off coke that deactivates the catalyst.

1.3. Classification of catalysts

Catalysts are classified in accordance to the reactions they catalysed. Redox, acid-base and multifunctional catalysts are the three main classes of catalysts.

Redox catalysts catalyse reactions such as oxidation, hydrogenation, halogenation, dehydrogenation, etc. Typically, the redox catalysts involve transition metals, such as Pd, Pt, Ni, Ag, etc., and transition metal compounds such as oxides, sulfides, chlorides, metal complexes, etc. that have metal atoms or metal ions as active sites.

Acid-base catalysts catalyse reactions such as alkylation, cracking, isomerisation, dehydration, etc. These catalysts include inorganic and organic acids and bases. Heterogeneous acid-base catalysts are represented by zeolites, metal oxides, metal salts and supported mineral acids, for example, zeolite HZSM-5, SiO_2-Al_2O_3, H_3PO_4/SiO_2, ZnO, MgO and CaO. The acidity and basicity of these catalysts are important properties affecting their activity. Their active sites are represented by Brønsted and Lewis acid sites and base sites that are present on the catalyst surface [20].

Multifunctional catalysts have active sites of different functionalities that can act simultaneously to effect different reactions in a one-pot or single-bed catalyst system. These catalysts can have characteristics of both redox and acid-base catalysts [21]. For example, in the one-step synthesis of methyl isobutyl ketone from acetone in the gas or liquid phase, Pd supported on Zn(II)–Cr(III) mixed oxide behaves as a bifunctional metal-acid catalyst [22].

Another example of bifunctional catalyst is Pt/HZSM-5 in the hydroisomerisation of n-alkanes [23,24].

1.4. Heterogeneous catalysis

1.4.1. Active sites

The concept of active sites is at the heart of heterogeneous catalysis. The active site is an atom (ion) or a group of atoms (ions) in the catalyst involved in catalytic reaction. This concept was first introduced by Taylor (defects, 1930s) and further advanced by Balandin (multiplets) and Kobozev (ensembles, 1940s).

According to Taylor [25], the structure of solid surfaces is extremely complex, non-uniform on the atomic scale, with a variety of imperfections and defects. These defects expose atoms or ions with low coordination which are able to bond reactant molecules and thus capable of acting as active sites. The active sites of redox and acid-base catalysts are shown schematically in Figure 1.3. Knowledge about active sites is obtained by surface scientists from various characterisation techniques some of which will be briefly discussed later.

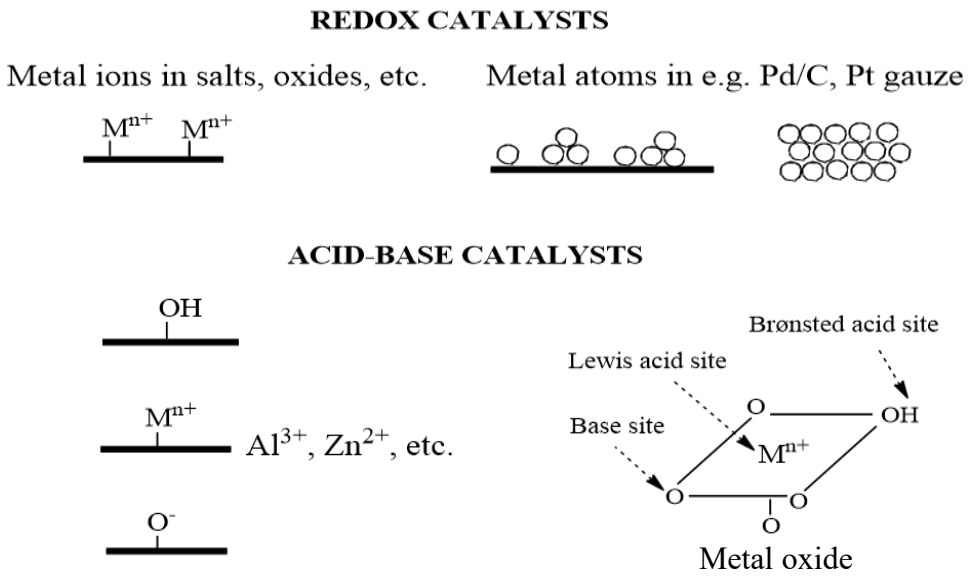

Figure 1.3. Active sites in redox and acid-base catalysts [2].

1.4.2. Key steps and regimes of reactions on porous solid catalysts

Figure 1.4 schematically shows a porous catalyst granule surrounded by a boundary layer (stagnant fluid film) causing resistance to external mass transfer. There are seven key reaction steps on solid porous catalysts [26], as illustrated in Figure 1.4 for a reaction A → B. These include:

1) External transport of reactant from bulk fluid phase (gas or liquid) through the boundary layer to the outer surface of catalyst granule (film diffusion)
2) Internal transport of reactant through the pores to active sites on the interior surface (pore diffusion)
3) Adsorption (chemisorption) of reactant
4) Chemical reaction on the surface
5) Desorption of product

6) Internal transport of product through the pores to the external surface

7) External transport of product through the boundary layer to bulk fluid phase.

Steps (3)–(5) are strictly chemical, (1) and (7) purely physical and (2) and (6) both chemical and physical.

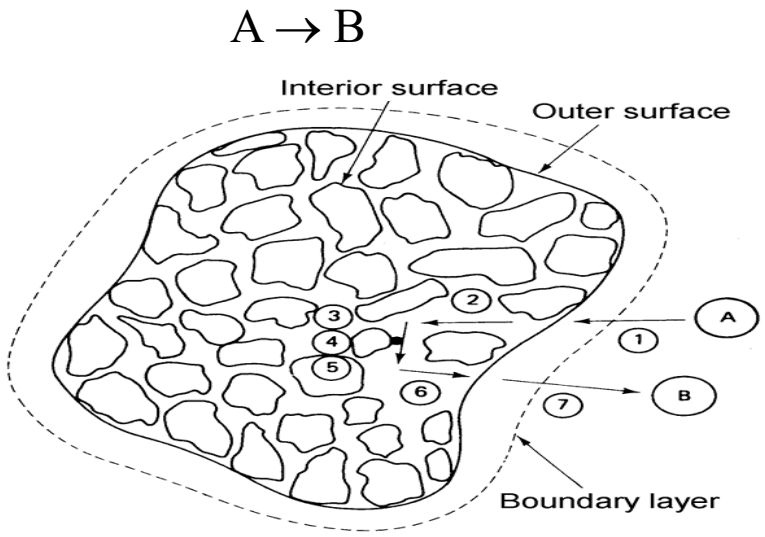

Figure 1.4. Individual steps of a heterogeneous reaction in the gas phase over a solid porous catalyst [26].

In general, any of these steps can be rate-limiting. For irreversible reactions when the products are continuously removed, it is usually step (1), (2) or (4) that can be the rate-limiting ones. Accordingly, three reaction regimes are recognized [26]:

- Kinetic regime (chemical reaction control) – step (4) rate-limiting
- Internal-diffusion regime (pore diffusion control) – step (2) rate-limiting
- External-diffusion regime (film diffusion control) – step (1) rate-limiting.

1.4.3. Mechanism of heterogeneous catalytic reactions

1.4.3.1. Unimolecular reaction

A unimolecular reaction A → X occurring on a solid catalyst is represented in Fig. 1.5. It is assumed that this reaction proceeds in kinetic regime (no diffusion limitations) and involves fast adsorption of reactant A followed by slow surface reaction $A_{ads} \rightarrow X_{ads}$ and fast desorption of product X. If the adsorption and desorption steps are at equilibrium and obey the Langmuir adsorption isotherm, the rate of reaction (r) will be given by the Langmuir equation (1.1), where k is the rate constant, θ_A is the fractional coverage of A, b_A is the adsorption coefficient and p_A is the partial pressure of reactant A [26].

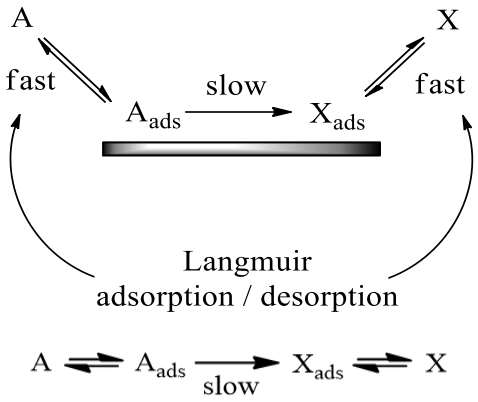

Figure 1.5. Unimolecular reaction on a solid catalyst.

$$r = k\Theta_A = \frac{kb_A p_A}{1 + b_A p_A} \qquad (1.1)$$

Figure 1.6 shows the pressure dependence of the reaction rate. The rate changes from the first order at low pressure to the zero order at high pressure as the surface becomes saturated with A and $\theta_A \approx 1$ [2,27].

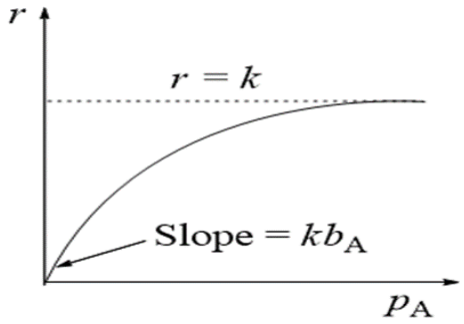

Figure 1.6. Pressure dependence for the rate of unimolecular reaction that follows Langmuir kinetics [27].

1.4.3.2. Biomolecular reaction

Now let us consider a bimolecular reaction A + B → X occurring on a solid catalyst in kinetic regime. The Langmuir-Hinshelwood mechanism and the Eley-Rideal mechanism are the two ways that this reaction can take place on the surface. Figure 1.7 illustrates these two mechanisms. Again the reaction rate is dependent on the reactant pressure. The pressure dependency of reaction rate is different for these mechanisms and can be used to discriminate them [27].

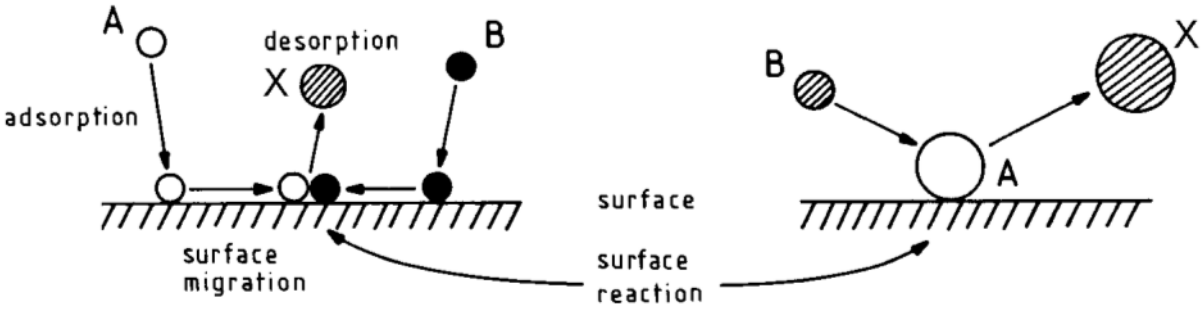

Figure 1.7. The diagram on the left illustrates the Langmuir-Hinshelwood mechanism and on the right the Eley-Rideal mechanism [2].

The Langmuir-Hinshelwood mechanism involves fast adsorption of A and B on adjacent catalyst sites through fast surface migration, followed by slow surface reaction of adsorbed A and B in the rate-limiting step and fast product desorption. Equation (1.2) shows the overall reaction rate for the Langmuir-Hinshelwood mechanism, where the notation is similar to that in equation (1.1).

$$r = \frac{k b_A b_B p_A p_B}{(1 + b_A p_A + b_B p_B)^2} \qquad (1.2)$$

In accordance with equation (1.2), the reaction is second-order at low pressure. If any reactant has a weak adsorption, then the term for that co-adsorbate will be taken out of the denominator. A poisoned reaction occurs as a result of high coverage of the adsorbate with a stronger binding. Equation (1.3) represents the rate when adsorption is weak in B and strong in A [27].

$$r = \frac{k b_B p_B}{b_A p_A} \qquad (1.3)$$

If one species fails to absorb at all, the Eley-Rideal mechanism is in operation. In this case, the adsorption of A takes place on the surface, and B reacts through impulsive collision with the adsorbed A. In B, it is a simple first-order reaction, while in A it is a Langmuir form of the reaction. The Eley-Rideal mechanism leads to the overall reaction rate equation (1.4).

$$r = \frac{k b_A p_A p_B}{1 + b_A p_A} \qquad (1.4)$$

Therefore, Langmuir-Hinshelwood and Eley-Rideal mechanisms can be discriminated by rate dependency on reactant pressure. The Langmuir-Hinshelwood mechanism holds far

more frequently. The Eley-Rideal mechanism is relatively rare; this mechanism is likely when B is a highly reactive species (free radical, carbenium ion, etc.) [2].

1.4.4. Mass transfer limitations in porous solid catalysts

Mass and heat transfer limitations within solid porous catalyst can strongly affect reaction kinetics (reaction rate, order and activation energy). This is sometimes referred to as "diffusion falsification" of kinetics [26]. The mass and heat transfer limitations are caused by concentration and temperature gradients that exist in such systems, which affect the course of chemical reaction.

There are two transport-controlled regimes: internal diffusion and external diffusion. These regimes are controlled by pore diffusion and film diffusion, respectively (Figure 1.4) [2,26,28].

In solid porous catalysts, the heat transfer and mass transfer limitations can have a very significant effect on the reaction rate, the activation energy, the reaction order and the product selectivity. To identify the reaction regime, several diagnostic criteria can be used, as outlined below [26].

In the internal diffusion regime, reaction rate decreases with increasing the catalyst particle size. This is due to a greater distance of diffusion in larger catalyst particles. The rate of diffusion is dependent on the size of catalyst pores, which is where the mass transfer takes place. Bulk (molecular) diffusion, Knudsen diffusion and configurational diffusion are the three forms of diffusion that occur in macro-, meso- and micropores, respectively [29]. On the other hand, the reaction rate in the internal diffusion regime does not depend on the flow rate which does not affect the rate of diffusion within pores.

In the external diffusion regime, the reaction rate is limited by film diffusion, i.e., mass transport to the outer surface of catalyst via the boundary layer (Figure 1.4). In this case, the

reaction rate increases with increasing the flow rate of the fluid phase due to an increase of the rate of film diffusion, This can help to identify the external diffusion regime.

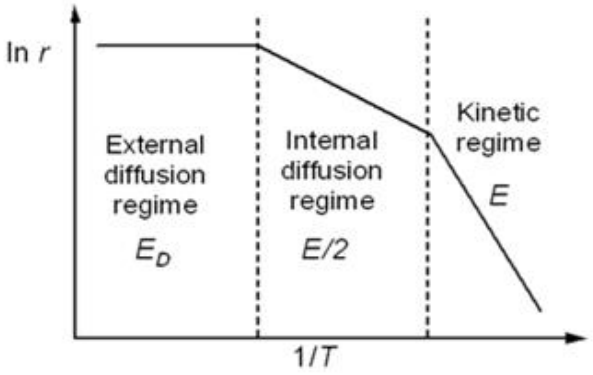

Figure 1.8. Effect of diffusion limitations on activation energy [2].

Strong impact of diffusion limitations on the activation energy can serve as an important diagnostic criterion to distinguish the reaction regime. In kinetic regime, chemical reactions occur with a high activation energy (E = 20 – 200 kJ/mol). Diffusion-limited reactions exhibit lower activation energies. A reaction with an activation E in kinetic regime will exhibit an apparent activation energy of $E/2$ in internal diffusion regime and a very low activation energy of 5 – 10 kJ/mol in external diffusion regime [2,26,28] (Figure 1.8). Diagnostic criteria for distinguishing reaction regimes on porous solid catalysts are summarised in Table 1.4.

Table 1.4. Diagnostic criteria for reaction regimes on solid porous catalysts.

Reaction regime	**Criteria**
Kinetic regime	E = 20 – 200 kJ/mol Reaction rate independent of particle size and flow rate
Internal diffusion	$E_a \approx E/2$ Reaction rate decreases with increasing particle size, but independent of flow rate
External diffusion	$E_a \approx E_D$ (5 –10 kJ/mol) Reaction rate increases with flow rate (at a constant contact time)

1.4.5. Catalyst characterisation

There is a wide range of techniques for the characterisation of bulk and surface properties of catalysts. Most frequently used techniques are shown below in Table 1.5 together with the information obtained about catalyst properties. Some of these techniques were used in our research including physisorption (BET method), chemisorption, powder X-ray diffraction, temperature programmed techniques (TGA, H_2-TPR, CO_2-TPD) and infrared spectroscopy in DRIFTS mode (diffuse reflectance infrared Fourier transform spectroscopy).

Table 1.5. Catalyst characterisation techniques.

Method	**Information obtained**
Adsorption (physisorption, chemisorption)	Catalyst texture: surface area, porosity, particle size
Powder X-ray diffraction (XRD)	Phase composition of catalysts
Temperature-programmed techniques (TGA, TPR, TPO, TPD)	Catalyst stability and phase transition (TGA), redox properties (TPR, TPO), strength of acid, base and other sites (TPD)
Electron microscopy (TEM, SEM)	Particle size on various length scales
Infrared (IR) spectroscopy	Bulk and surface analysis of catalysts
Solid state NMR (Magic-Angle Spinning (MAS) NMR)	Chemical and structural environment of atoms in catalysts

1.4.6. Catalyst optimisation

Many factors need to be taken into consideration for the preparation and development of a catalyst used in a specific catalytic reaction. The first factor is the catalyst active phase, which is crucial for maximising catalyst activity (represented as product yield per unit time or space-time yield). The second of the factors is the surface area and porosity of catalyst. Usually,

to achieve a better productivity, the catalyst should have a high surface area. Yet, in some cases, a moderate surface area is needed to prevent formation of undesired products, for example in selective oxidation to avoid over-oxidation. Long-term catalyst stability during the reaction is the third important factor, as most catalysts decay in activity with reaction time. This may be caused by (i) poisoning, which reduces active sites density on the catalyst; (ii) coke formation on the catalyst surface via organic compound side reactions; (iii) deposited metal sintering, which reduces the surface area of active phase. The fourth factor is catalyst shape, which significantly affects catalyst efficiency, as well as its mechanical strength and stability. Additionally, catalyst cost needs to be lower than the selling price of the product produced. Another factor is that the catalyst needs to be environmentally friendly, minimising the toxic by-product levels, while the catalyst itself must not release toxic chemicals into the environment.

1.5. Ketonisation of carboxylic acids

Ketonisation reaction takes place when two carboxylic acid molecules react to produce a ketone, together with carbon dioxide and water co-products [30–32], as represented by equation (1.5). Ketonisation thus makes a new C-C bond and removes three oxygen atoms. In contrast to catalytic hydrodeoxygenation, no hydrogen is required for the ketonisation of carboxylic acids.

Ketonisation of carboxylic acids was first used in 1858 in an attempt to make acetone by decomposition of calcium acetate [33]. Since then the ketonisation of carboxylic acids has been widely used as a clean way to synthesise ketones [34]. Homo-ketonisation is the reaction between two identical acid molecules yielding a symmetrical ketone (equation 1.5). Cross-ketonisation occurs between two different acid molecules to give an asymmetrical ketone together with symmetrical ketones corresponding to each reacting carboxylic acid (equation

1.6). The rate of cross-ketonisation can be greater by a factor of two compared with the homo-ketonisation. The rate of ketonisation depends on the acid chain length; the longer the acid chain, the lower the rate of the ketonisation [35].

$$RCOOH + RCOOH \rightarrow R_2CO + CO_2 + H_2O \quad (1.5)$$

$$RCOOH + R'COOH \rightarrow R_2CO + R'_2CO + RR'CO + CO_2 + H_2O \quad (1.6)$$

Ketonisation has long been employed as a clean method for the synthesis of ketones [34,36]. Currently, this reaction attracts significant interest for the upgrading of biomass-derived oxygenates, for example, bio-oil produced by fast pyrolysis of biomass. Bio-oil, among other oxygenated compounds, contains lower C_1-C_4 carboxylic acids, which make the oil unstable and corrosive. Ketonisation can eliminate the adverse effects of carboxylic acids by converting them to non-corrosive ketone products with higher caloric value. The ketones thus produced can be further subjected to aldol condensation to increase the carbon chain length to the gasoline/diesel range [10,36,37]. Therefore, there is much ongoing research and development work on the catalytic ketonisation of carboxylic acids.

1.5.1. Ketonisation catalysts

Ketonisation of carboxylic acids has been extensively studied both in the gas phase and in the liquid phase [34,36]. In the gas phase, the reaction is catalysed by many metal oxides in the temperature range of 200-500 ^oC [34,36,38-47]. It is suggested that the high activity of metal oxides results from bifunctional catalysis by surface acid-base pairs M-O involving a Lewis acid site (low-coordinate metal cation) and the neighbouring oxygen anion as the base side [44, 45]. However, despite numerous research efforts, the reaction mechanism and the nature of catalytically active sites and intermediates is still under debate [34,36,44-47].

A wide range of basic, acidic and amphoteric metal oxides and mixed-oxides catalyse

the ketonisation between 300 and 500 ºC [33-35,38,39,41,48–50]. Although the exact nature of the catalytically active sites is unknown, it is commonly thought that the basic sites play an important role in ketonisation carboxylic acids [34]. However, the gas-phase ketonisation of propionic acid has been reported to proceed over acid catalysts such as heteropoly acid $H_3PW_{12}O_{40}$ and its acidic Cs salt $Cs_{2.5}H_{0.5}PW_{12}O_{40}$ as well [50].

It is believed that amphoteric oxides may have more favourable activity compared with pure acidic and basic oxides [30,51–53]. Metal oxides used to ketonise carboxylic acids include CeO_2 [54,55], MnO_2, Cr_2O_3 [56–58], ZrO_2, PbO_2, BiO_3 [56], ZnO [59], TiO_2 [60], SiO_2 [42], mesoporous base catalysts [31], MgO [61], Nd_2O_3 [30] and Al_2O_3 [59,62]. In addition, mixed oxides Mn_2O_3-CeO_2 and ZrO_2-CeO_2 have shown high activity between 350 ºC and 450 ºC [63]. Glinski et al. have studied the activity of oxides of 32 elements for the gas-phase ketonisation of propanoic acid [64]. Zeolites have also been found to be an active catalyst in the ketonisation reaction [42,65].

Supported metal oxides have also been used as ketonisation catalysts [66]. Table 1.6 provides the results for the ketonisation of acetic acid catalysed by various metal oxides supported on silica at 10% metal oxide loading in the temperature range of 375-400 ºC [66]. It can be seen that La_2O_3, MnO_2, CdO and CeO_2 give the best acetone yield at 400 ºC.

Various properties, which determine the ketonisation of carboxylic acids over oxides, have been studied both experimentally and theoretically, for example, the interaction of carboxylic acids with catalysts, redox properties, dopants and pre-treatment of catalysts. When adsorbed onto the surface of a catalyst, carboxylic acids produce surface carboxylate and hydroxyl groups associated with metal and oxygen atoms in various coordination structures [67,68].

Table 1.6. Activity of silica-supported metal oxides 10% MO_x/SiO_2 for ketonisation of acetic acid [66].

Catalyst	Yield of acetone (%)	
	375 °C	400 °C
B_2O_3	2	3
MoO_3	4	5
WO_3	6	5
P_2O_5	10	12
V_2O_5	9	21
Bi_2O_3	11	18
NiO	31	
Al_2O_3	15	37
CuO	29	39
ZnO	19	33
PbO	36	76
Cr_2O_3	48	39
Fe_2O_3	66	59
CoO	50	63
MgO	53	59
Nd_2O_3	22	61
La_2O_3	50	87
MnO_2	72	96
CdO	76	94
CeO_2	96	97

Acid-base properties of metal oxides have a major impact on the activity during ketonisation of carboxylic acids. A variety of methods to characterise both the basicity and acidity of catalysts have been used including FTIR-pyridine spectroscopy, NH_3 adsorption and the TPD of CO_2. The basic sites of CeO_2, MgO and ZrO_2 have been studied using CO_2 adsorption, and the density of the basic sites has been calculated to compare these catalysts. MgO possesses the greatest strength of basic sites, while CeO_2 has a larger basic site density compared with ZrO_2 and MgO [69].

To study the impact of second metal additives on the gas-phase acetic acid ketonisation, transition metals such as Co and Pd were added to CeO_2. The results revealed that the ketonisation activity increased when Co and Pd were added [51]. Adding ZrO_2 to CeO_2 increased ketonisation activity because it increased both the number of Lewis acid sites and oxygen vacancies. Similarly, CeO_2 and MnO_2 supported on Al_2O_3, TiO_2 and SiO_2 have been analysed for the ketonisation of carboxylic acids. They were shown to have an impact on the activity in the ketonisation: Al_2O_3 and TiO_2 noticeably enhanced the catalytic activity compared with SiO_2 as a result of including the acid function of the support and the basic sites of the supported oxides [66].

Benaissa et al. [48] tested P-Mo-V heteropoly acids and their Cs salts as catalysts for the hydrogenation and ketonisation of hexanoic acid to the relevant aldehydes, ketones and other products at 350 °C and 1 bar H_2 pressure in the vapour phase. During this reaction, $H_4[PMo_{11}VO_{40}]$ and its Cs salts showed greater thermal stability. The selectivity to the ketonisation product 6-undecanone reached 71–76% by raising the content of Cs in the catalysts. Post reaction, the heteropoly compounds (HPCs) were found to decompose to their

oxides, having increased the activity in the hydrogenation of hexanoic acid, compared with the parent HPCs. MoO_2 achieved a 95% conversion with a 75% selectivity to hexanal.

The reaction of aliphatic carboxylic acids over oxidic catalysts has been studied by Pestman et al. [56]. Ketones are the main product in this reaction. In the case of acetic acid, it is suggested that the ketone can be formed via two different routes. On oxides with a low lattice energy, bulk acetates are formed, decomposition of which leads to acetone. On oxides with a high lattice energy, the reaction to acetone takes place on the surface and leaves the bulk structure of the catalyst unaltered [56].

The deoxygenation of propionic acid has been studied using Pt-, Pd- and Cu-loaded heteropoly salt $Cs_{2.5}H_{0.5}PW_{12}O_{40}$ (CsPW) in the gas phase in both N_2 and H_2 atmosphere. All these catalysts were active for the ketonisation of propionic acid to 3-pentanone between 250 and 400 ºC. However, the best ketonisation activity was observed for CsPW and $30\%H_3PW_{12}O_{40}/SiO_2$ without added metal at 250 ºC (100 and 80% 3-pentanone selectivity, respectively) [50].

The gas-phase ketonisation of acetic, propionic and butyric acid on a chromium-zinc-manganese catalyst between 330 and 400 ºC with addition of water has been studied. The yield at 325 ºC stood at 96% acetone, 95% diethyl ketone and 92% dipropyl ketone. There was a positive effect on the yield as a result of reducing the amount of water. At 1:0.5 of acetic acid to water, the selectivity of acetone achieved 98% with a 100% conversion of acetic acid at 375 ºC [70].

Pestman et al. [62] studied iron, vanadium, zirconium and titanium oxides. At low temperatures, only acetone formed on TiO_2; however, at high temperatures, acetaldehyde also formed. The selectivity of the products relied on the presence of α-hydrogen atoms. It is possible that ketene is an intermediate for ketone formation, as implied in the literature [71].

The longer the contact time, the more ketene was formed, which showed that ketene must be an intermediate in the process of converting acetic acid to acetone.

The ketonisation of many types of carboxylic acids has been studied using 10–20 wt% of metal oxide catalysts supported on SiO_2, Al_2O_3 and TiO_2. Although an increase in reaction temperature enhanced the acid conversion, the ketone selectivity dropped. MnO_2/Al_2O_3 at 20 wt% was found to have the greatest level of activity when heated to 400 °C and provided a 95% yield of 7-tridecanone in heptanoic acid ketonisation. A good long-term stability was observed in the reaction at 400 °C [72].

The use of red-mud bauxite resulted in unselective ketonisation of carboxylic acids. When reduced, however, it produced an active catalyst for propionic, iso-pentanoic and n-pentanoic acis ketonisation at 365 °C under H_2 flow in the liquid phase. The recycled catalyst remained active without suffering any loss of activity [73].

Studies of the ketonisation of propionic acid to form 3-pentanone and cross-ketonisation of a range of carboxylic acids with CeO_2 modified with Mn, Mg, Al, Ni, Fe and Zr at 300–425 °C have revealed that CeO_2-Mn_2O_3 is the most active catalyst for this reaction. The level of reactivity fell slightly for the cross-ketonisation of propionic acid with another linear carboxylic acid on CeO_2-Mn_2O_3 at 375 °C due to the increased length of the chain. Furthermore, branched acids were not as reactive due to steric hindrance. Branched acids without α-hydrogen reduce reactivity in the ketonisation of acid by both homo- and cross-ketonisation [39].

Martinez et al. [60] synthesised TiO_2-functionalised silica monoliths using the hydrolysis of titanium isopropoxide on the surface of the silica. The catalyst was used for ketonisation of acetic acid to form acetone between 533 and 680 °C and exhibited high selectivity to acetone.

Kobune et al. [74] studied the effect of calcination of CeO_2 on its ketonisation activity. The calcination affected the particle size of the catalyst, and it was shown that the greater the particle size, the greater the activity in ketonisation of propionic acid. The acid, ketonised over cerium oxide at 350 ºC using a range of particle sizes, produced 3-pentanone with a selectivity of more than 99% and a 50% conversion of propionic acid.

A bifunctional metal-acid catalyst was used to test the ketonisation of pentanoic acid. A 70% yield of 5-nonanone was produced from γ-valerolactone (GVL) in a single bed on Pd/Nb_2O_5. The yield rose to 90% when a double-bed reactor was used over Pd/Nb_2O_5 + $Ce_{0.5}Zr_{0.5}O_2$ at temperatures of 325 and 425 ºC [75].

Dumesic et al. [76] have used a multistep strategy to create ketones. The work aimed to convert cellulose into diesel and gasoline fuel in a cascade strategy for biomass deoxygenation. In the initial stage, cellulose was decomposed in an aqueous solution of H_2SO_4, producing a mixture of formic and levulinic acids. Following this, GVL was produced over Ru/C at 150 ºC and further converted to 90% 5-nonanone. Pd/Nb_2O_5 + $Ce_{0.5}Zr_{0.5}O_2$ mixed catalyst was selected as it provided an optimum hydrothermal stability with greater activity for producing GVL [76].

Using a citrate method, an active phase of MnO_x/CeO_x on mesoporous silica (HMS and MCM-41) has been created [30]. The catalyst was used for the ketonisation of propionic acid to form 3-pentanone. A 98% ketone selectivity was obtained with a 73% conversion of propionic acid over MnO_x/CeO_x-MCM-41 at 410ºC. However, much lower conversion was achieved for propionic and butyric acid cross-ketonisation [30].

The catalyst, $Ru/TiO_2/C$, was prepared through impregnation followed by air calcination then reduced in H_2. It was used for acetic acid ketonisation in the liquid phase, with water and organic solvents (n-hexane and n-methyl-2-pyrrolidone) at 180 °C. High selectivity and activity were observed when organic solvents were used for the ketonisation [77].

During the ketonisation of hexanoic [41] and pentanoic acids [78] in liquid phase, a ceria-zirconia catalyst was tested. For the ketonisation of hexanoic acid, 2-butanone and 1-pentanol were used as solvents. The ketonisation reaction was not as fast as esterification at low temperatures, and this fits with the activation energies of esterification and ketonisation. Adsorption of acids onto the surface of catalyst played an important role. The ketonisation of ester was found to be indirect because the ether had been first hydrolysed by water and the acid then ketonised. This means that the ketonisation of the ester had not occurred in this system. The activation energy of the ketonisation was greater than that of the esterification, 132 versus 40 kJ/mol [41].

Pr_6O_{11}, Nd_2O_3, CeO_2 and La_2O_3 were among the 14 rare earth oxides studied in the gas-phase ketonisation of acetic acid at 350 °C. The selectivity of acetone was recorded at 99.9% with the conversion of acetic acid at 38–80%. An acetone yield of 80% was provided by Pr_6O_{11}. The two key stages of this reaction were the formation of MO(AcO) surface acetates, where M = La, Pr or Nd and the production of acetone and carbon dioxide through the decomposition of the surface acetates. Furthermore, the reaction of MO(AcO) with acetic acid produced water [29].

A host of environmental issues is created by biomass waste being either buried in landfills or burnt. To conserve the environment, there is a need to invest in new methods to dispose of and process biomass waste. Hydrothermal modification is one of those methods. Ketones and other chemicals can be generated from waste materials, such as livestock manure. According to Funai et al. [79], acetone was produced from biomass waste over ZrO_2-FeO_x, Fe_2O_3 and ZrO_2/FeOx at 300–500 °C, presumably by ketonisation of acetic acid. Adding zirconia to iron oxide improves the activity of the catalyst. ZrO_2/FeO_x generated significant quantities of CO_2 instead of acetone in comparison to ZrO_2-FeO_x. Acetone yield increased with temperature before starting a downward trend at 500 °C; the optimal temperature was 450 °C.

The acetone concentration increased with increasing acetic acid content in the slurry.

Ni/Al_2O_3 was utilised as the catalyst for steam reforming of acetic acid at varied temperatures. The higher the Ni loading, the less of the ketonisation of acetic acid was observed. This occurred because of a cracking reaction instead of acetic acid ketonisation. The optimal activity and the lowest coking occurred at a 12 wt% Ni loading, as revealed by thermogravimetric analysis [80].

Carboxylic acid ketonisation in the production of biofuel requires high temperatures to remove oxygen and acidity from the source material. By managing the temperature of calcination, it is possible to ensure that ketonisation takes place at lower temperatures. The temperature of calcination has an impact on both the crystallinity and oxidation state of the oxide catalysts. For example, cerium oxide acted as a catalyst for acetic acid ketonisation already at 230 ^oC by increasing the temperature of the calcination of the catalyst [52].

It is difficult to ensure liquid-phase ketonisation at a moderate temperature. When metal oxides were used in the liquid phase, the catalytic activity for ketonisation of carboxylic acids was very low because of the blockages of active sites and competitive adsorption of water [81].

Catalyst deactivation is a serious problem in the commercialisation of catalytic ketonisation of carboxylic acids. Wang and Iglesia [82] sought to improve the stability and activity of TiO_2 and ZrO_2 catalysts by incorporating H_2 into the carrier gas stream and using a Cu/SiO_2 co-catalyst. They found that if located within the diffusion distance of the TiO_2 or ZrO_2 surface, the presence of Cu and H_2 significantly reduced the rate of catalyst deactivation. It is suggested that this is achieved by removing inert bidentate carboxylates to free up active binding sites.

1.5.2. Mechanism of ketonisation of carboxylic acids

Several mechanisms have been proposed for the acid ketonisation reaction including (i) decomposition of a metal carboxylate, (ii) via an acid anhydride intermediate, (iii) via a ketene intermediate route and (iv) via a β-ketoacid intermediate [36]. More recent theoretical calculations and experimental data favour the β-ketoacid intermediate route with the rate-limiting step of C-C bond formation [36,44,46,47]. Nevertheless, exact reaction mechanism and the requirements for catalytically active sites are still controversial [44]. From DFT analysis, different surface carboxylate species such as monodentate acetate [44] and bidentate bridging acetate [46,47] have been suggested as active intermediates in this reaction. Also different mechanisms of C-C bond formation have been proposed. These include the C-C coupling (i) between a surface carboxylate and a ketene (Scheme 1.1) [36], (ii) between an enolate species and a co-adsorbed acid [44], (iii) between an enolate species and a bidentate bridging carboxylate, (iv) between an enolate species and an acylium intermediate [46,47] and (v) via a concerted pathway (Scheme 1.2) [46]. The C-C coupling involving the enolate and a surface carboxylate or acylium species is currently considered to be the most plausible reaction mechanism [44,46,47].

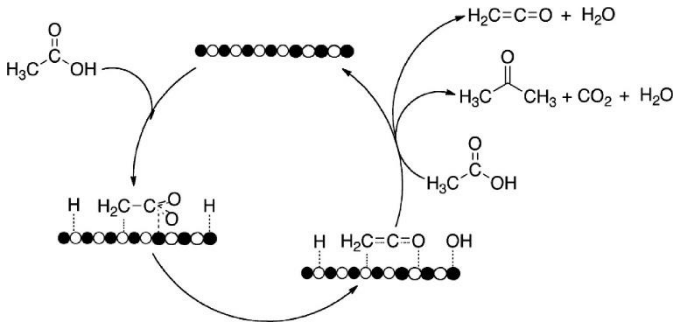

Scheme 1.1. Ketonisation of acetic acid to acetone via the ketene mechanism [36].

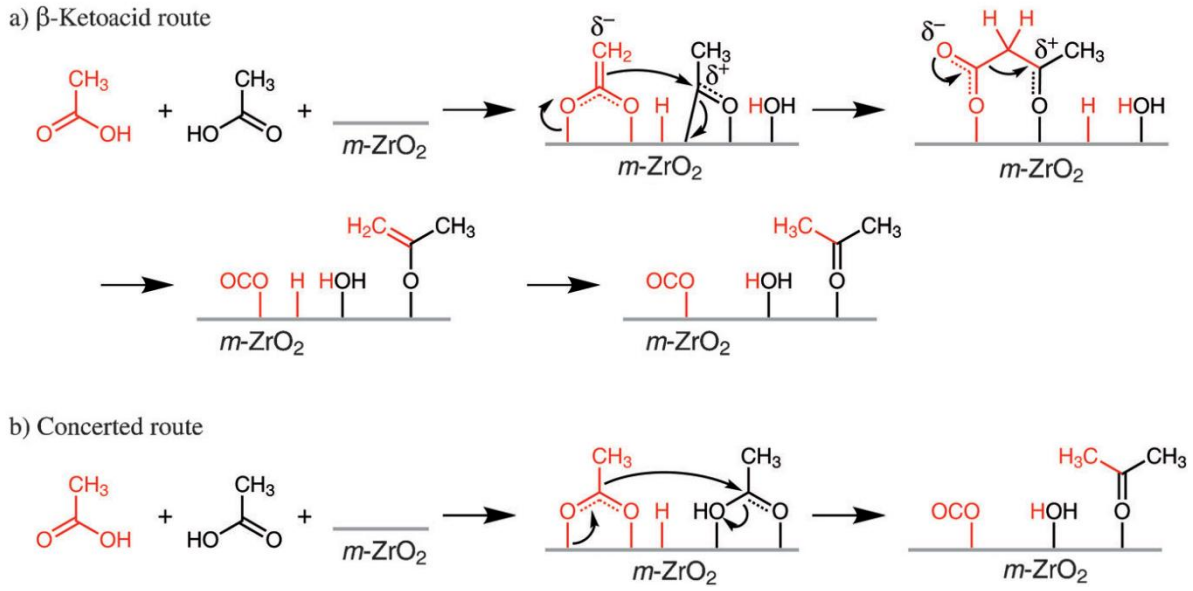

Scheme 1.2. Ketonisation of acetic acid to acetone on monoclinic ZrO_2 surface via β-ketoacid route and concerted route [46].

Yakerson et al. [83,84] demonstrated that two completely different phenomena can cause acetone to form from acetic acid. It was realised that oxides which have very high basicity (or low lattice energy), e.g., alkali and alkali earth oxides such as CdO, SrO, BaO, CaO, and MgO have a strong interaction with acetic acid. This interaction results in bulk carboxylate salts forming, followed by decomposition upon thermal treatment, leading to the generation of acetone, water and CO_2. These reactions are also seen over basic rare earth oxides such as Nd_2O_3, Pr_6O_{11} and La_2O_3 [30]. Contrastingly, in oxides with a higher lattice energy such as SnO_2, ZrO_2, CeO_2, TiO_2, etc., the reactions proceed via an alternative route and are restricted to the catalytic surfaces. These distinctions were then emphasised by Ponec et al. [85] in research covering many oxides, e.g., Cr_2O_3, Al_2O_3, TiO_2, and ZrO_2, which are active catalysts for the production of acetone from acetic acid. When H_2 is present and at a high temperature, some oxides are active for deoxygenating acetic acid to acetaldehyde. It was realised that low-lattice-energy oxides converted to acetate salts, and decomposition to acetone occurred, even when H_2 was present [36].

One of the distinctive elements appearing in every surface-catalysed ketonisation study is the requirement of an α-hydrogen in a carboxylic acid taking part in the reaction. α-Hydrogen is hydrogen which is bonded to carbon atoms in the α position relative to a carbonyl group. Such atoms display high acidity compared to other alkyl hydrogens. For example, whilst the pK_a values for alkyl C−H bond dissociation are usually ranged from 40−50, a α-hydrogen atoms range between 19−20 [86]. The vital role α-hydrogen has in the ketonisation of carboxylic acids is well known, primarily by H/D exchange research and a dependency of ketonisation activities on the α-hydrogens on the carboxylic acids [36].

A ketene forms by dehydrating a carboxylic acid, which contains an α-hydrogen atom [87]. Thus, since each of the connections requires an α-hydrogen, a ketene is usually thought to be a ketonisation intermediary. The mechanism which involves the coupling of adsorbed ketenes with a carboxylate was proposed by Munuera et al. [88] in 1978 and reinforced by Dooley et al. [89]. A carboxylate intermediate initially forms on a coordinatively unsaturated metal and then dehydrates to a surface ketene intermediary. The adsorbed intermediate is then coupled with an alkyl group of an adsorbed carboxylate for forming ketones. Therefore, the ketone acyl group is originated from ketenes rather than carboxylates [36].

Additionally, the vital part the α-hydrogen plays in the first activation is a crucial part in the coupling on the surface of the two species, with the intermediate forming with the ability of decomposition with evolution of water and CO_2 [36]. A species which fulfils the requirement is a β-ketoacid, which forms by being coupled with an enolate (enolised carboxylate) (alkyl fragment) and an acylium (carbonyl or acyl fragment) or a carboxylate. The β-ketoacids (or 3-oxocarboxylic acids) are organic compounds, which contain a ketone group on the second carbon (or β position) from the carboxylic acid group. These compounds can be decarboxylated and thus CO_2 and a ketone are produced when treated thermally (Scheme 1.3). The mechanisms for decarboxylation of β-ketoacids involve redistributing six electrons in a six membered cyclic

transition state to produce an enol, which is tautomerized to form a ketone. It should be noted that the simplicity of decarboxylation is a distinctive feature of β-ketoacids [90].

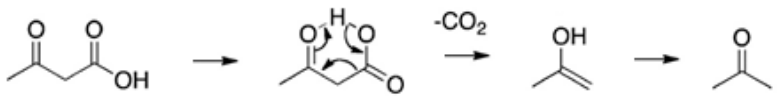

Scheme 1.3. Formation of acetone via the decarboxylation of the corresponding β-ketoacid, which forms and decomposes on the catalyst surface.

1.6. Objectives of research

Ketonisation of carboxylic acids catalysed by metal oxides is crucial for the reduction of the adverse effects of carboxylic acids in bio-oil because it can remove highly reactive carboxylic groups while increasing the length of the carbon chain to yield a more stable ketone product with a higher caloric value. However, despite numerous research efforts, the reaction mechanism and the nature of catalytically active sites and intermediates is still under debate. Besides, catalyst deactivation remains a serious problem in the commercialisation of catalytic ketonisation of carboxylic acids. Therefore, the understanding of reaction mechanism and the causes of catalyst deactivation as well as the improvement of catalyst stability remain a challenge.

The aim of this work is to study the performance of four typical metal oxide catalysts, namely γ-Al_2O_3, TiO_2, ZrO_2 and CeO_2, for the gas-phase ketonisation of acetic acid to acetone, primarily focussing on their activity and stability to deactivation. We also aim to provide new insights into the ketonisation mechanism and the site requirements of oxide surfaces using kinetic studies, the characterisation of catalyst acid and base sites and, in particular, IR spectroscopic investigation of reaction intermediates.

The ketonisation reactions will be carried out in a continuous-flow fixed-bed microreactor with on-line gas-chromatographic analysis of the reaction products. The catalysts will be characterised using the Brunauer–Emmett–Teller (BET) texture analysis, powder X-ray diffraction (XRD) and IR spectroscopy in DRIFTS (diffuse reflectance infrared Fourier transform spectroscopy) mode. Other techniques will include temperature programmed methods such TGA, H_2-TPR and CO_2-TPD. Elemental analysis (C and H analysis) will be used to determine the amount of coke deposited in spent catalysts.

Chapter 1 provides a general introduction to heterogeneous catalysis and a review of the literature on the ketonisation of carboxylic acids.

Chapter 2 describes the methods for preparing metal oxide catalysts and the techniques used for metal oxide catalyst characterisation. It also describes catalyst testing in the gas-phase ketonisation of acetic acid.

Chapter 3 describes the performance of the oxide catalysts in the gas-phase ketonisation of acetic acid.

Chapter 4 details the results catalyst stability and catalyst regeneration in the ketonisation of acetic acid.

Chapter 5 reports an investigation of reaction kinetics, including the determination of reaction orders, activation energies and kinetic isotope effect (KIE).

Chapter 6 reports the DRIFTs investigation of acetic acid adsorption on oxide catalysts and mechanistic insights.

Chapter 7 contains general conclusions.

References

1. G. Ertl, H. Knözinger and J. Weitkamp, *Handbook of heterogeneous catalysis*, VCH, 1997.

2. J. M. Thomas and W. J. Thomas, *Principles and Practice of Heterogeneous Catalysis*, VCH, Weinheim, 1997.

3. O. Deutschmann, H. Knözinger, K. Kochloefl and T. Turek, in *Ullmann's Encyclopedia of Industrial Chemistry*, Wiley-VCH Verlag GmbH & Co. KGaA, Editon edn., 2009.

4. J. Hagen, *Industrial Catalysis: A Practical Approach*, 2nd ed., Wiley-VCH, Weinheim, 2006.

5. P. T. Anastas, M. M. Kirchhoff and T. C. Williamson, *Applied Catalysis A: General*, 2001, **221**, 3-13.

6. G. Centi and S. Perathoner, *Catalysis Today*, 2003, **77**, 287-297.

7. R. A. Sheldon, I. W. C. E. Arends and U. Hanefeld, in *Green Chemistry and Catalysis*, Wiley-VCH Verlag GmbH & Co. KGaA, Editon edn., 2007, pp. 1-47.

8. J. Pyun, *Angewandte Chemie International Edition*, 2011, **50**, 46-48.

9. S. Chaturvedi, P. N. Dave and N. K. Shah, *Journal of Saudi Chemical Society*, 2012, **16**, 307-325.

10. E. L. Kunkes, D. A. Simonetti, R. M. West, J. C. Serrano-Ruiz, C. A. Gärtner and J. A. Dumesic, *Science*, 2008, **322**, 417-421.

11. S. Furuta, H. Matsuhashi and K. Arata, *Catalysis Communications*, 2004, **5**, 721-723.

12. S. Ha, R. Larsen and R. I. Masel, *Journal of Power Sources*, 2005, **144**, 28-34.

13. S. Park, J. M. Vohs and R. J. Gorte, *Nature*, 2000, **404**, 265-267.

14. T. R. Ralph and M. P. Hogarth, *Platinum Metals Review*, 2002, **46**, 117-135.

15. H. Liu, C. Song, L. Zhang, J. Zhang, H. Wang and D. P. Wilkinson, *Journal of Power Sources*, 2006, **155**, 95-110.

16. H. Knözinger and K. Kochloefl, in *Ullmann's Encyclopedia of Industrial Chemistry*, Wiley-VCH Verlag GmbH & Co. KGaA, Editon edn., 2000.

17. J. N. Armor, *Applied Catalysis A: General*, 2001, **222**, 407-426.

18. Y. Ren, Z. Ma and P. G. Bruce, *Chemical Society Reviews*, 2012, **41**, 4909-4927.

19. M. Misono, *Heterogeneous catalysis of mixed oxides*, Elsevier, 2013.

20. C.-C. Chang, A. R. Teixeira, C. Li, P. J. Dauenhauer and W. Fan, *Langmuir*, 2013, **29**, 13943-13950.

21. F. Cavani and F. Trifiró, *Catalysis Today*, 1997, **34**, 269-279.

22. F. Al-Wadaani, E. F. Kozhevnikova and I. V. Kozhevnikov, *Journal of Catalysis*, 2008, **257**, 199-205.

23. G. D. Pirngruber, K. Seshan and J. A. Lercher, *Journal of Catalysis*, 1999, **186**, 188-200.

24. X. Li and E. Iglesia, *Journal of Catalysis*, 2008, **255**, 134-137.

25. H. S. Taylor, *Proceedings of the Royal Society A*, 1925, **108**, 105-111.

26. M. Boudart, *Kinetics of Chemical Processes*, Prentice-Hall, 1968.

27. M. K. Bowker, *The basis and applications of heterogeneous catalysis*, Oxford University Press, Oxford, 1998.

28. R. Klaewkla, M. Arend and W. F. Hoelderich, *Mass Transfer-Advanced Aspects*, In Tech, Germany, 2011.

29. F. Lucio, *Catalysis Today*, 1999, **52**, 147.

30. Y. Yamada, M. Segawa, F. Sato, T. Kojima and S. Sato, *Journal of Molecular Catalysis A: Chemical*, 2011, **346**, 79-86.

31. A. D. Murkute, J. E. Jackson and D. J. Miller, *Journal of Catalysis*, 2011, **278**, 189-199.

32. T. Pham, D. Shi and D. Resasco, *Topics in Catalysis*, 2014, **57**, 706-714.

33. R. W. Snell and B. H. Shanks, *ACS Catalysis*, 2014, **4**, 512-518.

34. M. Renz, *European Journal of Organic Chemistry*, 2005, 979-988.

35. C. A. Gaertner, J. C. Serrano-Ruiz, D. J. Braden and J. A. Dumesic, *Industrial and Engineering Chemistry Research*, 2010, **49**, 6027-6033.

36. T. N. Pham, T. Sooknoi, S. P. Crossley and D.E. Resasco, *ACS Catalysts*, 2013, **3**, 2456-2673.

37. A. Corma, S. Iborra and A. Velty, *Chemical Review*, 2007, **107**, 2411-2502.

38. T. Yokoyama and N. Yamagata, *Applied Catalysis A: General*, 2001, **221**, 227-239.

39. O. Nagashima, S. Sato, R. Takahashi and T. Sodesawa, *Journal of Molecular Catalysis A: Chemical*, 2005, **227**, 231-239.

40. M. Glinski, J. Kijenski and A. Jakubowski, *Applied Catalysis A: General*, 1995, **128**, 209-217.

41. C. A. Gaertner, J. C. Serrano-Ruiz, D. J. Braden and J. A. Dumesic, *Journal of Catalysis*, 2009, **266**, 71-78.

42. H. Bayahia, E. Kozhevnikova and I. Kozhevnikov, *Chemical Communications*, 2013, **49**, 3842-3844.

43. H. Bayahia, E. F. Kozhevnikova and I. V. Kozhevnikov, *Applied Catalysis B: Environmental*, 2015, **165**, 253-259.

44. S. Wang and E. Iglesia, *Journal of Catalysis*, 2017, **345**, 183-206.

45. M. A. Hasan, M. I. Zaki and L. Pasupulety, *Applied Catalysis A: General*, 2003, **243**, 81-92.

46. A. Pulido, B. Oliver-Tomas, M. Renz, M. Boronat and A. Corma, *ChemSusChem*, 2013, **6**, 141-151.

47. S. Tosoni and G. Pacchioni, *Journal of Catalysis*, 2016, **344**, 465-473.

48. H. Benaissa, P. N. Davey, E. F. Kozhevnikova and I. V. Kozhevnikov, *Applied Catalysis A: General*, 2008, **351**, 88-92.

49. H. Benaissa, P. N. Davey, Y. Z. Khimyak and I. V. Kozhevnikov, *Journal of Catalysis*, 2008, **253**, 244-252.

50. M. A. Alotaibi, E. F. Kozhevnikova and I. V. Kozhevnikov, *Applied Catalysis A: General*, 2012, **447-448**, 32-40.

51. K. M. Dooley, A. K. Bhat, C. P. Plaisance and A. D. Roy, *Applied Catalysis A: General*, 2007, **320**, 122-133.

52. R. W. Snell and B. H. Shanks, *ACS Catalysis*, 2013, **3**, 783-789.

53. R. W. Snell, S. H. Hakim, J. A. Dumesic and B. H. Shanks, *Applied Catalysis A: General*, 2013, **464-465**, 288-295.

54. S. D. Randery, J. S. Warren and K. M. Dooley, *Applied Catalysis A: General*, 2002, **226**, 265-280.

55. L. Vivier and D. Duprez, *ChemSusChem*, 2010, **3**, 654-678.

56. R. Pestman, R. M. Koster, A. van Duijne, J. A. Z. Pieterse and V. Ponec, *Journal of Catalysis*, 1997, **168**, 265-272.

57. J. C. Kuriacose and R. Swaminathan, *Journal of Catalysis*, 1969, **14**, 348-354.

58. M. Gliński, W. Szymański and D. Łomot, *Applied Catalysis A: General*, 2005, **281**, 107-113.

59. R. Pestman, R. M. Koster, J. A. Z. Pieterse and V. Ponec, *Journal of Catalysis*, 1997, **168**, 255-264.

60. R. Martinez, M. C. Huff and M. A. Barteau, *Journal of Catalysis*, 2004, **222**, 404-409.

61. G. A. H. Mekhemer, S. A. Halawy, M. A. Mohamed and M. I. Zaki, *Journal of Catalysis*, 2005, **230**, 109-122.

62. R. Pestman, A. van Duijne, J. A. Z. Pieterse and V. Ponec, *Journal of Molecular Catalysis. A, Chemical*, 1995, **103**, 175-180.

63. C. Liu, A. Karim, V. Lebarbier, D. Mei and Y. Wang, *Topics in Catalysis*, 2013, **56**, 1782-1789.

64. M. Gliński, G. Zalewski, E. Burno and A. Jerzak, *Applied Catalysis A: General*, 2014, **470**, 278-284.

65. T. C. Keller, E. G. Rodrigues, J. Prez-Ramrez, *ChemSusChem*, 2014, **7**, 1729-1738.

66. M. Gliński, J. Kijeński and A. Jakubowski, *Applied Catalysis A, General*, 1995, **128**, 209-217.

67. A. G. Thomas and K. L. Syres, *Chemical Society Reviews*, 2012, **41**, 4207-4217.

68. H. Onishi, T. Aruga, C. Egawa and Y. Iwasawa, *Surface Science*, 1988, **193**, 33-46.

69. D. Martin and D. Duprez, *Journal of Molecular Catalysis A: Chemical*, 1997, **118**, 113-128.

70. W. Stonkus, J. Yuskovets, L. Leite, M. Fleisher, K. Edolfa, I. Liepina, A. Mishnev and A. Shmidlers, *Russian Journal of General Chemistry*, 2011, **81**, 1523-1528.

71. E. J. Grootendorst, R. Pestman, R. M. Koster and V. Ponec, *Journal of Catalysis*, 1994, **148**, 261-269.

72. M. Gliński and J. Kijeński, *Applied Catalysis A: General*, 2000, **190**, 87-91.

73. E. Karimi, I. F. Teixeira, L. P. Ribeiro, A. Gomez, R. M. Lago, G. Penner, S. W. Kycia and M. Schlaf, *Catalysis Today*, 2012, **190**, 73-88.

74. M. Kobune, S. Sato and R. Takahashi, *Journal of Molecular Catalysis A: Chemical*, 2008, **279**, 10-19.

75. J. C. Serrano-Ruiz, A. Pineda, A. M. Balu, R. Luque, J. M. Campelo, A. A. Romero and J. M. Ramos-Fernández, *Catalysis Today*, 2012, **195**, 162-168.

76. J. C. Serrano-Ruiz, D. J. Braden, R. M. West and J. A. Dumesic, *Applied Catalysis B: Environmental*, 2010, **100**, 184-189.

77. T. N. Pham, D. Shi, T. Sooknoi and D. E. Resasco, *Journal of Catalysis*, 2012, **295**, 169-178.

78. A. A. Shutilov, M. N. Simonov, Y. A. Zaytseva, G. A. Zenkovets and I. L. Simakova, *Kinetics and Catalysis*, 2013, **54**, 184-192.

79. S. Funai, T. Tago and T. Masuda, *Catalysis Today*, 2011, **164**, 443-446.

80. L. An, C. Dong, Y. Yang, J. Zhang and L. He, *Renewable Energy*, 2011, **36**, 930-935.

81. T. N. Pham, D. Shi and D. E. Resasco, *Applied Catalysis B: Environmental*, 2014, **145**, 10-23.

82. S. Wang and E. Iglesia, *The Journal of Physical Chemistry C*, 2016, **120**, 21589-21616.

83. V. I. Yakerson, L. I. Lafer, A. L. Klyachko-Gurvich and A. M. Rubinshtein, *Bulletin of the Academy of Science of the USSR*, 1966, **15**, 65.

84. V. I. Yakerson, English version is translated from *Izvestiya Akademi Nauk SSSR*, 1963, **6**, 1003.

85. R. Pestman, *Ph.D. Dissertation*, Leiden University, Leiden, The Netherlands, 1995.

86. J. E. McMurry, *Fundamentals of Organic Chemistry, 7th ed*.; Cengage Learning Publisher: Stamford, CT, 2010.

87. H. Staudinger, *Berichte der Deutschen Chemischen Gesellschaft*, 1905, **38**, 1735.

88. F. González, G. Munuera and J. A. Prieto, *Journal of the Chemical Society, Faraday Transactions*, 1978, **74**, 1517.

89. T. S. Hendren and K. M. Dooley, *Catalysis Today*, 2003, **85**, 333.

90. F. A. Bettelheim, W. H. Brown, M. K. Campbell and S. O. Farrell, *Introduction to General, Organic and Biochemistry, 9th edition*, 2010.

Chapter 2: Experimental

In this chapter, the experimental techniques used in the ketonisation of carboxylic acid with metal oxide catalysts in gas phase are described starting with preparation of catalysts. The catalysts were studied using various characterisation techniques to determine their properties such as thermal stability, surface area, porosity, crystallinity, carbon content in spent catalysts, etc. The carbon content was monitored in spent catalysts to determine catalyst coking. The ketonisation reactions were studied using a fixed bed microreactor with online gas-chromatographic analysis, which is also detailed in this chapter.

2.1. Chemicals and catalysts

Acetic acid (>99%), CD_3COOD (99% D) and CH_3COOD (99% D) were purchased from Sigma-Aldrich. γ-Al_2O_3 catalyst was Aluminiumoxide C from Degussa; it was washed with distilled water, calcined at 400 ^oC for 2 h and ground to a powder of 53-180 μm particle size. Degussa P25 titanium dioxide was used as received without further modification. ZrO_2 and CeO_2 were prepared in-house by the literature procedures [1,2] and calcined in air, ZrO_2 at 400 ^oC for 5 h and CeO_2 at 500 ^oC for 3 h, then ground to a powder of 45-180 μm particle size. All gases were supplied by the British Oxygen Company.

2.2. Catalyst preparation

2.2.1. Pretreatment of alumina catalysts

A suspension of 10 g alumina (Degussa) in 90 ml aqueous solution was stirred in a closed glass vessel for 2 h at room temperature, followed by drying at 45 ^oC using a rotary evaporator and calcination under air at 400 ^{o}C for 2 h and temperature ramp rate of 5 ^{o}C /min. The catalyst was ground into a powder of 53-180 μm particle size.

2.2.2. Preparation of CeO_2

The CeO_2 catalyst was synthesised by calcination of Ce(III) nitrate hexahydrate. $Ce(NO_3)_3 \cdot 6H_2O$ (5 g) was calcined at 500 °C in static air for 3 hours, using a 5 °C/min temperature ramp rate according to the method described by Liu et al. [3]. CeO_2 preparation occurred by equation (2.1):

$$2Ce(NO_3)_3 \rightarrow 2CeO_2 + 6NO_2 + O_2 \qquad (2.1)$$

Cerium dioxide was calcined in air at 500 ^oC for 3 h and crushed with a mortar and pestle to a fine powder of 45-180 μm particle size.

2.2.3. Preparation of Cu/SiO_2

5%Cu/SiO_2 was prepared using the procedure described elsewhere [4,5]. It included wet impregnation of silica with an aqueous solution of Cu(II) nitrate, $Cu(NO_3)_2 \cdot 2.5H_2O$, followed by drying in a rotary evaporator, air calcination at 400 ^oC for 2 h and final reduction with H_2 at 400 ^oC for 2 h.

2.2.4. Preparation of ZrO_2

Hydrous zirconium dioxide was prepared by reaction (2.2) using the literature procedure [6].

$$ZrOCl_2 + 2NH_3 + H_2O \rightarrow ZrO_2 + 2NH_4Cl \qquad (2.2)$$

Aqueous ammonia (25%) was added dropwise to an aqueous solution of $ZrOCl_2$ (30 g) in 400 ml of distilled water at room temperature and intense stirring to bring the solution to a pH of 10, which was confirmed using pH paper. The white hydrogel produced was left to age for a 24-hour period. Then it was filtered using a Buchner funnel and washed with distilled water until chloride free as controlled by $AgNO_3$. The hydrous oxide was air dried in an oven at 100

^{o}C for a 24-hour period, after which air calcination took place for a 5-hour period at 400 °C [6].

2.2.5. Sol-gel synthesis of TiO_2-ZrO_2

All TiO_2-ZrO_2 mixed oxide catalysts were prepared by a sol-gel synthetic procedure, which is a modification of the method described by Pfleiderer et al. [7]. The mixed oxide catalysts were prepared via hydrolysis and condensation of a mixture of titanium propoxide $Ti[OC_3H_7]_4$ and zirconium propoxide $Zr[OC_3H_7]_4$ in propanol. In order to avoid unwanted effects due to a change in the water to alkoxide ratio, this ratio was fixed to 4:1 for all catalysts by mixing 160 mmol water and 42 mmol of the metal propoxide in total. The ratios of the metal propoxides that were used are given in Table 2.1.

The two alkoxides were mixed at room temperature in a beaker and stirred in order to achieve a homogenous mixture. 3 mL of distilled water was added, and the stirring speed increased due to the high viscosity resulting from the emerging precipitates. After stirring for ten minutes, a further 20 mL of water was added and then heated to 50 ^{0}C in a water bath. The mixture was stirred at this temperature for 30 min. After heating, the resulting solid was filtered under vacuum and washed thoroughly with distilled water. The mixed oxide was dried in an oven for 3 h and finally calcined in air in a furnace for 5 h at 400 ^{0}C with a heating ramp of 5 ^{0}C/min. As well as all mixed oxides, pure TiO_2 and ZrO_2 powders were synthesised in the same way, for comparison.

Table 2.1. Molar ratios and weights of starting materials involved in catalyst preparation.

TiO_2/ZrO_2 mol/mol	$Ti(OPr)_4$		$Zr(OPr)_4$	
	mmol	**g**	**mmol**	**g**
1:0	42	12.2	0	0
5:1	35	10.2	7.0	3.28
2:1	28	8.12	14	6.55
1:1	21	6.09	21	9.83
1:2	14	4.06	28	13.1
1:5	7	2.03	35	16.438
0:1	0	0	42	19.7

2.2.6. Preparation of TiO_2 by precipitation method

A precursor 0.5 M Ti (IV) oxychloride aqueous solution was prepared as follows [8]. Fifty mL of distilled water was cooled in a 500 mL beaker by magnetic stirring in an ice bath. Then, while stirring, 5 mL (0.05 mol) of $TiCl_4$ were added with an oven-dried Pasteur pipette in ~1 mL portions. To add the $TiCl_4$, the pipette was dipped into the water, and $TiCl_4$ was quickly released, generating white fumes. After adding the $TiCl_4$, the beaker containing white slurry was covered with parafilm, heated to 50 °C in a water bath and stirred at 50 °C until a clear solution was obtained.

To the clear Ti (IV) oxychloride solution, a 2% (1 M) NH_3 aqueous solution (200 mL) was added dropwise during magnetic stirring over about 0.5 h until a pH at 7.2–7.4 was reached (measured with pH paper) to precipitate white Ti (IV) hydroxide. At a pH from 4–5, the mixture became thick enough to impede the stirring. To dilute it, distilled water was added (ca. 50 mL or more). The mixture was further stirred for l h at 50 °C. When the stirring ended, the white precipitate settled down with a clear aqueous phase on top. The precipitate was filtered off by suction under vacuum through a paper filter and washed with distilled water until it was free of chloride (tested with drops of 0.1 M $AgNO_3$). Finally, it was dried in an oven at 100°C under an ambient atmosphere overnight and then calcined in air in a furnace at 400 °C for 5 h with a heating ramp of 5 °C/min.

2.2.7. Preparation of TiO_2-ZrO_2 (1:1) by precipitation method

A precursor 0.5 M Ti (IV) oxochloride aqueous solution was prepared as described above. An aqueous solution of 12.5 g (0.05 mol) of $ZrOCl_2.8H_2O$ (MW 322.2) in 200 mL of distilled water was prepared in a 500 mL beaker and slowly added to the Ti (IV) oxochloride solution under intense stirring. To the clear Ti(IV)-Zr(IV) oxochloride solution, a 2% (1 M) NH_3 aqueous solution (prepared from 30% NH_3, 15 M, d = 0.9 g/mL) was added (~250 mL) in small portions from a beaker at room temperature during magnetic stirring over about 0.5 h until a pH of 8 was reached (measured with pH paper) to precipitate white Ti-Zr (1:1) hydroxide. More distilled water was added if the slurry became too thick upon adding ammonia. The hydrogel formed was aged at room temperature overnight with stirring, then it was filtered through filter paper using a Buchner funnel with suction. The hydrous TiO_2-ZrO_2 mixed oxide thus obtained was washed with distilled water until free of chloride (tested with drops of 0.02 M $AgNO_3$). The oxide was dried in an oven at 100 °C for 24 h under an ambient atmosphere, yielding the 1:1 TiO_2-ZrO_2 mixed oxide in white lumps. The oxide was crushed to a powder and calcined in air in a furnace for 5 h at 400 °C with a heating ramp of 5 °C/min.

2.3 Catalyst characterisation techniques

2.3.1. Surface area and porosity analysis

When considering the activity, selectivity and stability of heterogeneous catalysts it is important to recognise that each of these characteristics is dependent on surface area, pore volume and pore distribution. According to IUPAC classification [9,10,11], pores by their diameter can be classified into one of three groups:

1. Micropores < 2 nm
2. Mesopores between 2 and 50 nm
3. Macropores > 50 nm

Commonly found heterogeneous catalysts have total surface areas in the range of 1-10^3 m^2 g^{-1}, though external surface area ranges from 0.01 to 10 m^2 g^{-1} [9]. It follows that as a result of the pore wall contribution, porous solid catalysts will normally have a much greater total surface area than the given external surface area. A number of techniques have been established in order to measure the surface area of catalysts and to characterise their porous structure [9,12,13]. The most common technique used to determine the surface area and porosity of catalysts is nitrogen adsorption at its boiling temperature (-196 °C). The method developed by Brunauer, Emmett and Teller (BET) in 1938 [9, 14] is the most widely used technique for determining surface area and porosity. The technique involves nitrogen adsorption at its boiling point and is widely used to calculate the monolayer volume of adsorbed N_2 gas (V_m) and the surface area of porous solid materials (A_s) by the following equation:

$$A_s = (V_m/22414)\, N_a\sigma \qquad (2.3)$$

In this equation, σ is the area covered by one nitrogen molecule (0.162 nm^2), N_a is the Avogadro number (6.022×10^{23} mol^{-1}) and the constant 22414 is the nitrogen molar volume (ml mol^{-1}) under standard conditions [13].

A Micromeritics ASAP 2010 adsorption apparatus (Figure 2.1) was used for the characterisation of the catalyst texture. The first step was degassing all the catalysts externally for 1.5 h at 150 °C in a vacuum. This is usually done by placing a sample (150-200 mg) in a sample tube and evacuating it at 250 °C on the Micromeritics ASAP 2010 and continuing the procedure until the vacuum reached 8 µmHg which would remove the adsorbed gasses. After the sample cooled at room temperature, it was immersed in liquid nitrogen; several nitrogen doses (usually 55 doses) were applied so as to obtain an adsorption isotherm.

Figure 2.1. The Micromeritics ASAP 2010 adsorption apparatus.

2.3.2. Power X-ray diffraction (XRD)

When it comes to the phase structure of solid materials, powder X-ray diffraction (XRD) is a vital analytical technique which can be employed to offer information. X-rays wavelengths are equivalent to the spaces between atoms in crystalline materials, which means that when they go through these materials the result is diffraction patterns. Several factors affect the angle of X-ray scattering, thus obeying Bragg's law (equation 2.4) [15]:

$$n\lambda = 2dSin\theta \qquad (2.4)$$

In this equation, n is the order of the reflection (an integer value), λ is the incident X-ray wavelength, d is the lattice planar spacing and θ is the diffraction angle.

The crystallinity of solid materials as well as the average particle size are some of the valuable information that can be obtained from the X-ray diffractogram. The average particle size can be calculated using the Scherrer equation (2.5) [16]:

$$D_p = 0.9\lambda / B\ Cos\theta \qquad (2.5)$$

In this equation, D_p is the particle size, λ is the incident X-ray wavelength, B (rad) is the full width at half the maximum of the diffraction peak, and θ is the diffraction angle.

A Bruker D8 Advance diffractometer in Bragg-Brentano geometry was used for the powder X-ray diffraction studies, and it included a Ge monochromator giving Cu Kα radiation (λ = 1.542 Å), which is available in the Department of Chemistry at University of Liverpool.

2.3.3. Thermogravimetric analysis (TGA)

Measuring the changes in the weight of a sample as its temperature increases is one means of acquiring catalyst characterisation and it makes use of thermogravimetric analysis (TGA). What causes this change in weight can be either chemical or physical in nature and expressed as a percentage value. The requirements for this procedure include a precision balance and the sample holder placed inside the furnace, which is subsequently electrically heated under a flow of nitrogen or air. The results can be seen as a curve where the weight percentage of original material is a function of temperature. A derivative curve can be employed to ascertain where the weight loss is most apparent. Since knowing the correct amount of reactants in catalyst synthesis is undoubtedly important, TGA proves useful in measuring the amount of physisorbed water in the samples as well as in determining the thermal stability of the catalysts.

Performing the TGA of catalyst samples (20-50 mg) under flow of nitrogen gas was done using a Perkin Elmer TGA 7 instrument; the heating rate necessary to increase the temperature from room temperature to 700 ºC ranged between 10 and 20 ºC min^{-1}.

2.3.4. Fourier transform infrared (FTIR) spectroscopy

FTIR spectroscopy is an analytical technique that can be useful in acquiring data about bulk and surface properties of solid catalysts, such as the nature of acid sites in solid acid catalysts [17].

In this work, we researched the structure of oxide catalysts using infrared spectroscopy in the region of the spectrum (500 – 4000 cm^{-1}). Furthermore, pyridine adsorption using diffuse reflectance infrared Fourier transform (DRIFT) spectroscopy in the range from 1540 cm^{-1} to 1450 cm^{-1} established the Brønsted and Lewis acid sites on the catalyst surface.

In order to do the DRIFT measurements, the catalyst samples were degassed for two hours, under vacuum, at 150 °C. The next step was diluting 5 mg of the catalyst with 45 mg of dried KBr powder and grinding that thoroughly, at room temperature, under a flow of dry nitrogen. To determine the acid sites using pyridine adsorption, the samples were mixed with dried KBr (to dilute samples to 10 wt%), then degassed under vacuum at 150 °C/1 Pa for one hour. Next the samples cooled at room temperature in a dry nitrogen atmosphere, while 1-3 drops of pyridine were added to each sample. After exposing the samples to pyridine at room temperature for an hour, they were degassed once more under vacuum for one hour at 150 °C in order to remove any physisorbed pyridine. Finally, the DRIFT spectrum of adsorbed pyridine was recorded at room temperature.

A Nicolet NEXUS FTIR spectrometer was used for the FTIR studies which were carried out in absorbance mode at room temperature by averaging 254 scans in the 4000–500 cm^{-1} range with a resolution of 4 cm^{-1}.

2.3.5. C,H,N analysis

Measuring the amount of C and H in spent solid catalysts [18] can be done through combustion analysis. Normally, a small amount of catalyst (~5 mg) is put in the combustion reactor and heated up to 1000 °C under flowing He gas, then enriched with pure oxygen to cause the flash combustion to produce CO_2 and H_2O. Combustion quantities are detected when the gas mixtures pass to the GC detector. We used this analysis in order to measure the carbon content in spent catalysts to study the effect of coke on catalyst deactivation. For example, after ketonisation of acetic acid, there was 5.6% coke left in the spent CeO_2 catalyst, which could cause the metal and/or the acid sites in the catalyst to become blocked.

The Thermo Flash EA 1112 series analyser was used to analyse catalyst coking, which is available in the Department of Chemistry at Liverpool University.

2.3.6. Differential scanning calorimetry (DSC)

Thermogravimetric DSC is an analytical technique normally involved in catalyst characterisation [19], as it is crucial in ascertaining basic or acid properties such as the number of acid sites and their strength. Various chemical and physical transformations of catalysts, such as phase changes, crystallisation, adsorption, sublimation, decomposition, desorption, reduction, oxidation, surface reactivity and calcination can be studied using this technique [20]. Normally this is done through the ammonia pulse chemisorption method that we used in this research in order to determine the acid sites of the catalysts.

The DSC uses two open refractory tubes, crossing a heating furnace. Between the tubes there is a detection unit designed according to the Calvet principle. The sample cell is placed in the furnace and connected to the balance, while the reference sample is positioned on the other side of the furnace. A pressure regulator is built into the gas flow system.

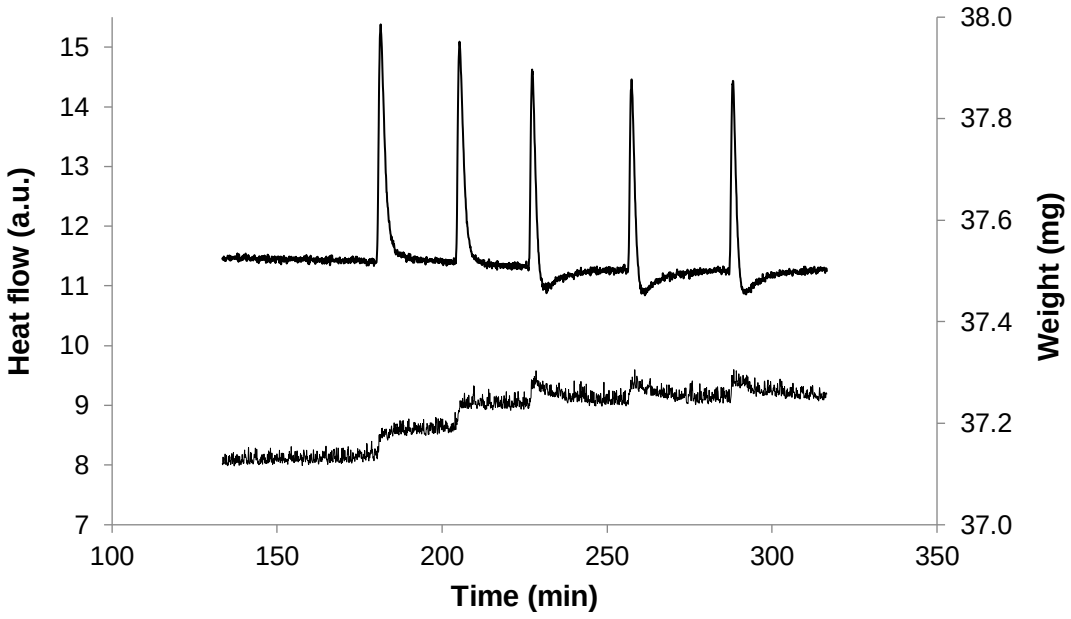

Figure 2.2. TG-DSC for ammonia adsorption on ZrO_2 at 150 °C: DSC (top profile) and TG (bottom profile). The first two NH_3 pulses (first two steps on the TG profile) represent practically irreversible NH_3 adsorption on stronger acid sites. Subsequent steps represent a reversible adsorption on weaker acid sites. From this TG profile, the total number of acid sites (stronger and weaker acid sites) was determined as the sum of adsorption amounts for the first three pulses.

In our study, the heat and the amount of ammonia adsorption on oxide catalysts were measured using a Setaram TG-DSC 111 differential scanning calorimeter by a pulse method in a flow system as described previously [1]. Catalyst samples (10–70 mg) were placed in the calorimeter and pre-treated under nitrogen flow (30 mL min^{-1}) at 300 °C for 1 h. Then the temperature was lowered to 150 °C and, after sample weight stabilisation (about 1 h), the measurement was performed at 150 °C by successive 2 mL pulses of pure ammonia into the N_2 flow using a loop fitted in a 6-port valve. Sufficient time was allowed after each pulse for adsorption equilibrium to be reached (about 30 min). Weight gain due to NH_3 adsorption and

the corresponding heat of adsorption were recorded, from which the enthalpy of NH_3 adsorption (ΔH) and the total amount of NH_3 adsorbed were determined as a measure of acid site strength and acid site density of catalysts, respectively. The ammonia pulses applied (2 mL) were large enough to ensure the accurate measurement of the amount of ammonia adsorbed. Such a pulse corresponded to a 30-40% of surface coverage of oxide catalysts. A representative example of TG-DSC analysis for ammonia adsorption on ZrO_2 is shown in Figures 2.2 and 2.3.

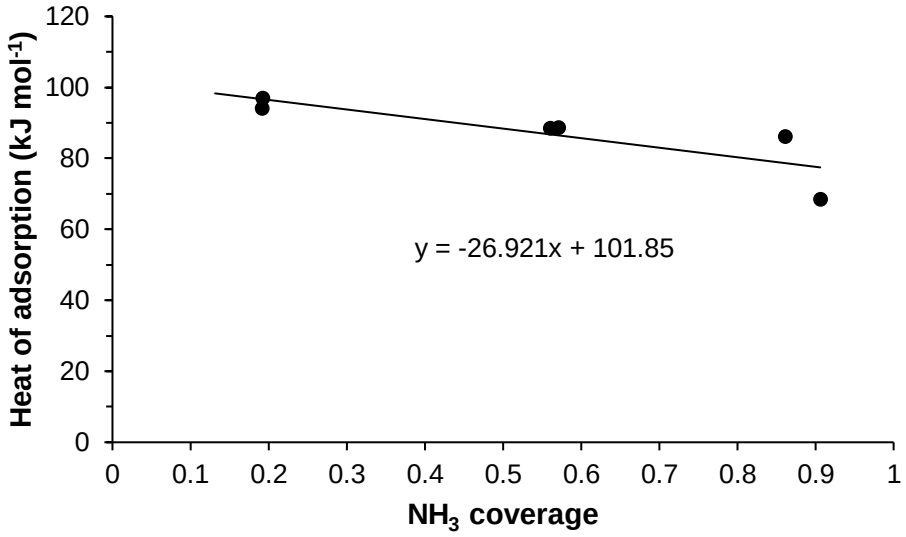

Figure 2.3. Heat of ammonia adsorption on ZrO_2 at 150 ^oC versus fractional surface coverage (the points represent two parallel measurements, one shown in Figure 2.2). Given the large NH_3 pulses, extrapolation to zero coverage is not reliable. For this reason, the adsorption heats at a fractional coverage of 0.3 were used to characterise the acid strength of all oxides.

2.4. Catalyst testing

2.4.1. Gas chromatography (GC)

Separating and analysing volatile compounds in the gas phase [21] can be achieved through an analytical technique, namely gas chromatography (GC). Firstly, a stream of an inert carrier gas such as He, Ar, H_2 or N_2 is used to transfer the volatilised sample as a mixture of volatiles through a heated column. According to their boiling specific points [22], each component in the mixture passes through the GC column at a different rate. Figure 2.4 provides a schematic diagram of a typical GC while Figure 2.5 shows the GC setup for this study.

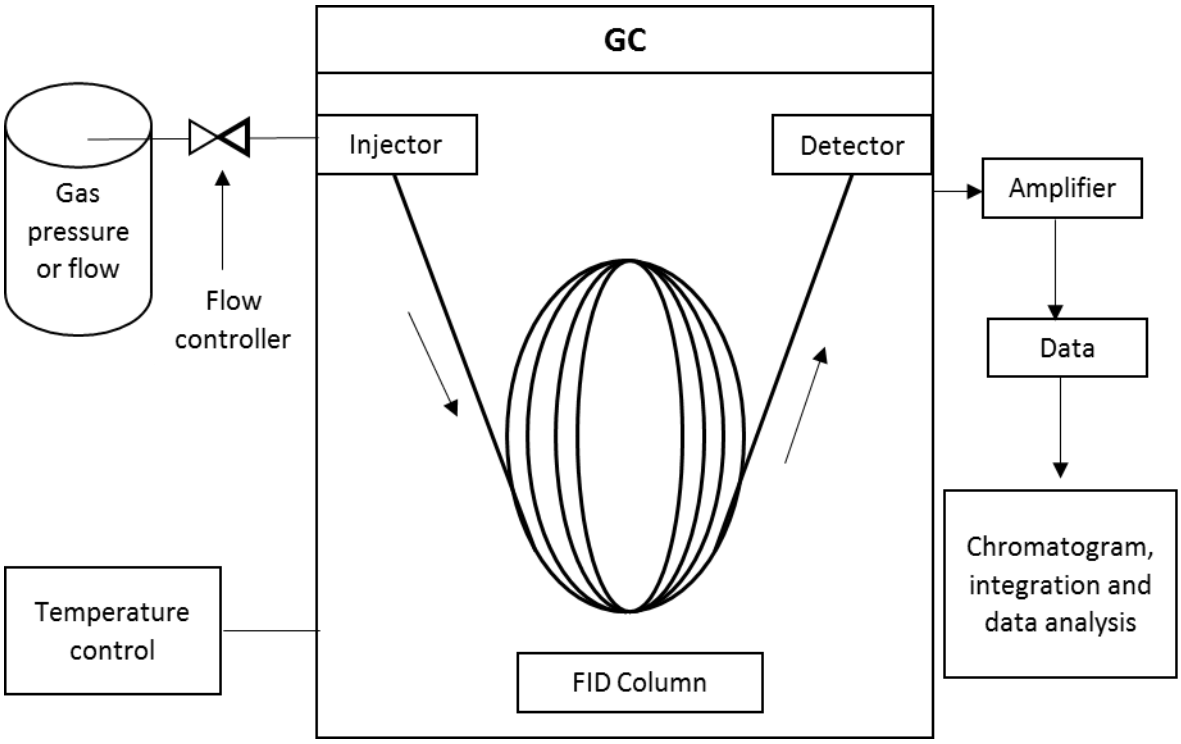

Figure 2.4. Schematic diagram of a typical GC.

The GC column is a long capillary tube with a stationary phase bonded to its wall. Because of a combination of volatility and the degree with which the various components of the gas mixture interact with the stationary phase, they are distributed between the stationary

phase of the column and the mobile phase (carrier gas). The rate at which these components pass is affected by factors such as the boiling points and the polarity of each compound.

A split/splitless injector, placed at the entrance of the GC column injects a controlled quantity of samples into the column (Figure 2.6). The ratio between the split flow rate and the column flow rate is known as the split ratio.

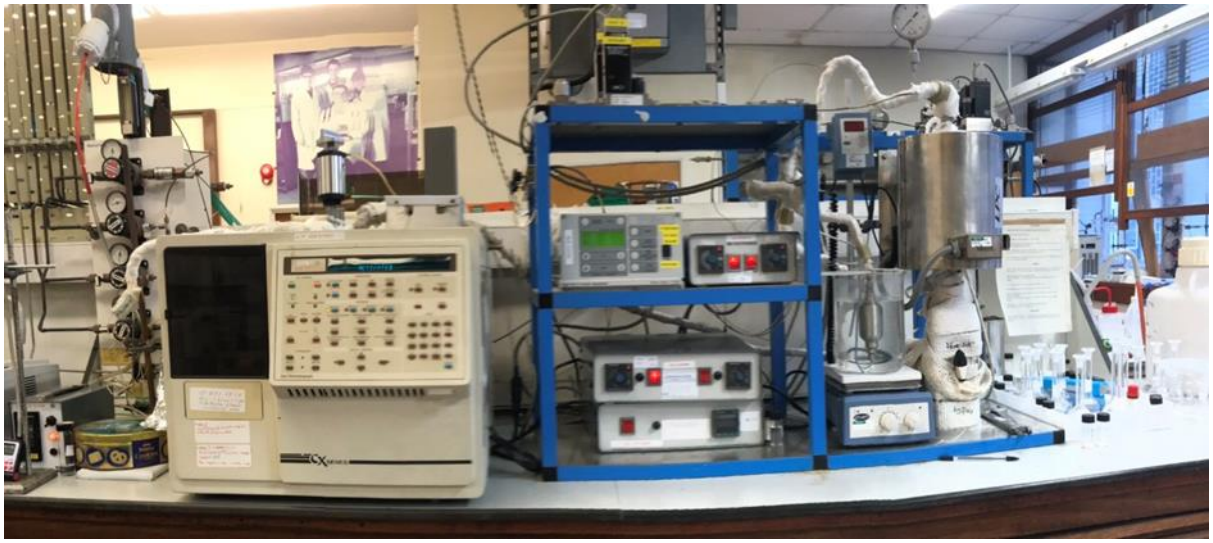

Figure 2.5. Varian 3400 GC connected to the fixed-bed reactor.

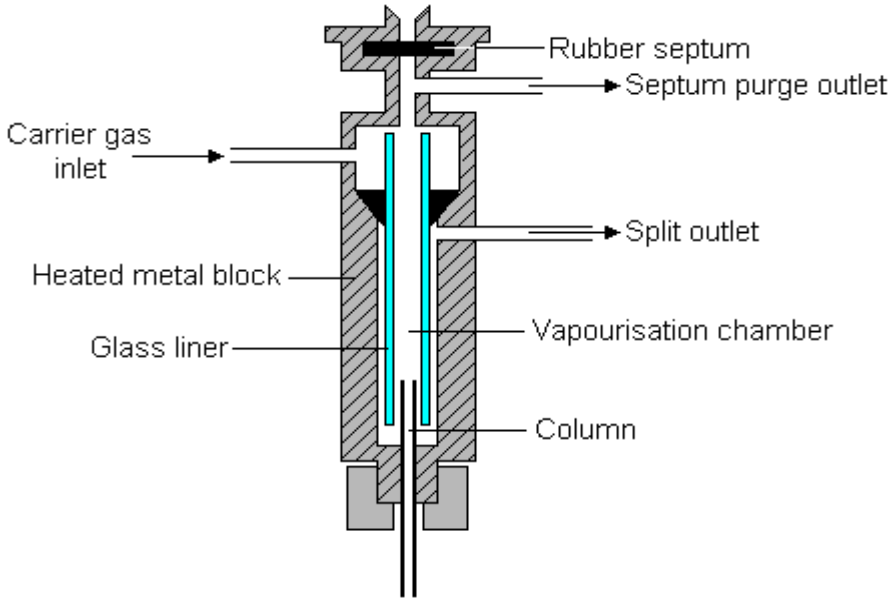

Figure 2.6. The split/splitless injector.

A detector is positioned at the end of the column. We used a flame ionisation detector (FID), as seen in Figure 2.7. Inside it, the analysed organic compounds are burned with high temperature flames, resulting from mixing H_2 and air at a small metal jet, which would ionise the compounds with low ionisation potentials and turn them into charged particles. These move towards the collector electrode. The amount of compound determines the amount of charge produced. The resulting current is amplified and plotted on the screen as a chromatogram. The retention time is the time each component needs to pass from the injector to the detector.

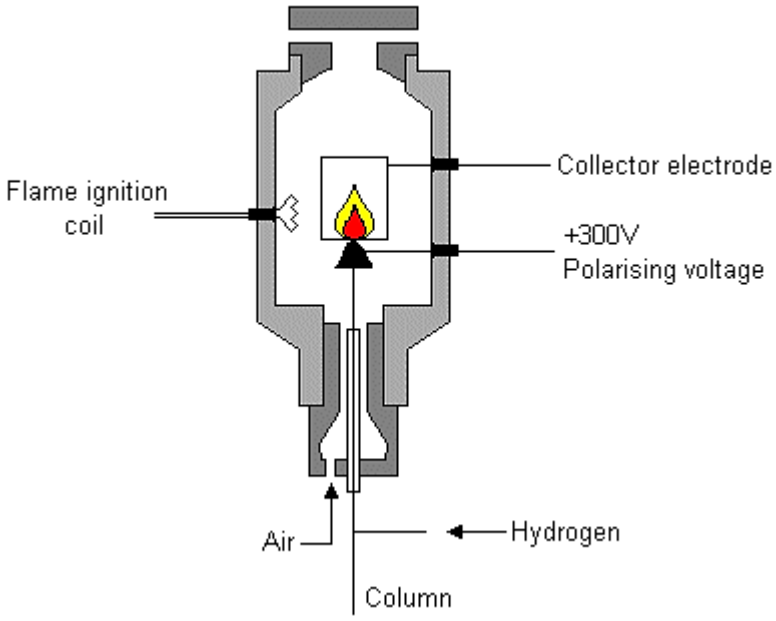

Figure 2.7. The flame ionisation detector [23].

For our research, we employed a Varian 3400 gas chromatograph with a 30 m x 0.32 mm x 0.5 μm CP-WAX capillary column and FID detector to analyse the reaction products on-line. Both the injector and detector temperature and were set at 247 °C. The nitrogen flow rate was 20 mL min^{-1}. The temperature of the column oven was set as can be seen in Figure 2.8.

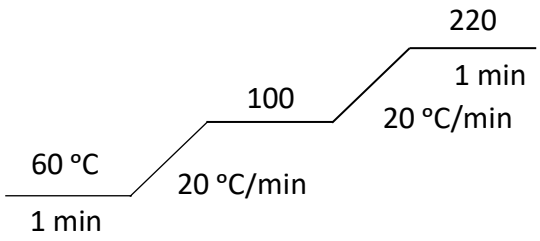

Figure 2.8. The temperature program of the column oven CP-WAX capillary column.

2.4.2. Product calibration

Equal peak areas for different compounds in a chromatogram are not always indicative of equal concentrations of these compounds, since the response characteristics of the detector influence these areas. Carrier gas flow rate as well as detector and column temperatures, can furthermore affect them. Standard internal or external methods can prove useful in removing the effects of these factors. In this work, acetone was calibrated against acetic acid as the standard, toluene was used as a solvent. The calibration data were represented using equation 2.6, which shows the ratio of the total peak area of acetone (S) to the total peak area of the standard (acetic acid) (S_o) against the ratio of the molar concentration of acetone (M) to the molar concentration of acetic acid (M_o).

$$\frac{M}{M_o} = K \frac{S}{S_o} \qquad (2.6)$$

Figure 2.9 and 2.10 show two repeated calibrations of acetone relative to acetic acid from toluene solution which are in very good agreement between them. From these calibrations, the response factors were calculated. Table 2.2 gives the molecular weights, boiling points, retention times and calibration factors for acetone and acetic acid.

Table 2.2. Molecular weights, boiling points, retention times and calibration factors for all compounds in the gas-phase ketonisation of acetic acid using Varian Star 3400 CP-WAX capillary column.

Compound	MW g mol^{-1}	Boiling point °C	Retention time min	Calibration factor
Acetone	58.10	56	1.3	0.47
Acetic acid	60.05	118	4.8	1

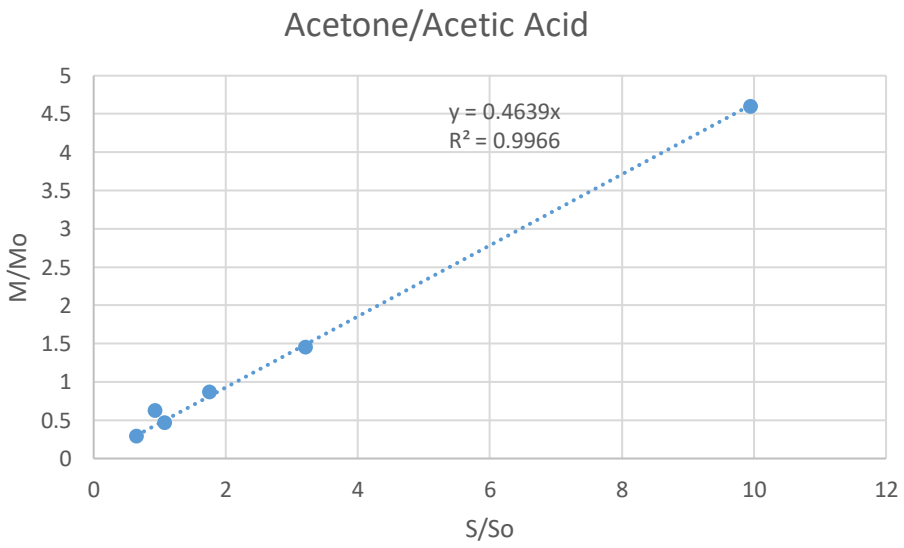

Figure 2.9 Calibration (1) for acetone relative to acetic acid.

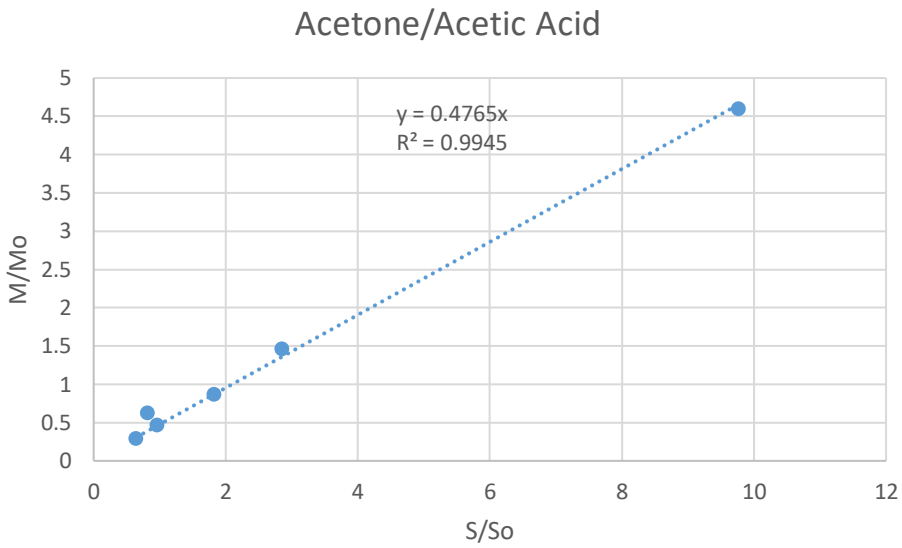

Figure 2.10 Calibration (2) for acetone relative to acetic acid.

2.4.3. Fixed bed flow microreactor for ketonisation of acetic acid

The ketonisation of acetic acid was carried out in the gas phase at 180-350 ^{o}C and atmospheric pressure in a vertical down-flow fixed-bed Pyrex reactor (9 mm internal diameter) as shown in Figure 2.5 with online gas chromatographic (GC) analysis (Varian Star 3400 CX instrument with a 30 m x 0.32 mm x 0.5 μm CP-WAX capillary column and a flame ionisation detector), as described elsewhere [24]. The temperature in the reactor was controlled by a Eurotherm controller using a thermocouple placed at the top of the catalyst bed. Acetic acid was fed by passing N_2 carrier gas flow controlled by a Brooks mass flow controller through a stainless steel saturator which held the liquid acid at appropriate temperature to maintain the chosen reactant concentration in the gas flow. Typically, the reaction was carried out at acetic acid partial pressure of 3.35 kPa and an N_2 flow rate of 20 mL min^{-1} unless stated otherwise. The downstream gas lines and valves were heated to 150 ^{o}C to prevent substrate and product condensation. The reactor was loaded with 0.10-0.20 g of catalyst powder (45-180 μm particle size). Prior to reaction, the catalysts were heated at the reaction temperature in N_2 flow for 1 h.

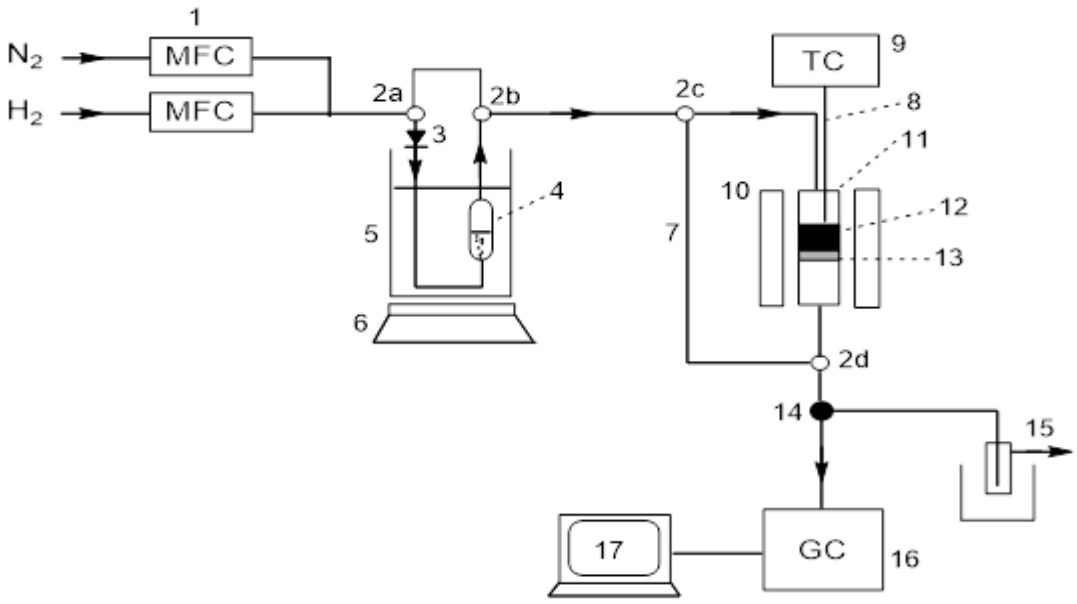

Figure 2.11. Continuous flow fixed-bed reactor setup for ketonisation of acetic acid: (1) Brooks mass flow controller, (2) 3-way valve, (3) check valve (non-return valve), (4) saturator containing liquid substrate, (5) temperature controlled water bath, (6) stirring hotplate, (7) bypass, (8) thermocouple, (9) Eurotherm temperature controller, (10) furnace, (11) quartz tubular reactor, (12) catalyst bed, (13) glass wool support, (14) Valco multiposition sampling valve with air actuator, (15) product trap, (16) Varian gas chromatograph, (17) computer.

Once reaction started, the downstream gas flow was analysed by the on-line GC to obtain reactant conversion and product selectivity. The product selectivity was defined as moles of product formed per one mole of acetic acid converted and quoted in mole per cent; thus 100% acetone selectivity would mean 1 mol of acetic acid converted to form 0.5 mol of acetone. CO_2 formed in the reaction was not quantified and not included in reaction selectivities. The mean absolute percentage error in conversion and selectivity was ≤ 5%. The molar balance between acetic acid and the reaction products (acetone and isobutene) was maintained within 95%. Reaction rates (R) were determined as $R = XF/W$ (in mol $g_{cat}^{-1}h^{-1}$),

where X is the fractional conversion of acetic acid, F is the molar flow rate of acetic acid (in mol h^{-1}), W is the catalyst weight (in grams) and W/F is the contact time (g_{cat} h mol^{-1}). For rate measurements, the reaction was carried out for 4 h time on stream (TOS) at differential conditions ($X \leq 0.1$), where X is directly proportional to the reaction rate. All oxide catalysts, except TiO_2, suffered from deactivation in the initial stage of reaction, reaching a steady conversion rate after ca. 1.5 h TOS. To minimise the effect of catalyst deactivation, the reaction rates were calculated from average acetic acid conversion over a TOS period of 1.5 – 4 h.

Figures 2.12 and 2.13 give examples of GC trace for ketonisation of acetic acid in gas phase.

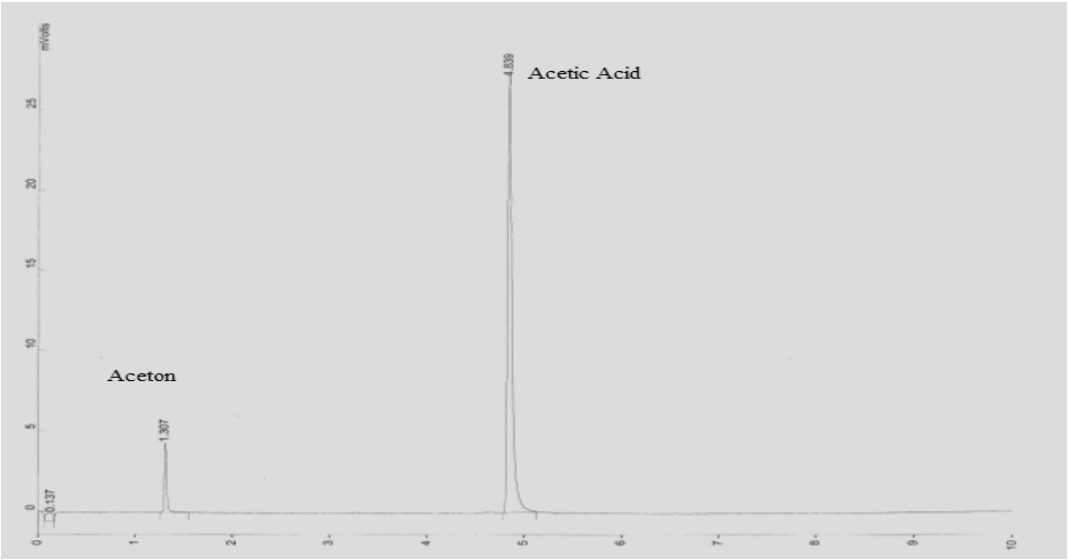

Figure 2.12. GC trace for ketonisation of acetic acid over Al_2O_3 at 320 ^oC, 20 ml min^{-1} flow rate.

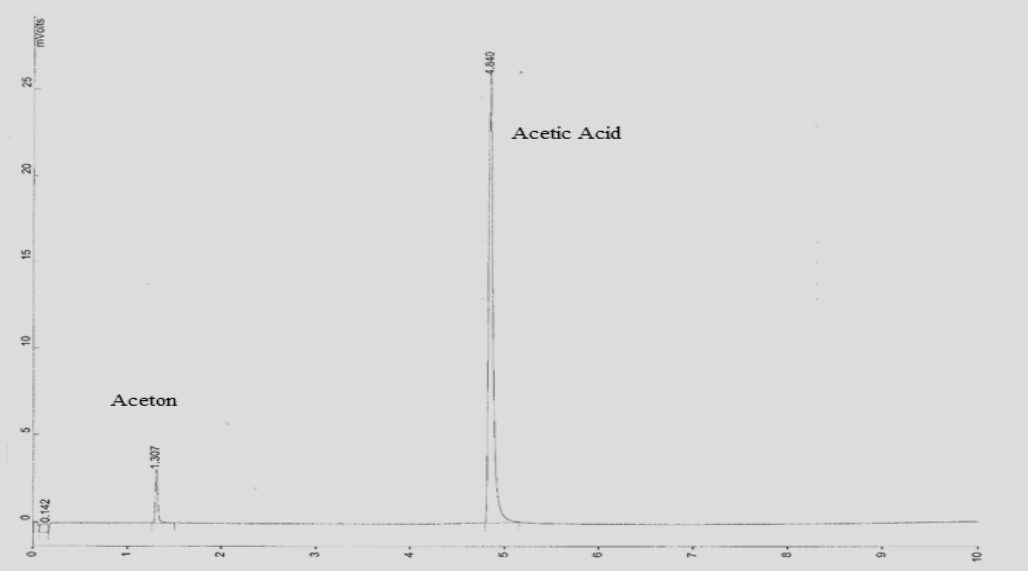

Figure 2.13. GC trace for ketonisation of acetic acid over TiO_2 at 270 ^oC, 20 ml min^{-1} flow rate.

2.4.4. Calculation of reaction results

In the processes of gas phase acid ketonisation, substrate conversion, product yield and selectivity were calculated by using equations 2.6, 2.7 and 2.8. The selectivity is moles of product formed per mole of substrate converted and quoted in mol per cent.

$$\text{Conversion of substrate (\%)} = \frac{\text{Moles of substrate reacted}}{\text{Moles of substrate fed}} \times 100 \qquad (2.6)$$

$$\text{Product yield (\%)} = \frac{\text{Moles of product}}{\text{Moles of substrate fed}} \times 100 \qquad (2.7)$$

$$\text{Product selectivity (\%)} = \frac{\text{Product yield}}{\text{Substrate conversion}} \times 100 \qquad (2.8)$$

References

1. M. Alsalme, P. V. Wiper, Y. Z. Khimyak, E. F. Kozhevnikova and I. V. Kozhevnikov, *Journal of Catalysis*, 2010, **276**, 181–189.
2. M.L. Dos Santos, R.C. Lima, C.S. Riccardi, R.L. Tranquilin, P.R. Bueno, J.A. Varela and E. Longo, *Materials Letters*, 2008, **62**, 4509–4511.
3. C.J. Liu, A. M. Karim, V. M. Lebarbier, D. H. Mei and Y. Wang, *Topics in Catalysis*, 2013, **56**, 1782-1789.
4. M. A. Alotaibi, E. F. Kozhevnikova and I. V. Kozhevnikov, *Journal of Catalysis*, 2012, **293**, 141-144.
5. S. Wang and E. Iglesia, *Journal of Catalysis*, 2017, **345**, 183-206.
6. A. Alsalme, E. Kozhevnikova, Y. Khimyak, P. Wiper and I. Kozhevnikov, *Abstracts of Papers- American Chemical Society*, 2011, **241**, 1.
7. S. J. Pfleiderer, D. Lutzenkirchen-Hecht and R. Frahm, *Journal of Sol-Gel Science and Technology*, 2012, **64**, 27-35.
8. D. -S. Seo, J. –K. Lee and H. Kim, *Journal of Crystal Growth*, 2001, **229**, 428-432
9. G. Leofanti, M. Padovan, G. Tozzola and B. Venturelli, *Catalysis Today*, 1998**, 41**, 207.
10. J. Rouquerol, D. Avnir, C.W. Fairbridge, D.H. Everett, J.H. Haynes, N. Pernicone, J.D.F. Ramsay, K.S.W. Sing and K.K. Unger, *Pure and Applied Chemistry*, 1994**, 66**, 1739.
11. G. Rothenberg, *Catalysis: Concepts and Green Applications*, Wiley-VCH, Weinheim, 2008.
12. G. Leofanti, G. Tozzola, M. Padovan, G. Petrini, S. Bordiga and A. Zecchina, *Catalysis Today*, 1997**, 34**, 329.
13. G. Leofanti, G. Tozzola, M. Padovan, G. Petrini, S. Bordiga and A. Zecchina, *Catalysis Today*, 1997**, 34**, 307.
14. S. Brunauer, P.H. Emmett and E. Teller, *Journal of American Chemical Society*, 1938**, 60**, 309.
15. P.W. Atkins, *Physical Chemistry*, Oxford University Press, 1998.

16. A.W. Burton, *Zeolite Characterization and Catalysis:* A 2009**,** 1.
17. G. Schwedt, *The Essential Guide to Analytical Chemistry*, John Wiley and Sons, Chichester, England, 1997.
18. J. Mendham, R.C. Denney, J.D. Barnes and M.J.K. Thomas, *Vogel's Textbook of Quantitative Chemical Analysis*, Preston Education Ltd, 2000.
19. Z. F. Pei and V. Ponec, *Applied Surface Science*, 1996, **103**, 171-182.
20. L.-F. Liao, C.-F. Lien and J.-L. Lin, *Physical Chemistry Chemical Physics*, 2001, **3**, 3831-3837.
21. I.A. Fowis, *Gas Chromatography*, ACOL-Wiley, Chichester, 1995.
22. D. Kealey and D.J. Haines, *Analytical Chemistry, (1st ed)*, Bio scientific, Oxford, 2002.
23. http://teaching.shu.ac.uk/hwb/chemistry/totorials/chrom/gaschrm.htm (accessed 13 March 2019).
24. H. Bayahia, E.F. Kozhevnikova and I.V. Kozhevnikov, *Applied Catalysis B: Environmental*, 2015, **165**, 253–259.

Chapter 3: Catalyst characterisation

In this chapter, catalyst characterisation results are described and discussed. The Physio-chemical properties of oxide catalysts were measured by various techniques. BET technique was used to measure catalyst texture features such as surface area, porosity and pore size. Crystallinity and phase composition were characterised using the XRD technique.

3.1. Surface area and porosity studies

3.1.1. Introduction

Nitrogen physisorption at boiling temperature (-196 °C) was utilised for determining the surface area of oxide catalysts and to characterise the porous texture. For generating the nitrogen adsorption isotherms, nitrogen volume adsorbed was plotted versus the relative pressure. The individual isotherm shape is dependent upon the solid catalyst texture. The IUPAC classification system states that 6 variations of isotherm can be identified [1-3]. Figure 3.1 shows four isotherms, which are generally found in solid catalysts [4].

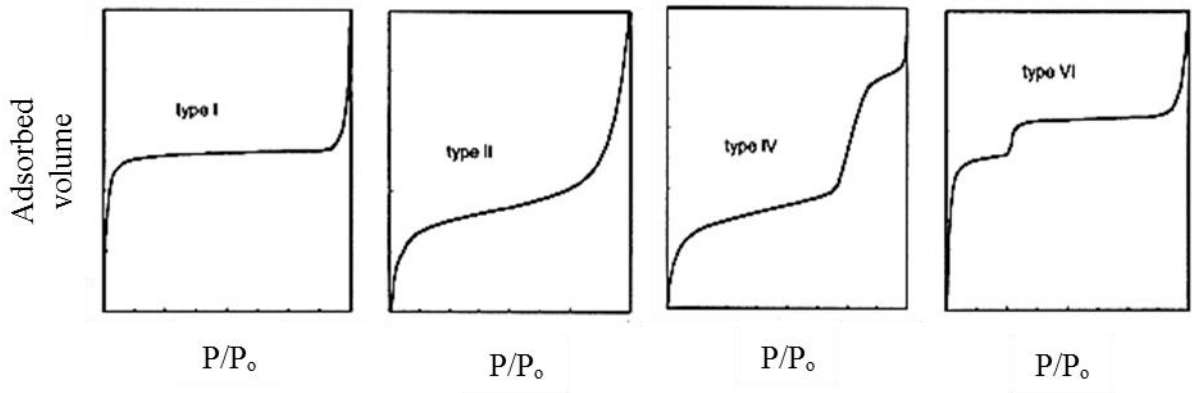

Figure 3.1. The four usual variations of nitrogen adsorption isotherm.

(1) Type I, II and IV isotherms represent microporous, macroporous and mesoporous materials, respectively. In microporous materials (type I), adsorption happens at a lower relative pressure. In this case, the adsorbate molecules do not have capillary condensation in the medium relative pressure area (<0.3) and have strong interactions with pore walls. At high relative pressures, the pores are totally filled

and adsorption continues on the external surface. Zeolites are an example of microporous materials.

(2) In macroporous materials (type II), the formation of monolayers of adsorbed molecules takes place at a lower relative pressure, while at high relative pressures multilayer adsorption happens. The thickness of the adsorbate layer increases with increasing pressure until condensation pressure is achieved.

(3) In mesoporous materials (type IV), the formation of the adsorption monolayer occurs at a lower relative pressure. At higher relative pressures, capillary condensation occurs to fill the mesopores, causing a sharp increase in the adsorption volume. The larger the mesopores in the solid catalyst, the higher the relative adsorption pressure will occur. When the mesopores are full, the adsorption will continue on external surfaces. An example of mesoporous materials are many metal oxides and supported HPA catalysts.

(4) When the catalyst surface is energetically uniform, the isotherm may take a step-like shape (type VI).

After measurement of the adsorption isotherm by a pressure increase until the adsorbate reaches saturation point, desorption is measured through a decrease in the pressure to evaporate the adsorbate from the surface and the pores. However, in mesoporous materials evaporation takes place at a pressure lower than condensation in the capillaries, which gives a hysteresis loop.

Four kinds of hysteresis for solid catalysts exist, according to IUPAC classification (Figure 3.2).

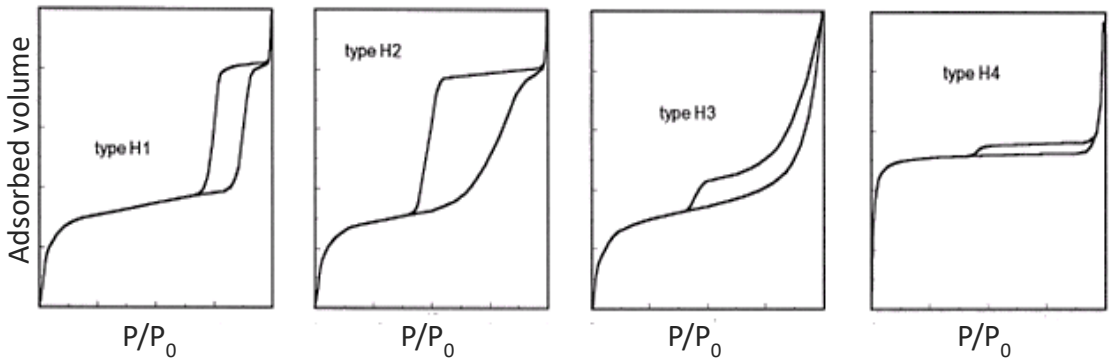

Figure 3.2. The four hysteresis shapes normally seen with N_2 adsorption.

Types H1 and H2 hysteresis are seen when analysed materials consist of particles with channels which are close to cylindrical in shape or are produced by an aggregate (consolidated) or agglomerate (unconsolidated) spheroid shape. For materials displaying type H1 hysteresis, a pore might be of uniform size and shape, while a pore with non-uniform sizes and shapes display type H2 hysteresis. Types H1 and H2 hysteresis are attributed to differences in size between pore bodies and pore mouths (e.g. pores shaped like ink bottles) or towards other behaviours in adsorption and desorption in a nearly cylindrical pore. Most mesoporous materials display these two hysteresis isotherms [4].

Types H3 and H4 hysteresis are seen in materials that consist of an aggregate or agglomerate particles producing a slit-shaped pore (a plate or edged particle similar in a cuboid shape). A pore uniform in size and/or shapes displaying type H4 hysteresis, while a pore with non-uniform size and/or shape will display type H3. Zeolites and active carbons are, respectively, examples of H3 and H4 isotherms.

Occasionally, no hysteresis is seen. This indicates materials with wedge-shaped, cone-shaped, and blind cylindrical pores. However, since a material pore is not usually regular in its size and shape, there are only observations of isotherms with a much reduced hysteresis.

3.1.2. Surface area and porosity analysis of metal oxide catalysts

Information about the metal oxide catalysts studied is given in Table 3.1 including catalyst surface area and porosity as well as the basicity of γ-alumina samples determined as the pH of 10% w/v aqueous suspension.

Table 3.1. Surface area and porosity of catalysts.[a]

Catalyst[b]	Surface area[c] m^2g^{-1}	Pore volume[d] cm^3g^{-1}	Pore diameter[e] Å	pH[f]
Al_2O_3 (1)	98	0.56	227	6.0
Al_2O_3 (2)	98	0.57	233	6.5
Al_2O_3 (3)	97	0.49	205	6.4
Al_2O_3 (4)	105	0.48	183	8.4
Al_2O_3 (5)	106	0.41	154	5.4
Al_2O_3 (6)	123	0.18	57	9.1
Al_2O_3 (7)	90	0.15	68	8.1
Al_2O_3 (8)	56	0.12	82	7.4
Al_2O_3 (9)	159	0.26	65	4.8
Al_2O_3 (10)	156	0.26	67	5.4
Al_2O_3 (11)	156	0.26	67	6.2
Al_2O_3 (12)	185	0.26	57	10.2
TiO_2	44	0.10	90	
ZrO_2	117	0.13	43	
CeO_2	85	0.22	104	

[a] The catalysts were pre-treated for 2 h at 240 °C in vacuum before measuring N_2 adsorption.

[b] γ-Alumina samples: (1) Degussa Aluminiumoxide C washed and air calcined at 400°C/2h; (2)

ditto, air calcined at 500°C/2h; (3) ditto, air calcined at 600°C/2h; (4) ditto, treated with 0.01 M aqueous KOH and air calcined at 400°C/2h; (5) ditto, treated with 0.5 M aqueous NH_3 and air calcined at 400°C/2h; (6) BDH alumina; (7) neutral alumina; (8) acidic alumina; (9) Sigma-Aldrich acidic alumina; (10) Sigma-Aldrich weakly acidic alumina; (11) Sigma-Aldrich neutral alumina; (12) Sigma-Aldrich basic alumina. [c] BET surface area. [d] Single point total pore volume. [e] Average BET pore diameter. [f] pH of 10% aqueous suspension.

Figures from 3.3 to 3.8 show nitrogen adsorption/desorption isotherms and pore size distribution for Al_2O_3, CeO_2 and ZrO_2. All oxides show hysteresis loops indicating the presence of mesopores.

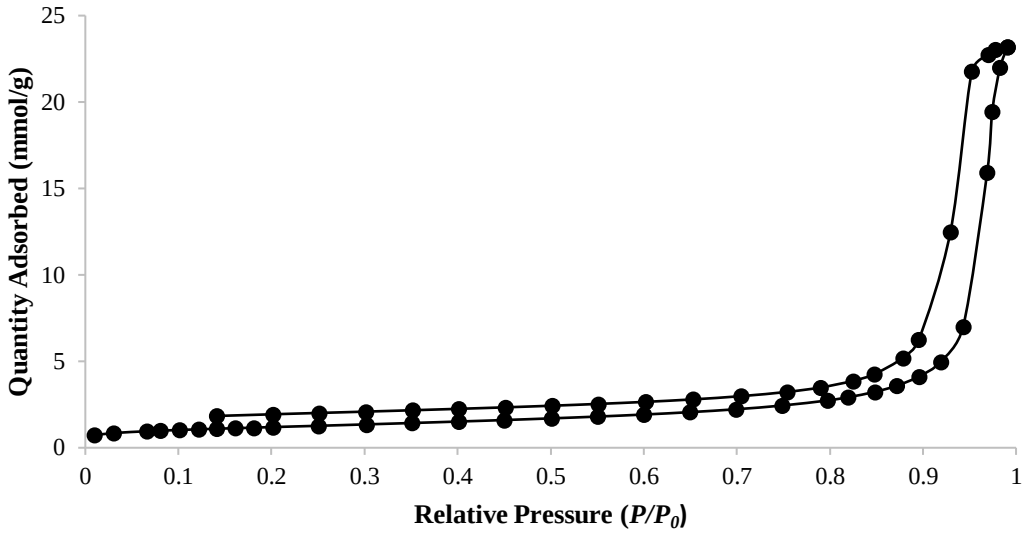

Figure 3.3. Nitrogen adsorption/desorption isotherm for Al_2O_3.

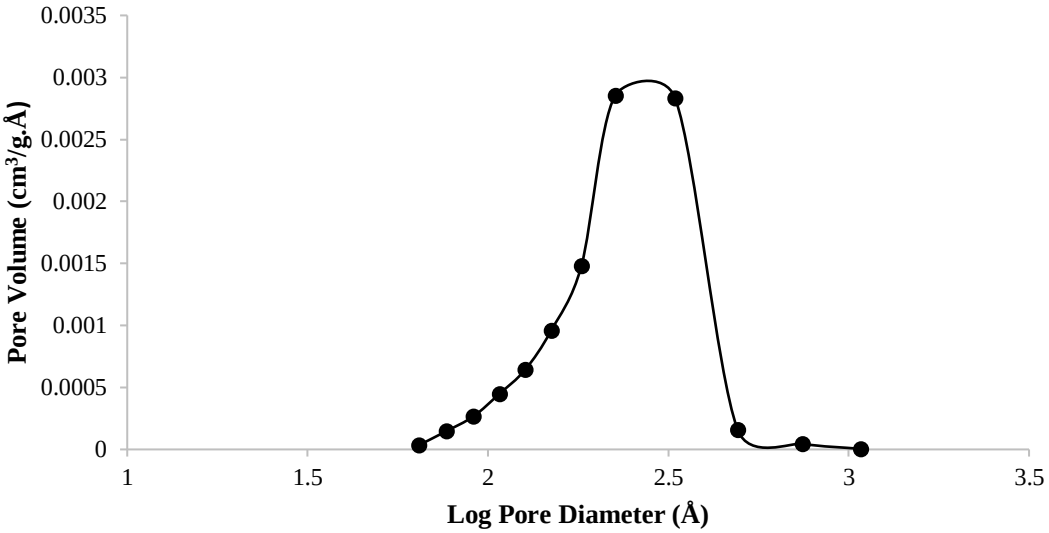

Figure 3.4. Pore size distribution for Al_2O_3.

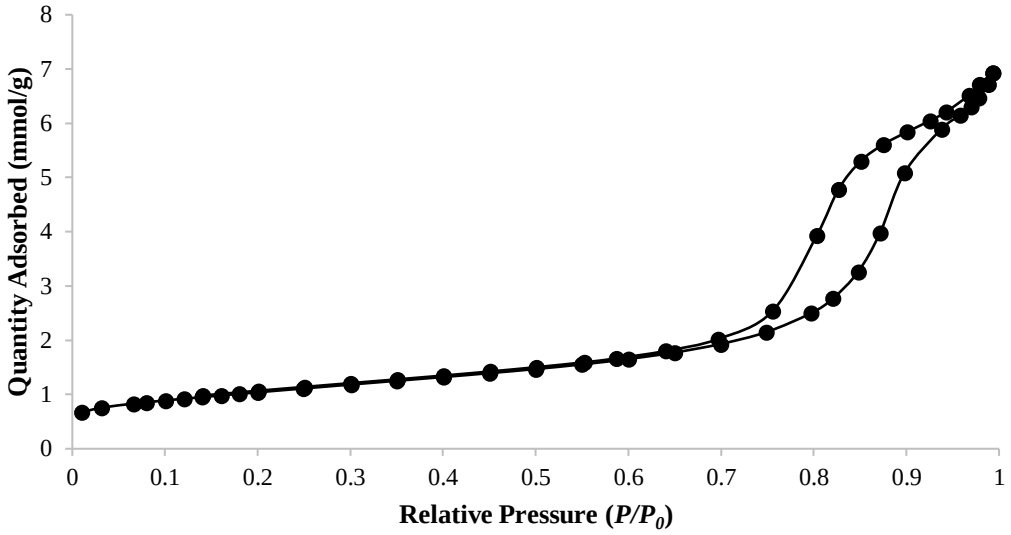

Figure 3.5. Nitrogen adsorption/desorption isotherm for CeO_2.

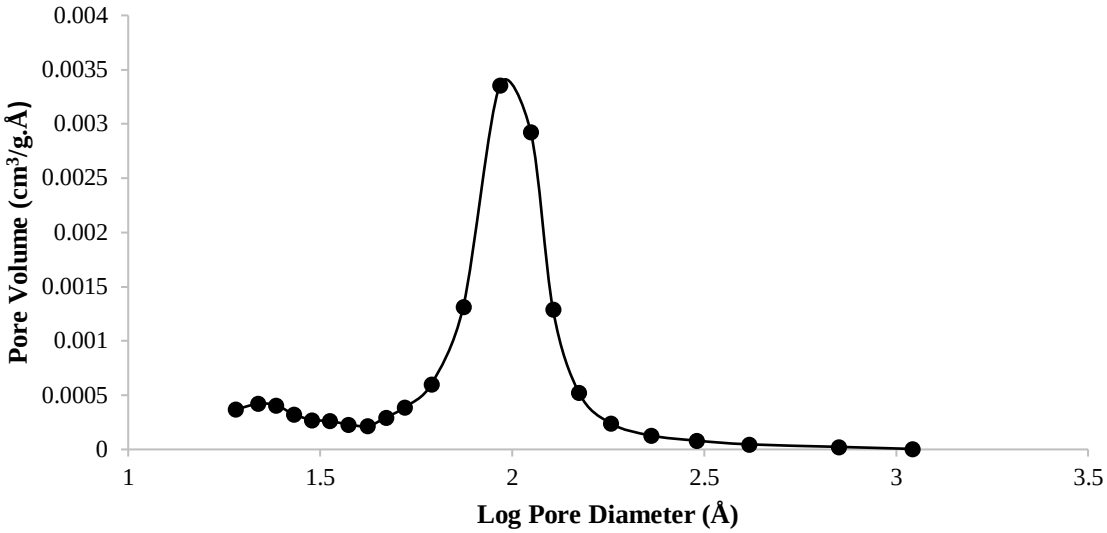

Figure 3.6. Pore size distribution for CeO_2.

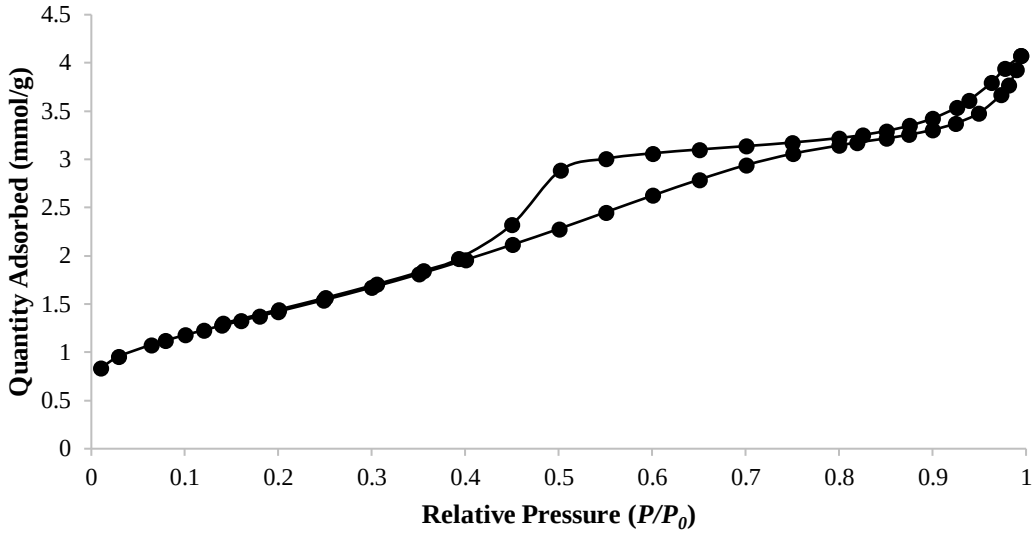

Figure 3.7. Nitrogen adsorption/desorption isotherm for ZrO_2.

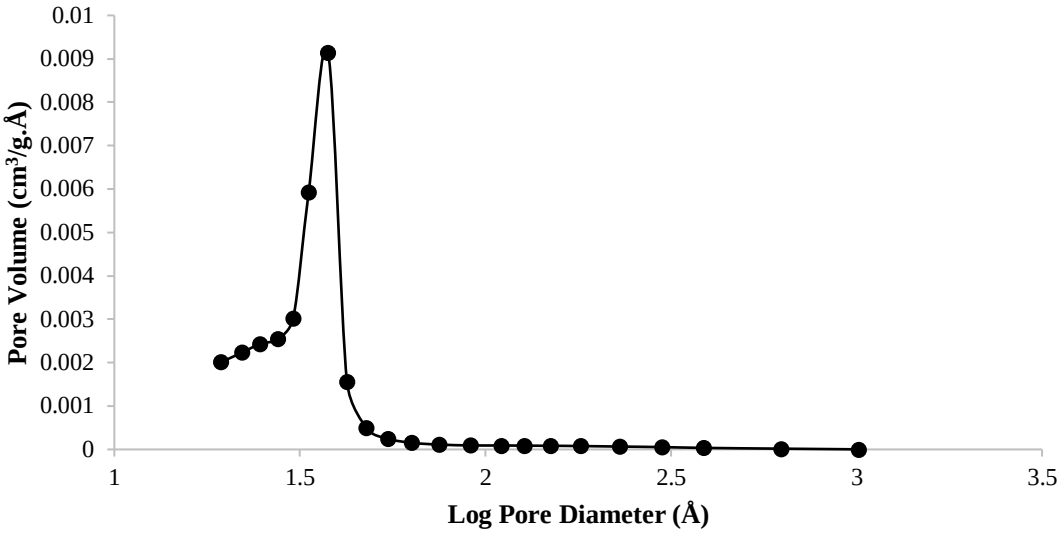

Figure 3.8. Pore size distribution for ZrO_2.

3.1.3 Surface area and porosity analysis of mixed oxide TiO_2-ZrO_2 catalysts

Table 3.2 gives information about the surface area, average pore diameter and average pore volume of the mixed-oxide TiO_2-ZrO_2, TiO_2 and ZrO_2 catalysts prepared by the sol-gel method (Chapter 2).

Table 3.2. Surface area and porosity of catalysts.

Catalyst	Surface area m^2g^{-1}	Pore volume cm^3g^{-1}	Pore diameter Å
TiO_2	83	0.106	49
5:1 TiO_2-ZrO_2	234	0.128	21
2:1 TiO_2-ZrO_2	277	0.169	23
1:1 TiO_2-ZrO_2	301	0.169	21
1:2 TiO_2-ZrO_2	217	0.138	25
1:5 TiO_2-ZrO_2	28	0.048	66
ZrO_2	16	0.035	85

The BET surface area was significantly higher for the mixed oxide catalysts when compared to the pure titanium oxide and pure zirconium oxide (all these catalysts prepared by the sol-gel method). This increase in surface area is also observed when decreasing the Ti/Zr ratio in the catalyst from 5:1 to 1:1 by 67 m^2/g from 234 m^2/g up to 301 m^2/g. Values for the surface area of the 1:1 mixed oxide have been widely reported in literature, but have had lower values. One such example includes research on the oxidation of H_2S to elemental sulfur. The Ti-Zr catalyst in that study was synthesised using a different method, producing a surface area of 169 m^2/g [5]. Hence, our 'sol-gel' method provided a 1:1 TiO_2-ZrO_2 catalyst with a surface area almost twice as high, which also led to a relatively high catalytic performance.

However, when the ratio of Ti/Zr was further decreased, the surface area began to decrease, to a value of 28 m^2/g for the 1:5 Ti/Zr, which was even lower than the pure TiO_2. The surface area then reached a minimum for pure ZrO_2, at just 16 m^2/g.

This trend in the surface area of the solids is also reflected in their performance (see Chapter 4), with the 1:1 TiO_2-ZrO_2 catalyst showing a higher conversion and selectivity compared to catalysts of significantly lower surface area.

The average pore diameter analysis also revealed that all catalysts were mesoporous [6], with pore sizes ranging from 21 Å to a maximum of 49 Å in pure TiO_2. For the mixed oxides, there is a clear trend in pore size and increasing the Zr/Ti molar ratio in the solid. Increasing the Zr/Ti molar ratio leads to a significant increase in the average pore size observed; with the 1:5 Ti-Zr mixed oxide showing the highest of its type with 66 Å. This upward trend is further displayed with the pure ZrO_2, showing the highest pore size of all catalysts with an average of 85 Å. This classification of pore size is further backed by the isotherm plots, with all solids displayed type IV adsorption-desorption plots [6] with hysteresis loops, typical of mesoporous solids (see Figures 3.9 and 3.10).

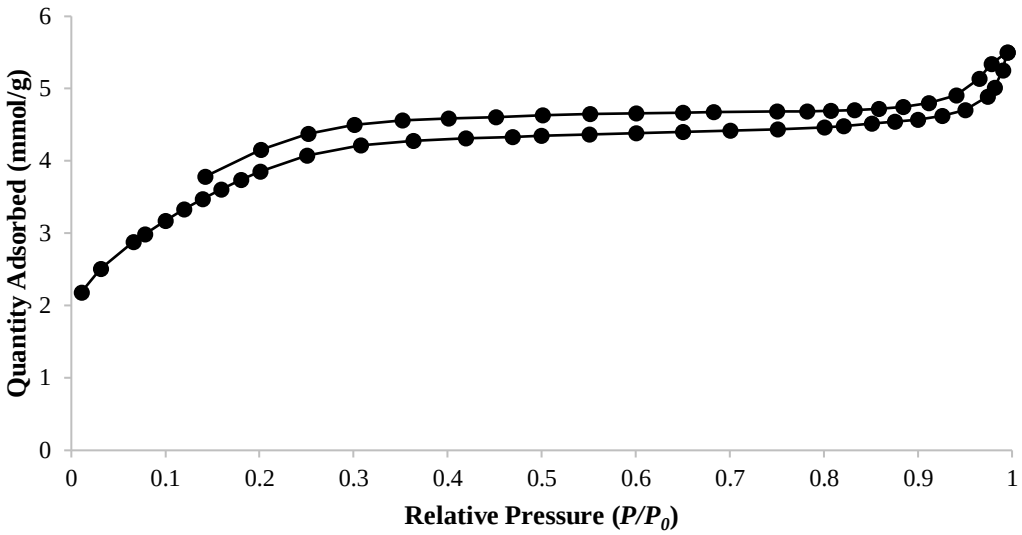

Figure 3.9. N_2 adsorption isotherm for 1:1 TiO_2-ZrO_2 catalyst.

The hysteresis loop displayed by the adsorption isotherm here most closely resembles that of a H4 hysteresis loop, which is indicative of narrow, slit like pores. The pore size distribution for this catalyst is shown in Figure 3.10.

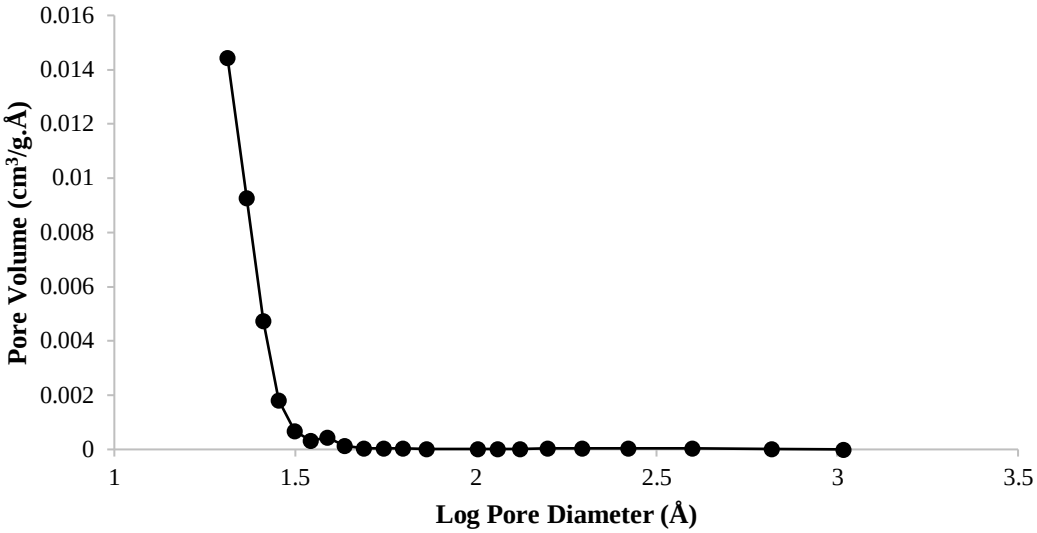

Figure 3.10. Pore size distribution for the 1:1 TiO_2-ZrO_2 catalyst.

The pore size distribution has a topmost point at log D = 1.38, which corresponds to a pore diameter D = 20.5 Å. This plot therefore provides further evidence that the average pore diameter for this catalyst is 21 Å.

The 1:2 TiO_2-ZrO_2 had one of the lowest surface areas (217 m^2/g) and a lower pore volume than both the 1:1 and 2:1 TiO_2-ZrO_2 catalysts. Like all others, the 1:2 TiO_2-ZrO_2 showed a type IV isotherm, and a pore size distribution with a topmost point at log D = 1.31 (D = 20.4 Å) (Figure 3.11 and 3.12).

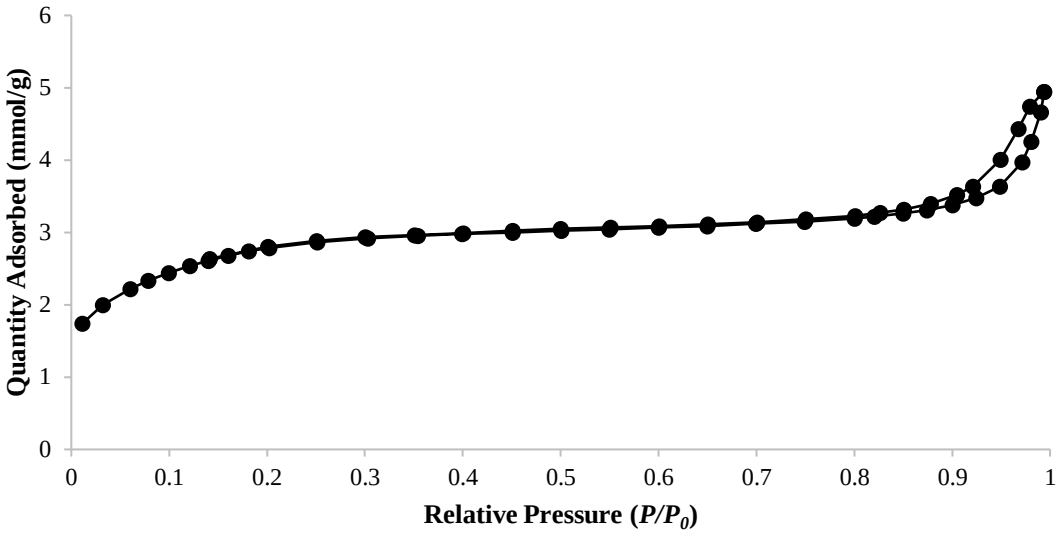

Figure 3.11. N_2 adsorption isotherm for 1:2 TiO_2-ZrO_2 catalyst.

The hysteresis loop displayed by this adsorption most resembles that of a H4 type hysteresis loop, therefore showing similar pore structures to the 1:1 mixed oxide.

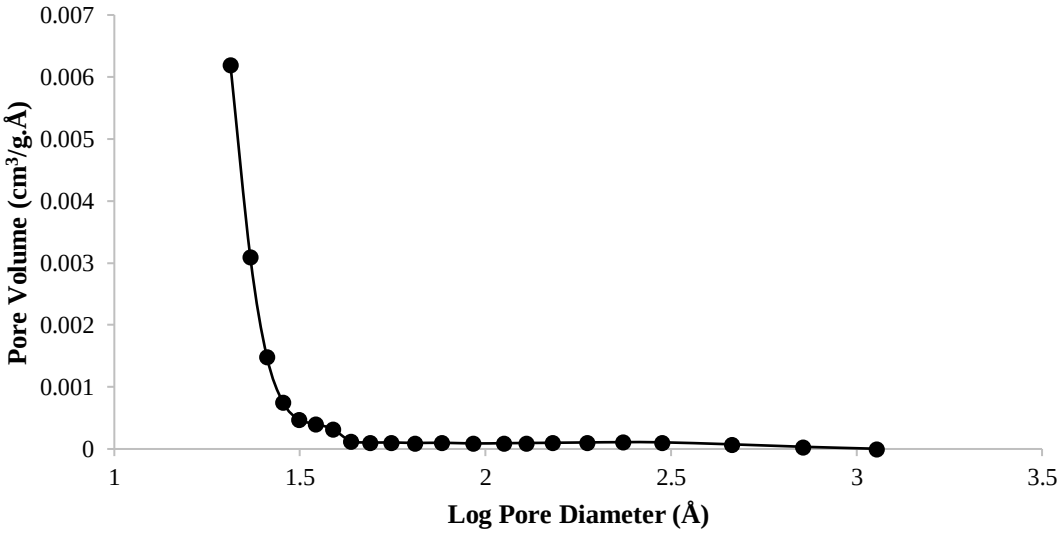

Figure 3.12. Pore size distribution for 1:2 TiO_2-ZrO_2 catalyst.

The pore size distribution for 1:2 TiO_2-ZrO_2 catalyst is similar to the 1:1 plot. The most common pore size seams to correspond to a log *D* value of around 1.4. This value leads to an

average pore diameter of 26 Å. However, the plot demonstrates that the distribution of pores covered a wider range than that of the 1:1 mixed oxide.

The only catalyst that did not show a type IV isotherm and a relatively narrow pore size distribution was the pure ZrO_2; its isotherm and pore size distribution are shown below in Figures 3.13 and 3.14.

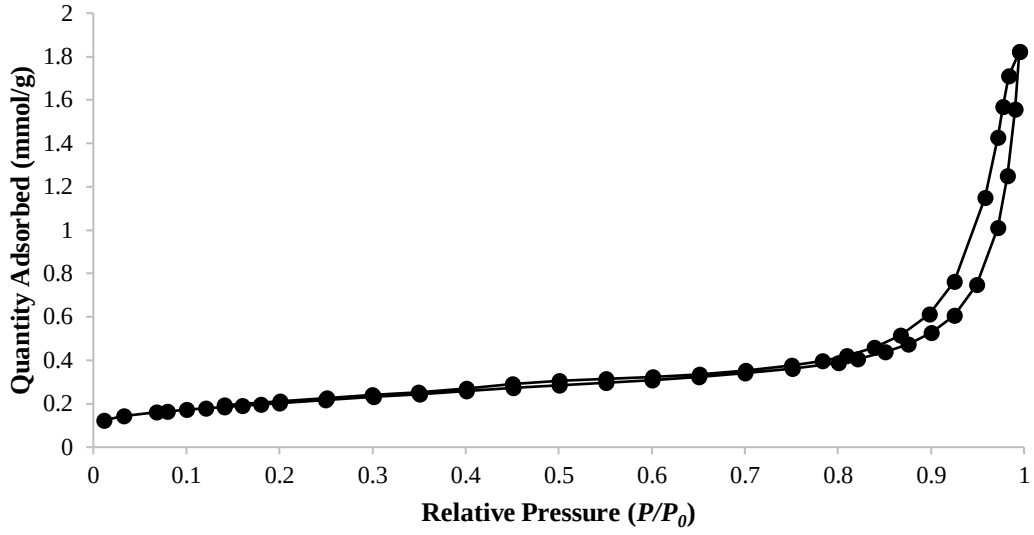

Figure 3.13. N_2 adsorption isotherm for the pure ZrO_2 catalyst.

Unlike all of the other catalysts, which display a type IV isotherm, this one shows a type V adsorption-desorption isotherm, with a H3 type hysteresis loop. This solid therefore shows slit-like pores, wider than those in all other samples.

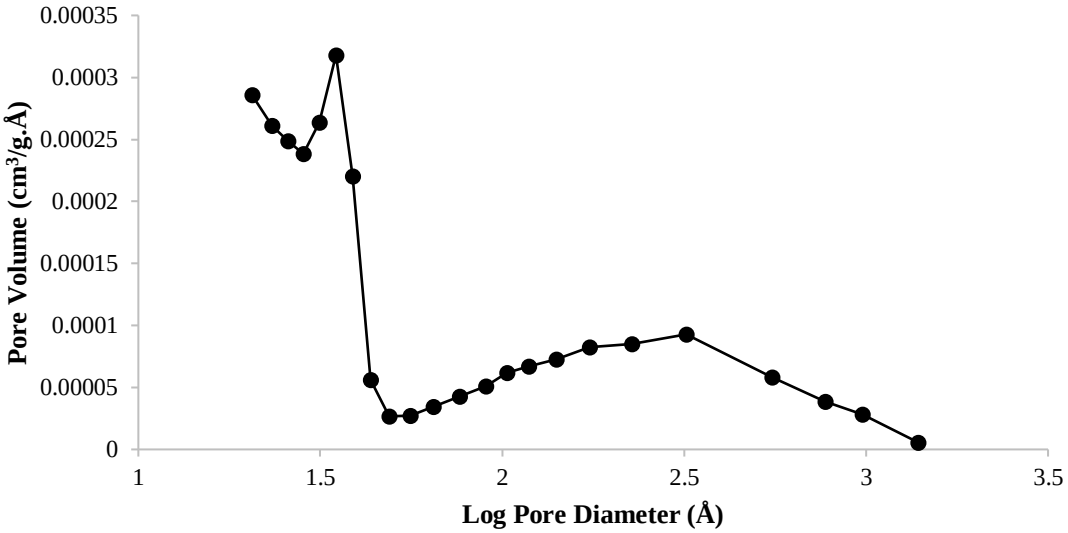

Figure 3.14. Pore size distribution of ZrO_2.

As depicted by the distribution curve above, this catalyst showed the greatest pore size diversity out of all the TiO_2-ZrO_2 samples. The sharpest peak is shown at a log *D* value of 1.54, corresponding to a pore diameter of 34 Å. However, this curve does not subsequently approach d*V*/d*D* = 0 unlike all other solids. Instead, the area under the curve remains significant, suggesting there is a large number of pore sizes present, particularly between log *D* of 1.9 and 2.8. Within this region, there is a range of approximately 900 Å; representing a vast variety of pore diameters.

It should be noted that the sol-gel TiO_2 and ZrO_2 samples (Table 3.2) had different texture in comparison to those in Table 3.1, i.e. commercial P25 Degussa TiO_2 and ZrO_2 prepared by precipitation.

3.2. Powder X-ray diffraction

Powder XRD was recorded for γ-Al_2O_3 Degussa catalyst, TiO_2 Degussa P25 catalyst, as well as for ZrO_2 and CeO_2 samples prepared in-house (Figure 3.15). The XRD patterns obtained are in agreement with the literature [7,8,9]. From these data, ZrO_2 contained tetragonal

and monoclinic zirconia in a weight ratio of 1.9:1. The TiO_2 catalyst contained anatase and rutile in a 2.4:1 weight ratio. These weight ratios were calculated as described elsewhere [8,9].

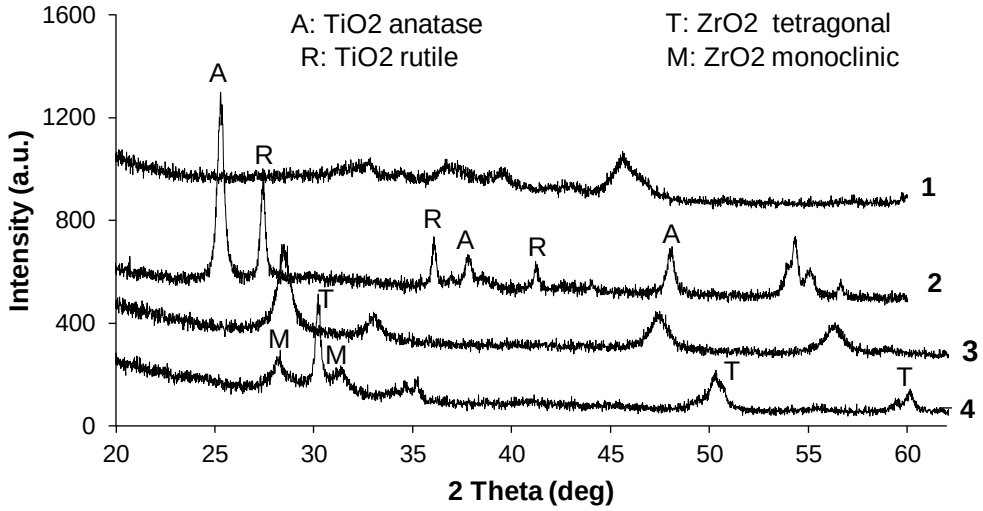

Figure 3.15. XRD patterns (CuKα radiation) for: (1) γ-Al_2O_3 Degussa catalyst air calcined at 400 ^oC for 2 h; (2) TiO_2 P25 Degussa catalyst, 2.4:1 w/w anatase/rutile ratio; (3) CeO_2 air calcined at 500 ^oC for 3 h, cubic fluorite structure; and (4) ZrO_2 air calcined at 400 ^oC for 5 h, 1.9:1 w/w tetragonal/monoclinic zirconia ratio.

All of the Ti-Zr mixed oxides showed amorphous-like structures when analysed by XRD, showing no clear, sharp peaks for specific structure types. Instead, broad peaks were observed, like for 1:1 Ti-Zr, which is shown in Figure 3.16.

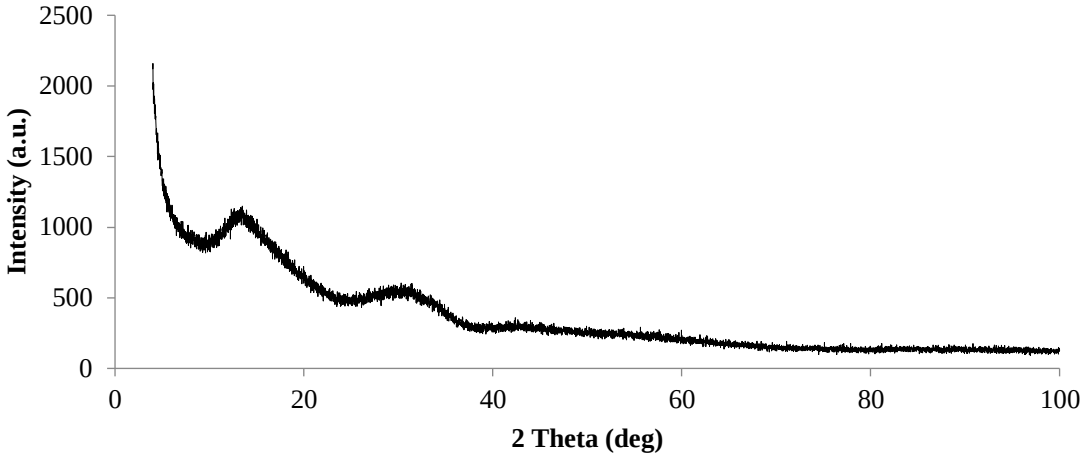

Figure 3.16. XRD plot for 1:1 TiO_2-ZrO_2 catalyst.

This amorphous XRD pattern of the mixed oxide may indicate much smaller particle size of the mixed oxide compared to that of pure TiO_2 and ZrO_2. It is also possible that the structure of mixed oxide was neither of those normally exhibited by pure TiO_2 or pure ZrO_2, but more of a mixture of all possible structures.

The pure TiO_2 catalyst exhibited almost exclusively anatase structure, with a sharp peak at a 2θ value of 25^o [10]. Using the Scherrer equation, $D_p = 0.9\lambda/\beta Cos\theta$ (where λ=1.54 Å, β is the line width at half height and θ is the Bragg angle) the average particle size D_p can be calculated. In this particular case, $\beta = 1.2^o$ and $\theta = 25.3^o$. This leads to a particle size of 7.1 nm.

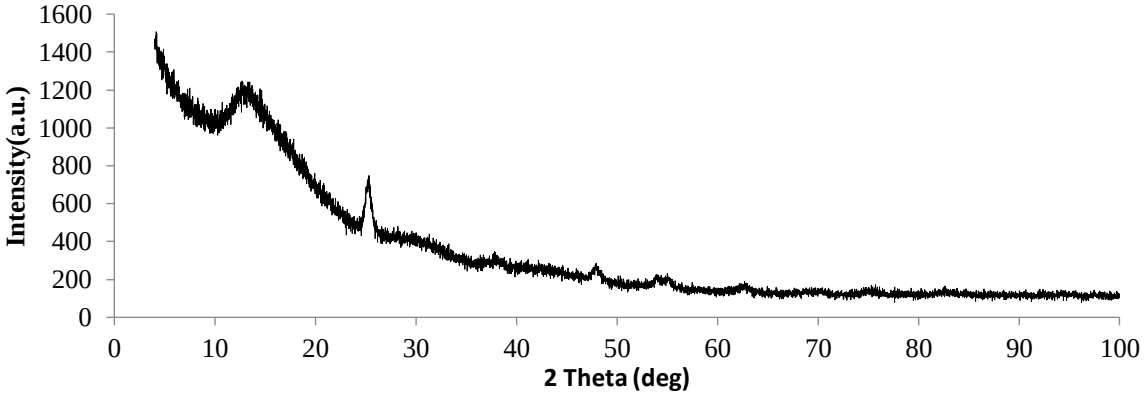

Figure 3.17. XRD plot for pure TiO_2 catalyst.

Figure 3.18 and 3.19 show 1:1 TiO_2-ZrO_2 catalyst (precipitation method) and pure TiO_2 catalyst (precipitation method), respectively.

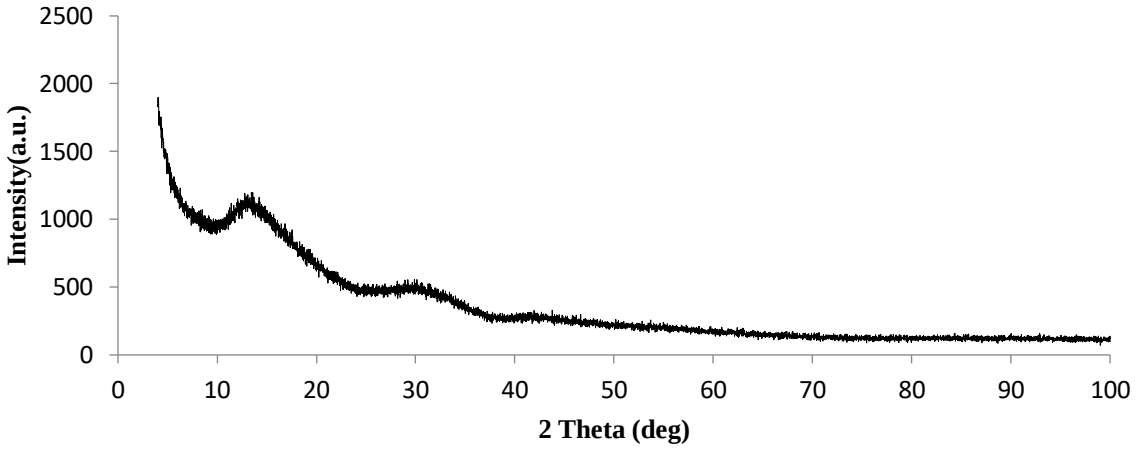

Figure 3.18. XRD plot for 1:1 TiO_2-ZrO_2 catalyst (precipitation method).

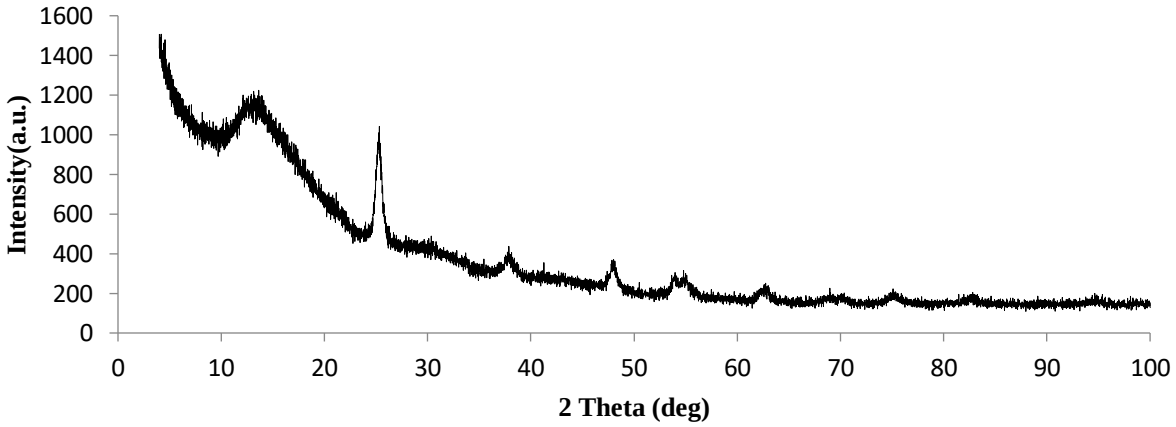

Figure 3.19. XRD plot for pure TiO_2 catalyst (precipitation method).

ZrO_2, on the other hand, displayed 2 structure types, tetragonal and monoclinic. Its XRD pattern is displayed in Figure 3.20.

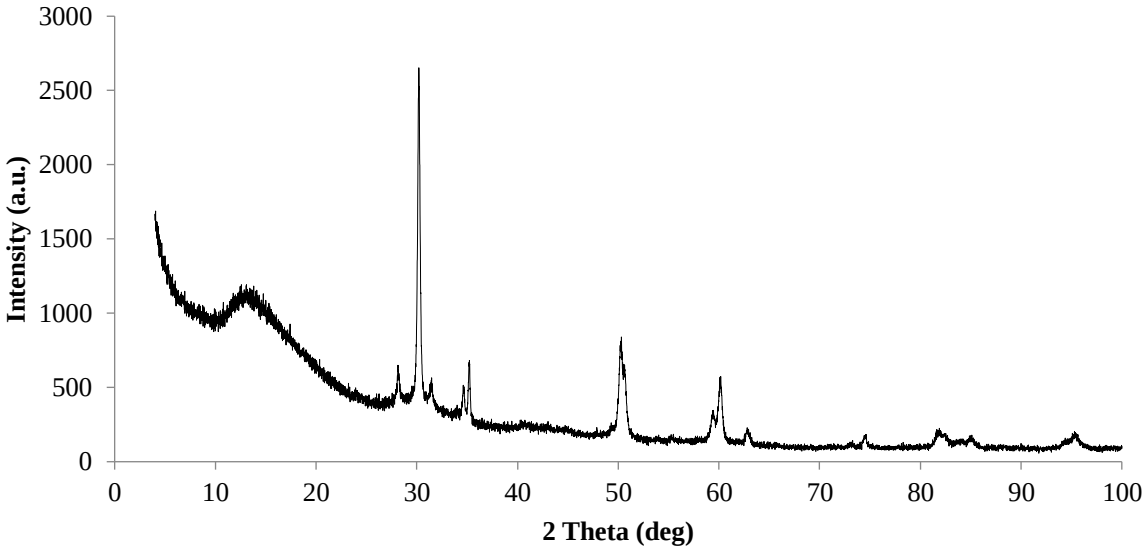

Figure 3.20. XRD plot for pure ZrO_2 catalyst.

The two relevant peaks appear at 2θ values of 30^0 and 31^0 for tetragonal and monoclinic zirconia, respectively. The ratio of the two phases can be calculated from the relative intensity ratio of the 111 plane diffractions, which are shown Figure 3.21.

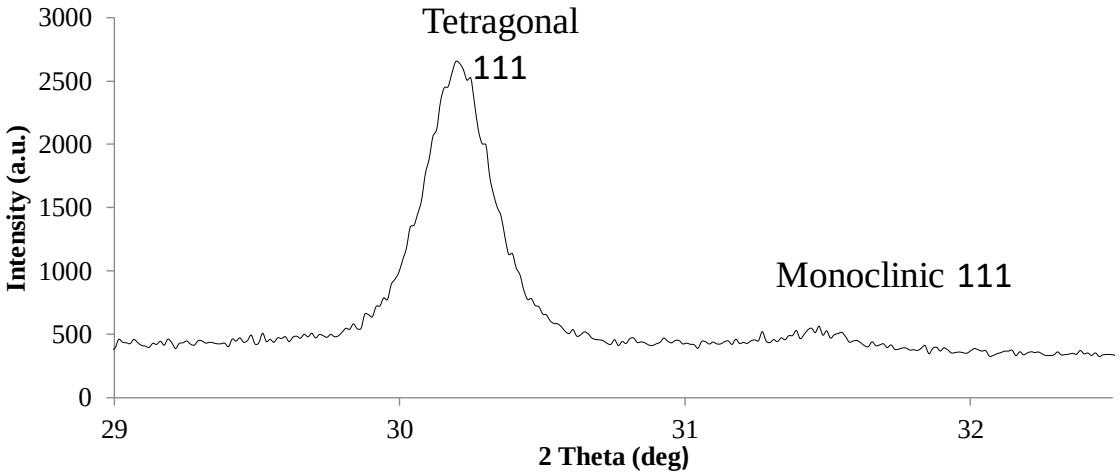

Figure 3.21. (111) tetragonal and monoclinic peaks for ZrO_2.

The content of monoclinic phase within the sample was found to be 5.1%, with tetragonal therefore representing 94.9%.

3.3. Fourier transform infrared (FTIR) spectroscopy

The relative number of Brønsted and Lewis acid sites (B/L) was determined by infrared spectroscopy of adsorbed pyridine (Figure. 3.22, Figure. 3.23) assuming equal integral extinction coefficients for infrared bands of Brønsted (1540-1550 cm^{-1}) and Lewis (1450-1460 cm^{-1}) acid sites [11-13].

All oxides possess predominantly Lewis acidity, in agreement with the literature [11–14]. The number of Brønsted acid sites is negligible (B/L ≈ 0), except for ZrO_2 having a B/L value of 0.1, in agreement with a previous IR study [14].

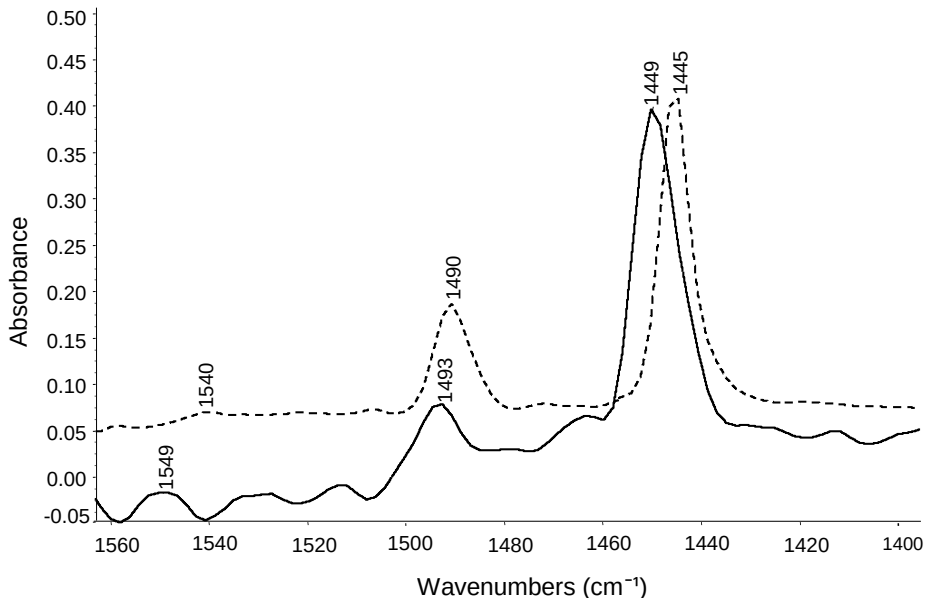

Figure 3.22. DRIFT spectra of pyridine adsorbed on γ-Al_2O_3 (solid line) and TiO_2 (broken line).

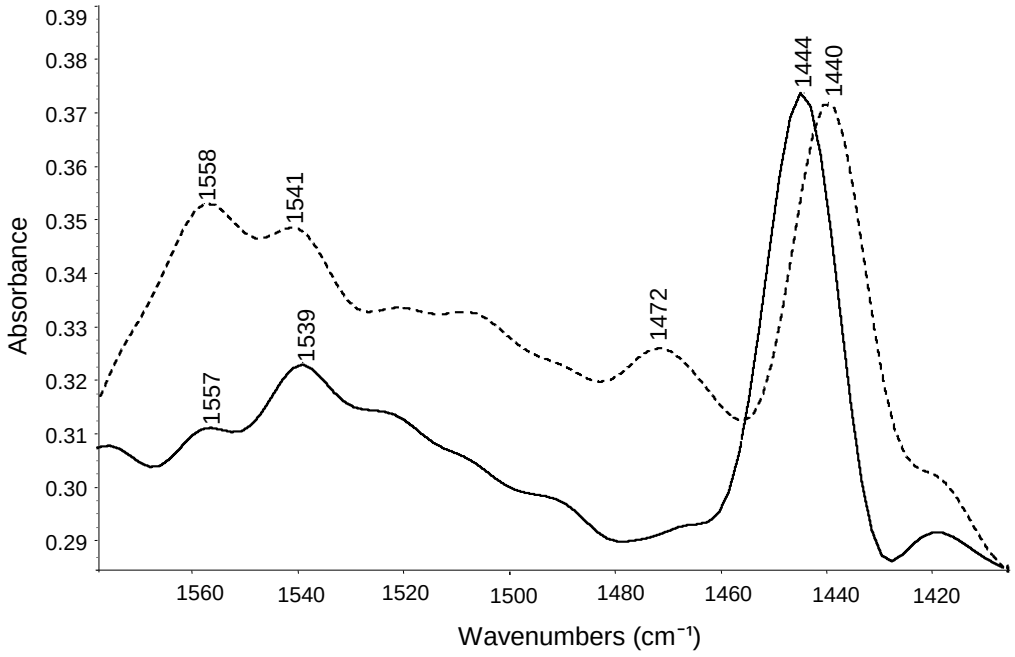

Figure 3.23. DRIFT spectra of pyridine adsorbed on ZrO_2 (solid line) and CeO_2 (broken line).

References

1. S. J. Gregg and K.S.W. Sing, *Adsorption, Surface Area and Porosity,* Academic Press, London, 1982.
2. K. K. Unger, J. Roquerol, K. S. W. Sing and H. Kral (Eds.), *Characterisation of Porous Solids I,* Elsevier, Amsterdam, 1988.
3. J. Roquerol, F. Rodriguez-Reinoso, K.S.W. Sing and K. K. Unger, *Characterisation of Porous Solids III,* Elsevier, Amsterdam, 1994.
4. G. Leofanti, M. Padovan, G. Tozzola and B. Venturelli, *Catalysis Today,* 1998, **41**, 207.
5. H. M. Tasdemir, S. Yasyerli and N. Yasyerli, *International Journal of Hydrogen Energy*, 2015, **40**, 9989-10001.
6. K. S. W. Sing, D. H. Everett, R. A. W. Haul, L. Moscou, R. A. Pierotti, J. Rouquerol and T. Siemieniewska, *Pure and Applied Chemistry*, 1985, **57**, 603-619.
7. M.L. Dos Santos, R.C. Lima, C.S. Riccardi, R.L. Tranquilin, P.R. Bueno, J.A. Varela and E. Longo, *Materials Letters*, 2008, **62**, 4509–4511.
8. K. Sakurai and M. Mizusawa, *Analytical Chemistry*, 2010, **82**, 3519–3522.
9. E. Djurado, P. Bouvier and G. Lucazeau, *Journal of Solid State Chemistry*, 2000, **149**, 399–407.
10. K. Sakurai and M. Mizusawa, *Analytical Chemistry,* 2010, **82**, 3519-3522.
11. E. A. Paukshtis, *Infrared Spectroscopy in Heterogeneous Acid-Basic Catalysis*, Nauka, Novosivbirsk, 1992 (in Russian).
12. H. Knözinger, G. Ertl, H. Knözinger, F. Schüth and J. Weitkamp (Eds.), Handbook of Heterogeneous Catalysis, 2008, **2**, Wiley-VCH, 1154.
13. E. A. Paukshtis and E. N. Yurchenko, *Russian Chemical Reviews (English Translation),* 1983, **52**, 242-258.
14. M. I. Zaki, M. A. Hasan and L. Pasupulety, *Langmuir*, 2001, **17**, 768-774.

Chapter 4: Ketonisation of acetic acid on metal oxides: catalyst activity and stability

4.1. Introduction

Carboxylic acids are readily available from renewable natural resources and can be used for the production of value-added chemicals and carbon-neutral bio-fuels [1,2]. For fuel applications, carboxylic acids require an increase in their caloric value which can be achieved by reduction in their oxygen content. Much current research is focussed on the deoxygenation of carboxylic acids, primarily using heterogeneous catalysis [3–7].

Ketonisation (Equation (1)) is a chemical reaction which converts two molecules of a carboxylic acid into a ketone, carbon dioxide and water [8,9], thus making a new C-C bond and removing three oxygen atoms. The ketonisation reaction occurs with carboxylic acids possessing α-hydrogen atoms at least in one of the reacting acid molecules. In contrast to catalytic hydrodeoxygenation, no hydrogen is required for the ketonisation of carboxylic acids.

$$CH_3COOH \rightarrow (CH_3)_2CO + CO_2 + H_2O \qquad (1)$$

Ketonisation has long been employed as a clean method for the synthesis of ketones ([8,9] and references therein). Currently, this reaction attracts significant interest for the upgrading of biomass-derived oxygenates, for example, bio-oil produced by fast pyrolysis of biomass.

Bio-oil, among other oxygenated compounds, contains lower C1–C4 carboxylic acids, which make the oil unstable and corrosive. Ketonisation can eliminate the adverse effects of carboxylic acids by converting them to non-corrosive ketone products with higher caloric value. The ketones thus produced can be further subjected to aldol condensation to increase the carbon chain length to the gasoline/diesel range [1,2,9].

Ketonisation of carboxylic acids has been extensively studied both in gas phase and liquid phase ([8,9] and references therein). In the gas phase, the reaction is catalysed by many

metal oxides in the temperature range of 200–500 °C [8–19]. The best catalytic activity have amphoteric oxides such as CeO_2, MnO_2, ZrO_2, TiO_2, etc., with CeO_2 showing particularly high activity [8,9,17]. It is suggested that the high activity of the amphoteric metal oxides results from bifunctional catalysis by surface acid-base pairs M-O involving a Lewis acid site (low-coordinate metal cation) and the neighbouring oxygen ion as the base side [16, 17]. However, despite numerous research efforts, the reaction mechanism and the nature of catalytically active sites and intermediates is not yet clear [8,9,16,17]. Besides, catalyst deactivation remains a serious problem in the commercialisation of catalytic ketonisation of carboxylic acids. Therefore, the understanding of causes of catalyst deactivation and improvement of catalyst stability is a challenge [9].

In this chapter, we investigate the ketonisation of acetic acid to acetone (Equation (1)) using a series of metal oxide catalysts including γ-Al_2O_3, TiO_2, ZrO_2 and CeO_2, primarily focussing on their relative activity, selectivity and stability to deactivation.

4.2. Ketonisation of acetic acid over Al_2O_3, TiO_2, ZrO_2 and CeO_2

4.2.1. Catalyst characterisation

Information about the catalysts studied is given in Table 4.1. This includes catalyst surface area and porosity as well as acid properties. The latter include the total density of acid sites (Brønsted and Lewis), the ratio of numbers of Brønsted and Lewis acid sites (B/L) and the enthalpy of ammonia adsorption as a measure of acid site strength. As can be seen, all oxides possess predominantly Lewis acidity, in agreement with the literature [20-23]. The number of Brønsted acid sites is negligible (B/L ≈ 0), except for ZrO_2 having a B/L value of 0.1, in agreement with a previous IR study [23]. This was determined by infrared spectroscopy of adsorbed pyridine (Chapter 3) assuming equal integral extinction coefficients for infrared bands of Brønsted (1540-1550 cm^{-1}) and Lewis (1450-1460 cm^{-1}) acid sites [20-22]. From the

enthalpies of ammonia adsorption, the acid strength of oxides decreases in the order: ZrO_2 > Al_2O_3 > $TiO_2 \geq CeO_2$. The total acid site density of ZrO_2 (0.23 mmol g^{-1}) measured at 150 ^oC is in agreement with the literature value of 0.27 mmol g^{-1} obtained from microcalorimetry of NH_3 adsorption at 80 ^oC [24]. In contrast, CeO_2 had the lowest acid site density and the weakest acid strength among these oxides (Table 4.1). This is also in agreement with data [24], which shows a much weaker acidity of CeO_2 compared to ZrO_2 [24].

Table 4.1. Information about catalysts.[a]

Catalyst	Surface area[b] m^2g^{-1}	Pore volume[c] cm^3g^{-1}	Pore diameter[d] Å	Acid site density[e] mmol g^{-1}	B/L[f]	ΔH[g] kJ mol^{-1}
Al_2O_3	98	0.56	227	0.24±0.01	~0	73
TiO_2	44	0.10	90	0.26±0.01	~0	68
ZrO_2	117	0.13	43	0.23±0.01	0.1	94
CeO_2	85	0.22	104	0.18±0.02	~0	66

[a] For BET analysis, the catalysts were pre-treated for 2 h at 240 ^oC in vacuum before measuring N_2 adsorption. [b] BET surface area. [c] Single point total pore volume. [d] Average BET pore diameter. [e] Total amount of NH_3 adsorbed on Brønsted and Lewis acid sites at 150 ^oC (from TG-DSC). [f] The ratio of numbers of Brønsted (B) and Lewis (L) acid sites from DRIFTS of adsorbed pyridine. [g] Enthalpy of NH_3 adsorption (±4 kJ mol^{-1}) at 150 ^oC and a fractional NH_3 surface coverage of 0.30 (from TG-DSC).

Comparing these results with the literature, it should be taken into account that the acid strength of oxides depends on their preparation and pre-treatment [21,22]. The heat of ammonia adsorption on solid acid catalysts depends on ammonia surface coverage, decreasing with increasing the NH_3 coverage [25]. Therefore, our ΔH values obtained at an NH_3 coverage of

30% will differ from those extrapolated to zero NH_3 coverage. An IR study of pyridine adsorption [23] has reported TiO_2 having the strongest Lewis acidity in the same series of oxides based on the shift of $\nu_{CC(N)}$ vibration band for H-bonded pyridine observed at 1600-1633 cm^{-1}. However, it has been demonstrated that this band is sensitive to the nature and coordination number of the metal centre and cannot be used for comparison of acid strength of different metal centres [20-22].

4.2.2. Comparison of catalyst activity and stability to deactivation

Table 4.2 compares the catalytic activity of Al_2O_3, TiO_2, ZrO_2 and CeO_2 in the ketonisation of acetic acid to acetone measured in the fixed-bed reactor (Chapter 2) at 300 ^oC, a contact time W/F = 120 g h mol^{-1} and 4 h time on stream (TOS). As seen, the activity increases in the order $Al_2O_3 << TiO_2 < ZrO_2 < CeO_2$. In all cases, the selectivity to acetone based on the converted acetic acid was ≥ 99 mol%, with traces of isobutene also found. Acetone condensation to form isobutene on metal oxides has been reported previously [26].

Table 4.2. Comparison of activity of Al_2O_3, TiO_2, ZrO_2 and CeO_2 oxides in ketonisation of acetic acid.[a]

Catalyst	Al_2O_3	TiO_2	ZrO_2	CeO_2
Conversion[b] (%)	3	48	73	100

[a] Reaction conditions: 0.20 g of catalyst, 300 ^oC, 3.35 kPa HOAc partial pressure, 20 mL min^{-1} N_2 flow rate, 4 h time on stream, contact time W/F = 120 g h mol^{-1}. [b] Average HOAc conversion between 1.5-4 h time on stream; acetone selectivity ≥ 99 mol% based on acetic acid converted.

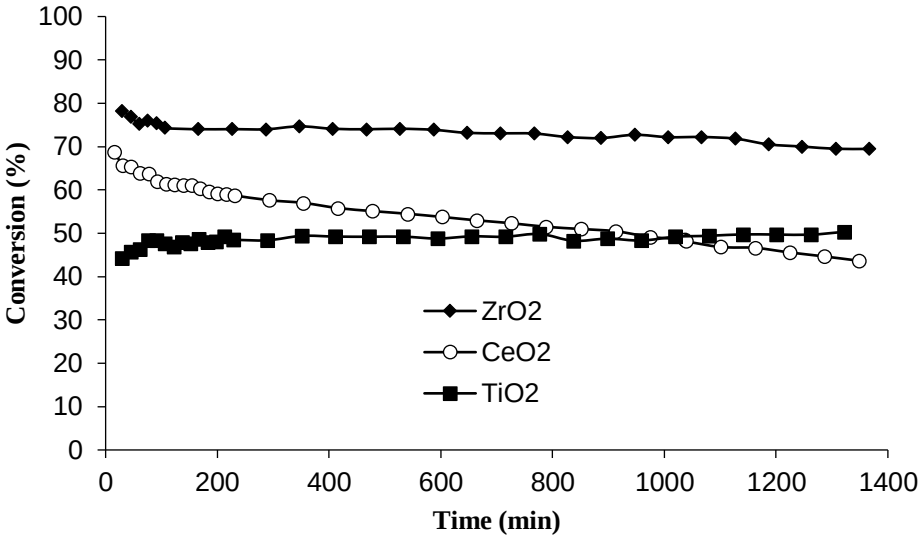

Figure 4.1. Comparison of catalyst activity and stability in acetic acid ketonisation over ZrO_2 (300 ^oC), TiO_2 (300 ^oC) and CeO_2 (250 ^oC) at *W/F* = 120 g h mol^{-1}, 3.35 kPa HOAc partial pressure; acetone selectivity in all cases ≥ 99 mol%.

Figure 4.1 compares a longer-term performance of the more active TiO_2, ZrO_2 and CeO_2 catalysts (24 h TOS) at a comparable conversion of 50-70%, revealing a different stability of these oxides to deactivation. It can be seen that the resistance to deactivation increases in the order CeO_2 << ZrO_2 < TiO_2, with TiO_2 exhibiting practically no deactivation and ZrO_2 only a small deactivation after reaching steady state. Based on their high activity and strong resistance to deactivation, TiO_2 (Degussa P25) and ZrO_2 exhibited the best catalytic performance in acid ketonisation among the oxides studied, in agreement with the literature [9].

The spent CeO_2 catalyst was notably darker than TiO_2 and ZrO_2, which indicates catalyst coking. Table 4.3 gives the carbon content in spent catalysts after the reactions shown in Figure 4.1. Regarding the amount of coke formed, CeO_2 clearly stands out with its 5.6% carbon content. Usually, coking of solid acid catalysts is the result of acid catalysed oligomerisation of organic molecules present in the reaction system [27]. This appears to be

unlikely for CeO_2 because its acidity is weaker than that of the other oxides (Table 4.1). An IR study [23] of acetone condensation on the same oxide series suggests that strong Lewis base sites found on the CeO_2 surface have a great capacity toward adsorption of condensation products and thus can be responsible for the profound deactivation of CeO_2 in acetone condensation. However, in the acid ketonisation reaction, strong base sites could be poisoned by CO_2 formed as the reaction by-product. As CeO_2 is a relatively strong one-electron oxidant, its intense coking might also result from a radical polymerisation initiated by the Ce(IV)/Ce(III) redox couple, however there is no proof of this as yet. The observed deactivation of oxide catalysts could therefore be primarily attributed to the catalyst coking, i.e., the most coked CeO_2 was the fastest to deactivate, whereas the least coked TiO_2 and ZrO_2 were more resistant to deactivation. Degussa P25 TiO_2, produced by flame hydrolysis of $TiCl_4$ with a moderate surface area of 44 $m^2\ g^{-1}$, was the most stable toward deactivation.

Table 4.3. Carbon content in spent catalysts.[a]

Catalyst	TiO_2	ZrO_2	CeO_2
Carbon content (%)	1.2	1.2	5.6

[a] From combustion chemical analysis of spent catalysts after reactions shown in Figure 4.1.

Ketonisation of acetic acid occurred with >99% selectivity to acetone with all oxide catalysts studied in the temperature range of 180-350 ^oC. At higher temperatures (380-400 ^oC), the selectivity was found to decrease due to acetone condensation to form isobutene as the main by-product (identified by GC-MS). The high-temperature condensation of acetone to isobutene in the gas phase on SiO_2-Al_2O_3 has been reported previously [26].

Figure 4.2 shows the effect of contact time on acetic acid conversion and product selectivity for the ketonisation over Al_2O_3 at 380 ^oC. The contact time was changed by varying

the catalyst weight (*W*) and the molar flow rate of acetic acid (*F*). This graph clearly demonstrates that acetone is the primary reaction product, which is further converted to isobutene in a consecutive reaction. This can occur through acetone condensation to mesityl oxide followed by mesityl oxide hydrolytic cleavage to produce isobutene and acetic acid [26], as shown in Equation (3).

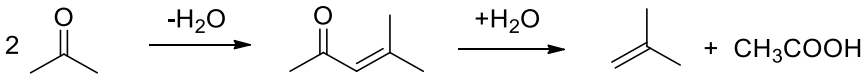

(3)

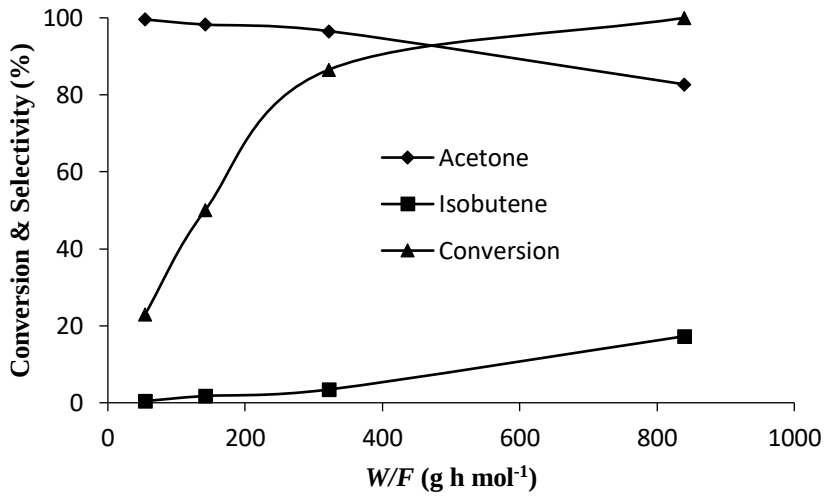

Figure 4.2. Effect of contact time (*W/F*) on acetic acid conversion and product selectivity over γ-Al_2O_3 Degussa catalyst (380 °C, 1.93 kPa HOAc partial pressure).

4.3. Catalyst regeneration

4.3.1. Effect of Cu and H_2 on catalyst deactivation

Previously, phase-pure anatase and rutile TiO_2 possessing larger surface areas (240 and 160 $m^2\ g^{-1}$, respectively) have been found to suffer from deactivation [16]. Addition of Cu/SiO_2 to the phase-pure TiO_2 and ZrO_2 by physical mixing and co-feeding H_2 have been reported to

reduce catalyst deactivation [16]. However, our attempt to decrease the deactivation of ZrO_2 by adding Cu/SiO_2 and H_2 had no effect; in the case of CeO_2, this even exacerbated the deactivation, which may be due to reduction of CeO_2 [28,29].

In our case, no deactivation of the mixed-phase P25 titania was observed (Figure 4.1). Our attempt to reduce the deactivation of ZrO_2 and CeO_2 catalysts by adding Cu and H_2 was unsuccessful. This had no effect on the performance of ZrO_2 (Figure 4.3). In the case of CeO_2, the addition of Cu and H_2 aggravated the deactivation (Figure 4.4), which may be due to reduction of CeO_2. The addition of H_2 without Cu did not increase the rate of CeO_2 deactivation at 180 ^oC (Figure 4.4). This is in agreement with the H_2-TPR data, which shows that CeO_2 surface is reduced with H_2 only above 350 ^oC [28,29]. However, in the presence of Cu the reduction could occur at lower temperature, taking into account that the contact time for ketonisation in a fixed-bed reactor is much longer than that in the H_2-TPR. Moreover, doping ceria with metals such as Rh and Pd is known to decrease the reduction temperature, which has been explained by hydrogen spillover from the metal to the ceria surface [29].

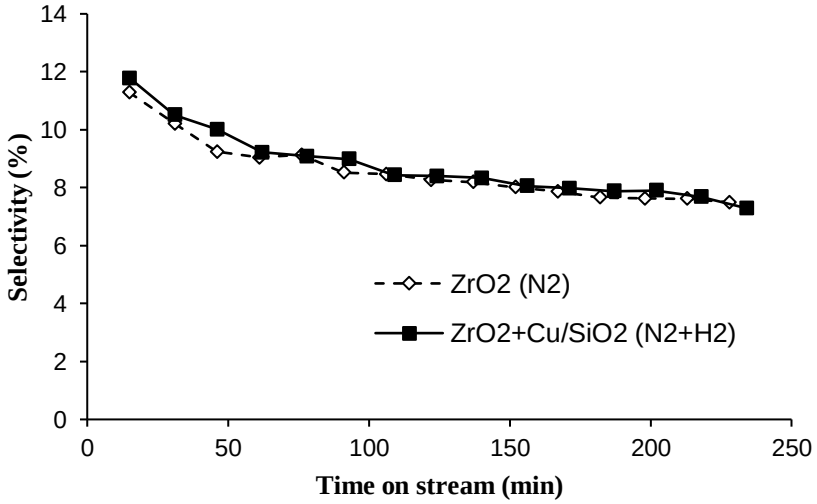

Figure 4.3. Time course for acetic acid ketonisation over ZrO_2 (0.10 g) in N_2 flow and over ZrO_2 + 5%Cu/SiO_2 (1:1 w/w) mixed catalyst (0.20 g) in N_2 + H_2 (1:1) flow (240 ^oC, 3.35 kPa HOAc partial pressure, 20 mL min^{-1} flow rate).

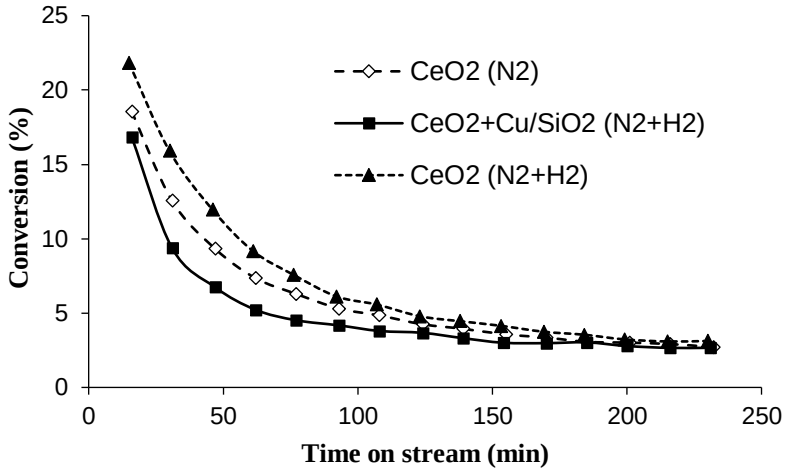

Figure 4.4. Time course for acetic acid ketonisation over CeO_2 (0.20 g) in N_2 and $N_2 + H_2$ flow and over CeO_2 + 5%Cu/SiO_2 (1:1 w/w) mixed catalyst (0.40 g) in $N_2 + H_2$ (1:1) flow (180 ^oC, 3.35 kPa HOAc partial pressure, 20 mL min^{-1} flow rate).

Figure 4.5 shows our H_2-TPR results for pure CeO_2 and 1:1 w/w physical mixture CeO_2 + 5%Cu/SiO_2. The H_2-TPR of pure CeO_2 occurs in two steps involving the reduction of surface CeO_2 between 360-600 ^oC followed by the reduction of bulk CeO_2 at 820 ^oC, in agreement with data [29]. It can be seen that the reduction of surface CeO_2 in the CeO_2 + Cu/SiO_2 mixture started at a significantly lower temperature (210 ^oC) than in the case of pure CeO_2, whereas the reduction of bulk CeO_2 was not affected by the presence of Cu/SiO_2. As expected, Cu/SiO_2 itself did not exhibit any H_2-TPR as Cu had already been reduced in this catalyst. Therefore these results confirm the possibility of reduction of CeO_2 surface in the reaction system, which could cause catalyst deactivation.

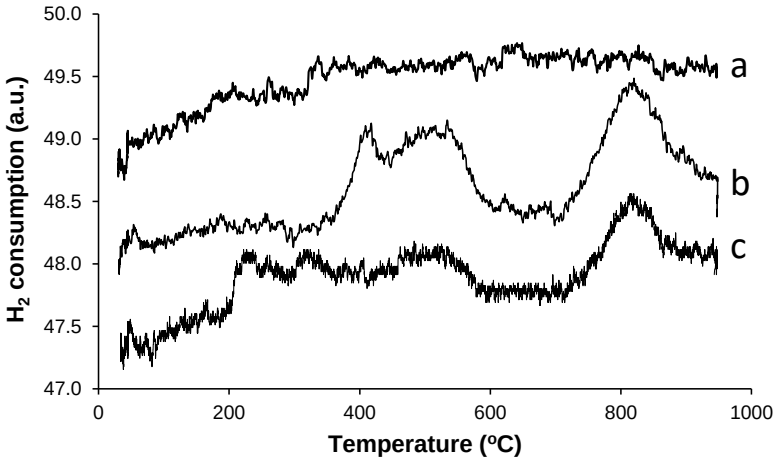

Figure 4.5. H_2-TPR in H_2-N_2 (5:95) gas flow: (a) 5%Cu/SiO_2 (20 mg), (b) CeO_2 (20 mg) and (c) CeO_2 + 5%Cu/SiO_2 (20 + 20 mg).

4.3.2. Effect of oxygen on CeO_2 deactivation

When the ketonisation reaction over CeO_2 was carried out using air instead of N_2 as the carrier gas, the catalyst had significantly better stability to deactivation. This is demonstrated in Figure 4.6, which shows two parallel runs in air in comparison with the reaction over CeO_2 in N_2 and CeO_2 + 5%Cu/SiO_2 in N_2 + H_2 (1:1) gas mixture at 180 °C. As can be seen, CeO_2 shows a better performance in air. The same was observed in longer term reactions with CeO_2 in N_2 and air for 24 h on stream at 200 °C (Figure 4.7). It is noteworthy that the air did not affect reaction selectivity below 200 °C; all these reactions had >99% selectivity to acetone. However, the selectivity to acetone sharply decreased when the reaction was carried out in air at 250 °C, which can be explained by acetone oxidation. These results support the view that CeO_2 deactivation, at least in part (in addition to catalyst coking), is caused by reduction of CeO_2 to Ce_2O_3. The latter is well known to re-oxidise to CeO_2 by O_2. Therefore, co-feeding oxygen can improve CeO_2 stability to deactivation without impairing acetone selectivity at the reaction temperature below 200 °C.

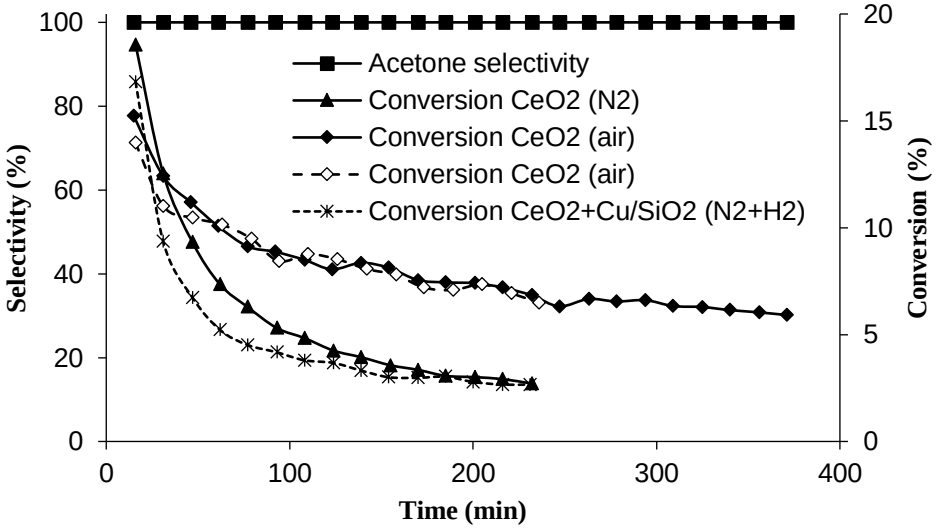

Figure 4.6. Time course for acetic acid ketonisation over CeO_2 (0.20 g) in air flow (two parallel runs) and N_2 flow and over CeO_2 + 5%Cu/SiO_2 (1:1 w/w) mixed catalyst (0.40 g) in N_2 + H_2 (1:1) flow (180 ^oC, 3.35 kPa HOAc partial pressure, 20 mL min^{-1} flow rate).

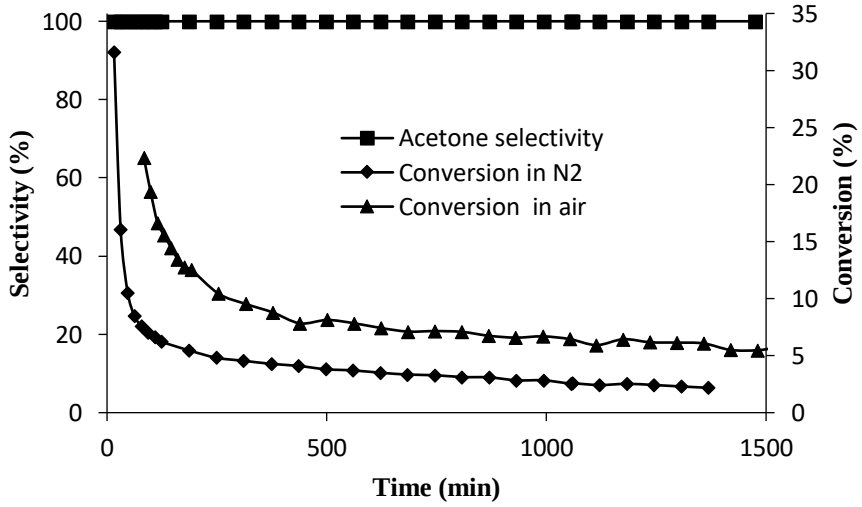

Figure. 4.7. Time course for acetic acid ketonisation over CeO_2 (0.20 g) in N_2 and air flow (200 ^oC, 3.35 kPa HOAc partial pressure, 20 mL min^{-1} flow rate).

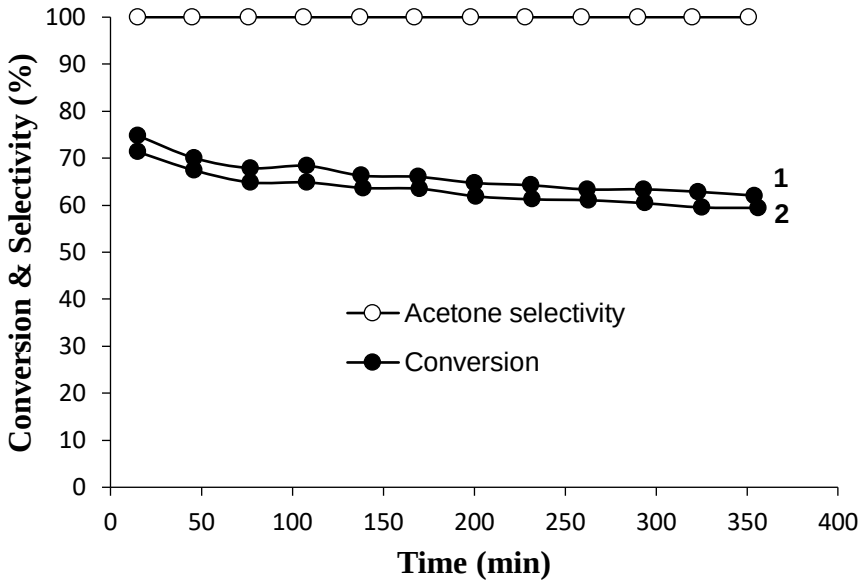

Figure 4.8. Effect of regeneration of CeO_2 catalyst by air calcination at 500 °C for 3 h: (1) first and (2) second run (250 °C, *W/F* = 120 g h mol^{-1}, 3.35 kPa HOAc partial pressure; acetone selectivity in all cases ≥ 99%).

We found that CeO_2 could be successfully regenerated by calcination of spent catalyst in air at 500 °C for 3 h (5 °C min^{-1} temperature ramp rate). Figure 4.8 shows two successive ketonisation runs on CeO_2 with catalyst regeneration after each run. As seen, almost full recovery of catalyst activity and selectivity was achieved. The catalyst, black after reaction, regained its initial light yellow colour after regeneration. Some reduction in the catalyst surface area was observed, though, from 85 m^2g^{-1} for fresh CeO_2 catalyst to 73 m^2g^{-1} after regeneration. Similar air calcination procedure (400 °C/5 h) was also successful for regeneration of ZrO_2.

4.4. Kinetic results

Our kinetic studies included the measurement of apparent activation energies, specific reaction rates and CH_3COOH/CH_3COOD kinetic isotope effects. We also looked at the effect of acetic acid pressure on the reaction rate. Recently, a thorough kinetic investigation of the ketonisation of C_2–C_4 carboxylic acids over phase-pure TiO_2 and ZrO_2 oxides complemented by DFT calculations has been published [16]. Kinetics of C_2–C_4 acid ketonisation over Ru/TiO_2 catalyst has also been reported [30].

Table 4.4. Apparent activation energies (E_a) and reaction rates for acetic acid ketonisation over oxide catalysts.

Catalyst	Temperature range ^oC	E_a kJ mol^{-1}	10^5 Rate[a] mol $g^{-1}h^{-1}$	10^5 Rate[a] mol $m^{-2}h^{-1}$
CeO_2	180-220	58±10	290	3.4
ZrO_2	230-260	106±3	200	1.7
TiO_2	270-300	115±5	47	1.1
Al_2O_3	300-350	110±3	4.6	0.047

[a] At 260 ^{o}C, extrapolated using the Arrhenius equation.

Table 4.4 summarises the apparent activation energies (E_a) obtained for acetic acid ketonisation over Al_2O_3, TiO_2, ZrO_2 and CeO_2 oxides. The corresponding Arrhenius plots are shown in Figure 4.9. Due to the large difference in activity of oxides (Table 4.2), these measurements had to be carried out in different temperature ranges in order to stay within the differential conditions (fractional conversion $X < 0.1$). The E_a values thus obtained can be used for extrapolation of reaction rates, but may not be quite comparable across the oxide series studied. As seen, the E_a values vary from 106 to 115 kJ mol^{-1} for Al_2O_3, TiO_2, ZrO_2; these high E_a values indicate no diffusion limitations in the reaction with these oxides [31]. For the most active catalyst CeO_2, a lower activation energy was obtained, E_a = 58 kJ/mol. This might be

thought to point to internal diffusion limitations [31] for the reaction with CeO_2. However, the Weisz-Prater criterion [32] calculated for CeO_2, $C_{WP} = 2 \cdot 10^{-3} << 1$, indicates no internal diffusion limitations for this catalyst either. The low E_a value for CeO_2 may be explained by the high reactivity of base sites on CeO_2 surface compared to the Al, Ti and Zr oxides, as suggested by the IR study of acetone condensation on these oxides [23]. It should be noted that the apparent activation energies E_a include enthalpy contributions from all reaction steps preceding the rate-limiting step. These steps include formation of surface acetate and enolate species, which involves interaction with the surface base sites (Chapter 6, Scheme 6.3), hence the importance of oxide base sites for acid ketonisation (see below).

Table 4.4 also shows the reaction rates extrapolated to 260 °C using the Arrhenius equation, which allow to compare the catalytic activity of different oxides based on unit catalyst weight and surface area. This shows that the specific catalyst activity (10^5 mol m^{-2} h^{-1}) decreases in the order: CeO_2 (3.4) > ZrO_2 (1.7) > TiO_2 (1.1) >> Al_2O_3 (0.047).

The reaction rate (R) was found to increase with increasing the partial pressure of acetic acid (P_{HOAc}), tending to level off at high partial pressures, as shown in Figure 4.10 for the reaction with Al_2O_3, TiO_2 and ZrO_2. The reaction with CeO_2 also had a close trend (not shown), although the kinetic data was less accurate due to strong catalyst deactivation. Similar kinetics have been reported for C_2–C_4 acid ketonisation over phase-pure TiO_2 and ZrO_2 catalysts [16]. These kinetics indicate saturation of catalyst surface with adsorbed acetic acid molecules as P_{HOAc} increases [16,30]. Rate equations assuming a mechanism involving fast adsorption of two molecules of acetic acid followed by a rate-limiting step leading to the formation of acetone have been derived elsewhere [16,30].

Kinetic isotope effect (KIE) was measured for the ketonisation of CH_3COOH and CH_3COOD catalysed by Al_2O_3, TiO_2, ZrO_2 and CeO_2. The reactions were carried out under differential conditions (fractional conversion $X < 0.1$); the details are shown in Table 4.5. Both acids CH_3COOH and CH_3COOD were found to react with the same rate, i.e., no H/D KIE was observed for all oxide catalysts studied: 0.98 ± 0.02 (Al_2O_3), 1.03 ± 0.02 (TiO_2), 1.03 ± 0.02 (ZrO_2) and 1.0 ± 0.2 (CeO_2). These results are in agreement with the previous report [16], which has found no KIE (acetic acid d_0/d_4) for the phase-pure TiO_2 and ZrO_2. The lack of acetic acid d_0/d_1 and d_0/d_4 KIE shows that dissociation of the O-H and C-H bonds of acetic acid is not the rate limiting step of ketonisation reaction [16].

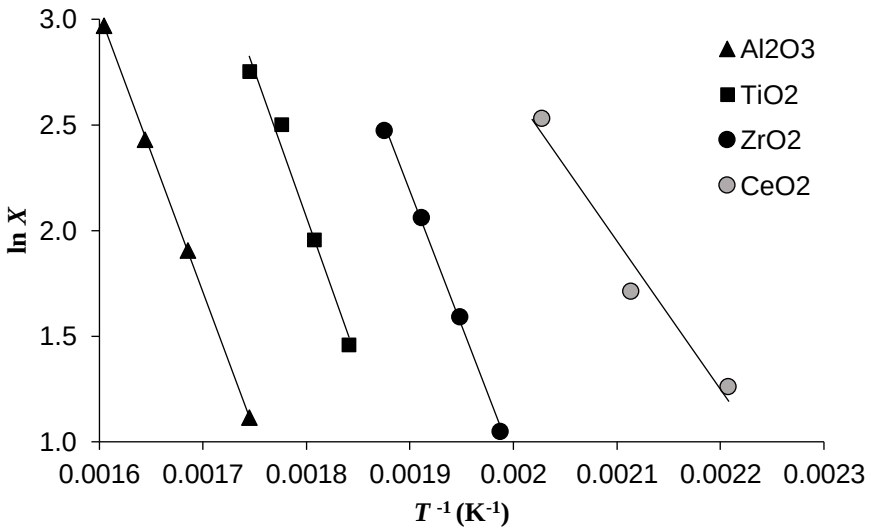

Figure 4.9. Arrhenius plots for acetic acid ketonisation over Degussa γ-Al_2O_3 (0.20 g), P25 TiO_2 (0.10 g), ZrO_2 (0.10 g) and CeO_2 (0.20 g) (3.35 kPa HOAc partial pressure, 20 mL min^{-1} flow rate; X is the conversion of HOAc) (E_a = 110, 115, 106 and 58 kJ mol^{-1}, respectively).

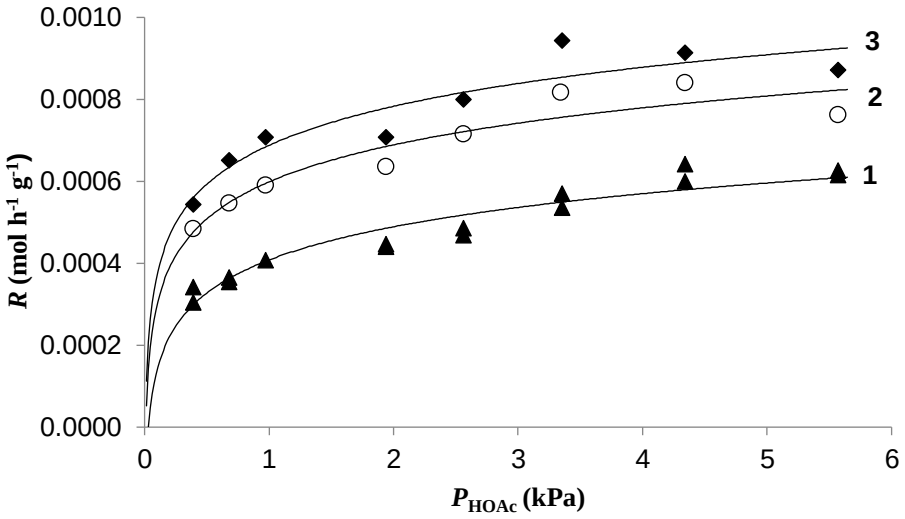

Figure 4.10. Effect of partial pressure of acetic acid on reaction rate over (1) Al_2O_3 (0.20 g), 320 °C, 20 mL min^{-1} flow rate), (2) ZrO_2 (0.10 g, 240°C, 20 mL min^{-1} flow rate) and (3) TiO_2 (0.10 g, 270°C, 20 mL min^{-1} flow rate).

Table 4.5. Kinetic isotope effect (KIE).[a]

Catalyst	Temperature (°C)	Conversion[b] (%)		H/D KIE
		CH_3COOH	CH_3COOD	
γ-Al_2O_3	320	6.64±0.10	6.75±0.08	0.98±0.02
TiO_2	270	6.21±0.05	6.05±0.11	1.03±0.02
ZrO_2	240	5.15±0.07	5.02±0.02	1.03±0.02
CeO_2	200	5.5±0.5	5.7±0.6	1.0±0.2

[a] Reaction conditions: 3.35 kPa partial pressure of acetic acid (d_o and d_1), catalyst weight 0.20 g (Al_2O_3 and CeO_2) or 0.10 g (TiO_2 and ZrO_2), 20 mL min^{-1} flow rate of N_2 carrier gas, 4 h time on stream; catalysts pre-treated in situ at reaction temperature for 1 h. [b] Mean value of two parallel measurements; the conversion value determined in each measurement as an average conversion after 100 min time on stream.

4.5. Effect of catalyst acidity and basicity

Comparison of reaction rates (see above) with acid strengths and densities of Brønsted and Lewis acid sites of the oxide catalysts (Table 4.1) shows that there is no direct relation between the ketonisation activity and the acid properties of oxide catalysts studied.

In acetic acid ketonisation over γ-alumina, the conversion of acetic acid was found to increase with increasing catalyst basicity (Figure 4.11). The basicity was characterised as the pH of 10% oxide suspension in water and varied in the pH range of 4.8 – 10.2 (Chapter 3, Table 3.1). It should be noted, however, that the γ-alumina samples had different surface areas varying from 56 to 185 m^2g^{-1} (Table 3.1). Although there is no direct correlation between acetic acid conversion and the catalyst surface area, the Sigma-Aldrich basic alumina (pH 10.2) having the largest surface area (185 m^2g^{-1}) showed the highest activity per catalyst weight among the γ-alumina samples studied. These results indicate the importance of catalyst basic sites in acid ketonisation over oxide catalysts (see below).

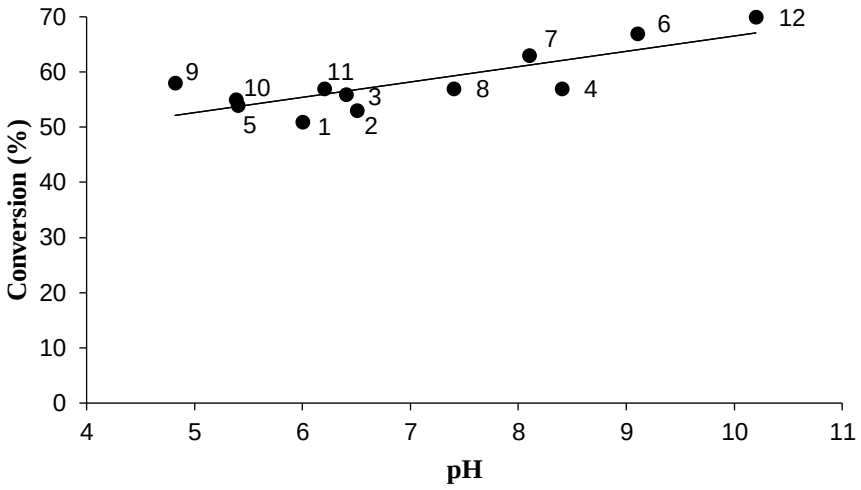

Figure 4.11. Plot of acetic acid conversion versus basicity of γ-alumina (0.20 g catalyst, 380°C, 3.35 kPa HOAc partial pressure, 20 mL min^{-1} flow rate; catalyst pre-treatment at 380°C/1h/N_2, 20 mL min^{-1} flow rate). For data labelling, see Table 3.1 in Chapter 3.

In order to gain an insight into the effect of catalyst basicity on ketonisation reaction, we examined base sites in the metal oxides using CO_2-TPD. As CO_2 is one of the reaction products (Equation (1)), it will poison strong base sites in oxide catalysts to make them unavailable for ketonisation reaction. Therefore, it was interesting to find out if there were relatively mild base sites in the oxide catalysts that would desorb CO_2 within the reaction temperature range to become available for the reaction. On the other hand, stronger base sites that desorb CO_2 at higher temperatures could hardly participate in the ketonisation. CO_2-TPD has been reported for these oxides [33–35], however, to our knowledge, it has not been used for correlation with ketonisation activity in this series of oxide catalysts.

Figure 4.12 shows CO_2 desorption from CeO_2, ZrO_2, TiO_2 and Al_2O_3 within the temperature range of 100–450 °C, which covers the temperature range of ketonisation reaction on these oxides. The oxides were pre-treated at 450 °C then saturated with pure CO_2 at 100 °C

and after that the CO_2-TPD was measured. It should be noted that such pre-treatment would not release strong base sites with CO_2 desorption temperatures above 450 °C. The CO_2-TPD results obtained are in agreement with the literature data [33–35]. As seen, the most active oxides, CeO_2, ZrO_2 and TiO_2, show a CO_2 desorption peak in the temperature range 160–200 °C (at 168, 176 and 191 °C, respectively), corresponding to relatively weak base sites, with the base strength increasing in that order. In contrast, Al_2O_3 shows a large peak with an onset at 320 °C centred at ca. 420 °C, which corresponds to stronger base sites. There is also a small peak in CO_2-TPD of Al_2O_3 centred at 150 °C corresponding to very weak base sites, which are probably too weak to be active in the ketonisation reaction. It should be noted that an IR study [23] suggests very strong base sites on CeO_2 surface, as compared to ZrO_2, TiO_2 and γ-Al_2O_3. This does not contradict our results as we probed only the mild base sites that were released upon pre-treatment of these oxides at 450 °C. Unfortunately, our CO_2-TPD data are not accurate enough to quantify the number of base sites for these oxides. Nevertheless these results indicate that the relatively weak catalyst basicity is important for the ketonisation reaction over metal oxides. It can be seen that there is an inverse correlation between the ketonisation activity and the strength of base sites of oxide catalysts. In the presence of CO_2 in the reaction system, poisoning catalyst base sites, the stronger the catalyst basicity, the higher the temperature required to release the base sites for the reaction. From the CO_2-TPD (Figure 4.12), the CO_2 desorption temperature increases in the order $CeO_2 < ZrO_2 < TiO_2 << \gamma\text{-}Al_2O_3$. This order is in line with the catalytic activity of these oxides in acetic acid ketonisation. Ce(IV), Zr(IV) and Ti(IV) oxides, due to the presence of relatively weak base sites on their surfaces, are the more active ketonisation catalysts operating at relatively low temperatures above their CO_2 desorption temperatures. In contrast, the more basic γ-Al_2O_3 requires a higher temperature for the reaction to occur due to the stronger CO_2 adsorption.

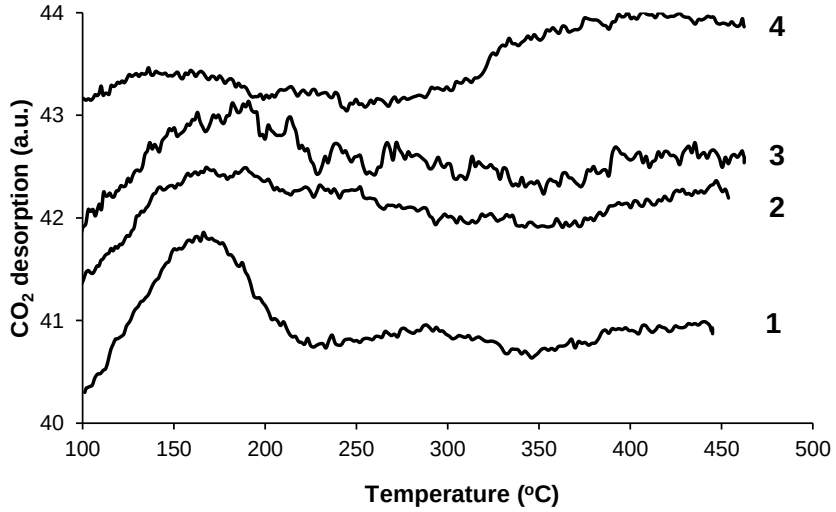

Figure 4.12. CO_2-TPD in He flow: (1) CeO_2 (0.294 g), (2) ZrO_2 (0.432 g), (3) TiO_2 (0.112 g, scaled up 2-fold), (4) γ-Al_2O_3 (0.403 g); pre-treatment at 450 ^oC/1h in He flow, CO_2 adsorbed at 100^oC, 20 ^oC min^{-1} temperature ramp rate.

4.6. Conclusions

Ketonisation of acetic acid to acetone was studied in the gas phase using γ-Al_2O_3, TiO_2, ZrO_2 and CeO_2 as the catalysts in the temperature range of 180-350 ^oC and ambient pressure. Catalyst activity was found to increase in the order Al_2O_3 << TiO_2 < ZrO_2 < CeO_2. CO_2-TPD showed that relatively weak base sites on oxide surfaces are essential for the ketonisation activity, whereas no relation between oxide acidity and catalytic activity was observed. Catalyst resistance to deactivation increased in the order CeO_2 << ZrO_2 < TiO_2 in parallel with the amount of coke formed. TiO_2 (Degussa P25) and ZrO_2 were found to exhibit the best performance as represented by their activity and stability to deactivation. CeO_2 and ZrO_2 could be regenerated by air calcination to regain their activity.

References

1. A. Corma, S. Iborra and A. Velty, *Chemical Reviews*, 2007, **107**, 2411–2502.
2. E. L. Kunkes, D.A. Simonetti, R.M. West, J.C. Serrano-Ruiz, C.A. Gaertner and J.A. Dumesic, *Science*, 2008, **322**, 417–421.
3. M. Snare, I. Kubickova, P. Maki-Arvela, K. Eranen and D.Yu Murzin, *Industrial & Engineering Chemistry Research*, 2006, **45**, 5708–5715.
4. H. Bernas, K. Eranen, I. Simakova, A.-R. Leino, K. Kordas, J. Myllyoja, P. Maki-Arvela, T. Salmi and D.Yu Murzin, *Fuel*, 2010, **89**, 2033–2039.
5. J.G. Immer, M.J. Kelly and H.H. Lamb, *Applied Catalysis A: General*, 2010, **375**, 134–139.
6. P. T. Do, M. Chiappero, L.L. Lobban and D. Resasco, *Catalysis Letters*, 2009, **130**, 9–18.
7. M. Arend, T. Nonnen, W.F. Hoelderich, J. Fischer and J. Groos, *Applied Catalysis A: General*, 2011, **399**, 198–204.
8. M. Renz, *European Journal of Organic Chemistry*, 2005, 979–988.
9. T. N. Pham, T. Sooknoi, S.P. Crossley and D.E. Resasco, *ACS Catalysis*, 2013, **3**, 2456–2673.
10. T. Yokoyama and N. Yamagata, *Applied Catalysis A: General*, 2001, **221**, 227–239.
11. O. Nagashima, S. Sato, R. Takahashi and T. Sodesawa, *Journal of Molecular Catalysis A* 2005, **227**, 231–239.
12. M. Glinski, J. Kijenski and A. Jakubowski, *Applied Catalysis A: General*, 1995, **128**, 209–217.
13. C. A. Gaertner, J.C. Serrano-Ruiz, D.J. Braden and J.A. Dumesic, *Journal of Catalysis*, 2009, **266**, 71–78.

14. H. Bayahia, E. Kozhevnikova and I. Kozhevnikov, *Chemical Communication*, 2013, **49**, 3842–3844.

15. H. Bayahia, E.F. Kozhevnikova and I.V. Kozhevnikov, *Applied Catalysis B: Environmental*, 2015, **165**, 253–259.

16. S. Wang and E. Iglesia, *Journal of Catalysis*, 2017, **345**, 183–206.

17. M. A. Hasan, M.I. Zaki and L. Pasupulety, *Applied Catalysis A: General*, 2003, **243**, 81–92.

18. A. Pulido, B. Oliver-Tomas, M. Renz, M. Boronat and A. Corma, *ChemSusChem*, 2013, **6**, 141–151.

19. S. Tosoni and G. Pacchioni, *Journal of Catalysis*, 2016, **344**, 465–473.

20. E. A. Paukshtis, *Infrared Spectroscopy in Heterogeneous Acid-Basic Catalysis*, Nauka, Novosivbirsk, 1992 (in Russian).

21. H. Knözinger, G. Ertl, H. Knözinger, F. Schüth and J. Weitkamp (Eds.), *Handbook of Heterogeneous Catalysis*, 2008, **2**, Wiley-VCH, 1154.

22. E. A. Paukshtis and E.N. Yurchenko, *Russian Chemical Reviews*, 1983, **52**, 242–258 (English Translation).

23. M. I. Zaki, M.A. Hasan and L. Pasupulety, *Langmuir*, 2001, **17**, 768–774.

24. M. G. Cutrufello, I. Ferino, R. Monaci, E. Rombi, V. Solinas, *Topics in Catalysis*, 2002, **19**, 225–240.

25. N. C. Martinez, J.A. Dumesic, G. Ertl, H. Knözinger, F. Schüth and J. Weitkamp (Eds.), *Handbook of Heterogeneous Catalysis*, 2008, **2**, Wiley-VCH, 1122–1135.

26. M. Demorest, D. Mooberry and J.D. Danforth, *Industrial & Engineering Chemistry*, 1951, **43**, 2569–2572.

27. M. Guisnet and P. Magnoux, *Applied Catalysis*, 1989, **54**, 1–27.

28. Y. Zhang, Y. Zhao, H. Zhang, L. Zhang, H. Ma, P. Dong, D. Li, J. Yu and G. Cao, *RSC Advances*, 2016, **6**, 70653–70659.

29. G. R. Rao and B.G. Mishra, *Bulletin of the Catalysis Society of India*, 2003, **2**, 122–134.

30. T. N. Pham, D. Shi and D.E. Resasco, *Journal of Catalysis*, 2014, **314**, 149–158.

31. R. Dittmeyer, G. Eming, G. Ertl, H. Knözinger, F. Schüth and J. Weitkamp (Eds.), *Handbook of Heterogeneous Catalysis*, 2008, **3**, Wiley-VCH, 1727–1784.

32. P. B. Weisz and C.D. Prater, *Advances in Catalysis*, 1954, **6**, 143–196.

33. S. Hegde, K. Tharpa, S.R. Akuri, K. Rakesh, A. Kumar, R. Deshpande and S.A. Nair, *Physical Chemistry Chemical Physics*, 2017, **19**, 8034–8045.

34. G. Tang, H.-L. Bao, C. Jin, X.-H. Zhong and X.-L. Du, *RSC Advances*, 2015, **5**, 99678–99687.

35. W. Cai, J. Yu, C. Anand, A. Vinu and M. Jaroniec, *Chemistry of Materials*, 2011, **23**, 1147–1157.

Chapter 5: Ketonisation of acetic acid over TiO_2-ZrO_2 mixed oxide catalysts

5.1. Introduction

Titanium dioxide TiO_2 was first employed in large-scale catalytic processes in the 1970s in air pollution control. It was found to be highly selective in the reduction of NO_x compounds contained within flue gas from stationary combustion equipment [1]. Although this application has since been modified using various techniques, TiO_2 still remains a compound of interest when developing novel catalytic processes. One such example uses a mix of titanium oxide and graphene, which is used to remove antibiotics, antibiotic-resistant bacteria, and anti-bacterial genes from urban waste water [2]. This process takes advantage of titania's photocatalytic activity, which reduces energy costs in an environmentally sustainable way [3]. One of the most important pieces of information to come from this study was titanium oxide's effectiveness in removing *E. coli* from the water, showing a 75% decrease in ERY-resistant *E. coli* and a 39% decrease in SMX-resistant *E. coli* [3]. These results show that pure TiO_2 has important contemporary applications, not just in typical chemical reactions but also in advanced medicine and medical research.

Pure zirconium oxide ZrO_2 has been used in heterogeneous catalysis, but more often it has been employed in mixed-metal oxide catalysts. One such example includes the use of a Ni-Zr oxide catalyst for the hydrogenation of bio-derived methyl levulinate to γ-valerolactone in water under low hydrogen pressure [4]. This is important because γ-valerolactone has been identified as a key intermediate for the production of fuels and value-added chemicals [5, 6].

An example of mixed titanium and zirconium oxide in the past was the selective oxidation of H_2S to elemental sulphur [7]. As well as using Ti-Zr oxides, other titanium-based oxides were employed, including Ti-Fe and Ti-Cr. It was found that the Ti-Zr mixed oxides showed the lowest conversion of H_2S than the other mixed oxides but showed the highest selectivity for sulfur.

In Chapter 4, the ketonisation performance of individual TiO_2 and ZrO_2 oxides was investigated together with γ-Al_2O_3 and CeO_2 oxides. In this study, commercial P25 Degussa TiO_2 and in-house prepared ZrO_2 (by precipitation) were used as the catalysts. These TiO_2 and ZrO_2 catalysts were found to exhibit the best performance in the ketonisation of acetic acid to acetone amongst the metal oxides studied, showing high catalytic activities as well as strong resistance to deactivation. It was interesting, therefore, to test the performance of mixed oxides Ti-Zr catalysts in this reaction.

This study will investigate the effectiveness of mixed Ti-Zr oxides in the gas-phase ketonisation of acetic acid to acetone at 300 °C (Scheme 5.1). The mixed oxides will have varying Ti/Zr molar ratios, and pure TiO_2 and ZrO_2 samples of the respective metal oxides will also be investigated for comparison.

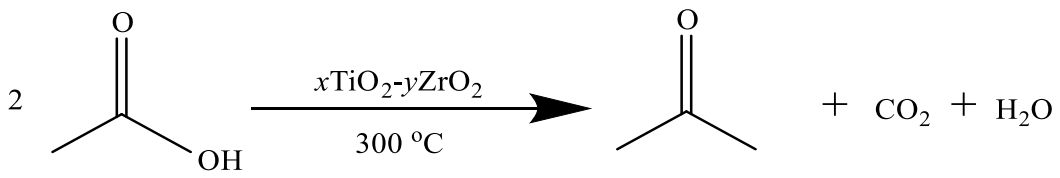

Scheme 5.1. Ketonisation of acetic acid to acetone over Ti-Zr oxides; *x* and *y* are the relative molar stoichiometry in the mixed-oxide catalyst.

5.2 TiO_2-ZrO_2 mixed oxide catalysts

The mixed oxide TiO_2-ZrO_2 catalysts were prepared by two methods (Chapter 2). First, the sol-gel synthesis procedure was used, which is described by Pfleiderer et al. [8]. The mixed-oxide catalysts were prepared via hydrolysis and condensation of a mixture of titanium

propoxide $Ti(OC_3H_7)_4$ and zirconium propoxide $Zr(OC_3H_7)_4$ in propanol, as described in Chapter 2. Second, precipitation methods for pure TiO_2, ZrO_2 and 1:1 TiO_2-ZrO_2 were used, the details of which are also described in Chapter 2.

Table 5.1 gives information about the surface area, average pore diameter and pore volume (single point total pore volume) of the mixed-oxide TiO_2-ZrO_2, TiO_2 and ZrO_2 catalysts prepared by the sol-gel method and precipitation method. These results are discussed in Chapter 2 in detail.

Table 5.1. The surface area and porosity of TiO_2-ZrO_2 catalysts.[a]

Catalyst	BET surface area m^2g^{-1}	Pore volume cm^3g^{-1}	Average pore diameter Å
TiO_2	83	0.106	49
5:1 TiO_2-ZrO_2	234	0.128	21
2:1 TiO_2-ZrO_2	277	0.169	23
1:1 TiO_2-ZrO_2	301	0.169	21
1:2 TiO_2-ZrO_2	217	0.138	25
1:5 TiO_2-ZrO_2	28	0.048	66
ZrO_2	16	0.035	85
ZrO_2[b]	117	0.130	43
TiO_2[b]	106	0.179	68
1:1 TiO_2-ZrO_2[b]	320	0.273	34

[a] The catalysts were prepared by two methods: sol-gel synthesis and precipitation method. The catalysts were pre-treated at 240 ^oC for 2 h before measurement. [b] Catalysts prepared by the precipitation method.

All of the Ti-Zr mixed oxides were amorphous as analysed by powder X-ray diffraction, showing no clear, sharp peaks for specific structure types.

The pure TiO_2 catalysts prepared by sol-gel and precipitation methods exhibited almost exclusively anatase structure with a sharp peak at a 2θ value of 25° (Chapter 3). Both sol-gel and precipitation ZrO_2 were crystalline materials containing tetragonal and monoclinic zirconia (Chapter 3).

5.3. Testing TiO_2-ZrO_2 catalysts for acetic acid ketonisation

Each catalyst was tested using the method described in the experimental section at 300 °C with a run time of 24 h. The performance of each solid was measured using an online gas chromatography analysis to obtain figures for selectivity and conversion. Although all of the catalysts showed varying conversions, all of them, including pure TiO_2 and ZrO_2, showed excellent selectivity for acetone, that is, greater than 98%. This high selectivity for Ti-Zr mixed oxides can be found in the literature, with the study by Tasdemir et al. [7] reporting 100% selectivity for 1:1 Ti-Zr.

Figure 5.1 shows the selectivity and conversion time course for the TiO_2 precipitation catalyst, which gave 49% acetic acid conversion (average over 24 h on stream). The sol-gel TiO_2 was less active giving 40% conversion. Figure 5.2 shows the selectivity and conversion for the 1:1 TiO_2-ZrO_2 precipitation catalyst, which gave a 46% average acetic acid conversion, similar to the sol-gel 1:1 TiO_2-ZrO_2 (see below).

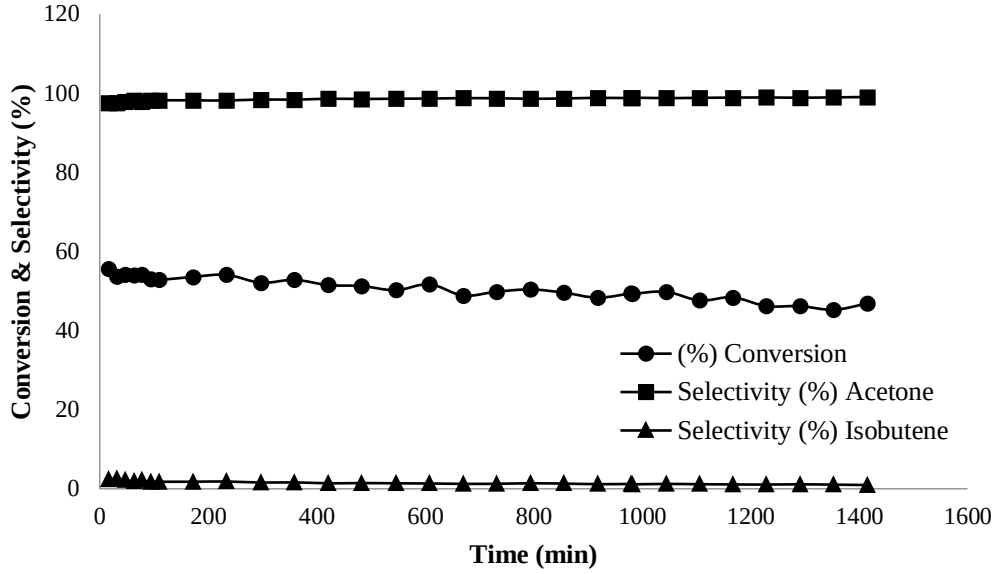

Figure 5.1. The selectivity and conversion for the TiO_2 precipitation catalyst (0.20 g, 300 ^oC, 3.35 kPa HOAc partial pressure, 20 mL min^{-1} flow rate).

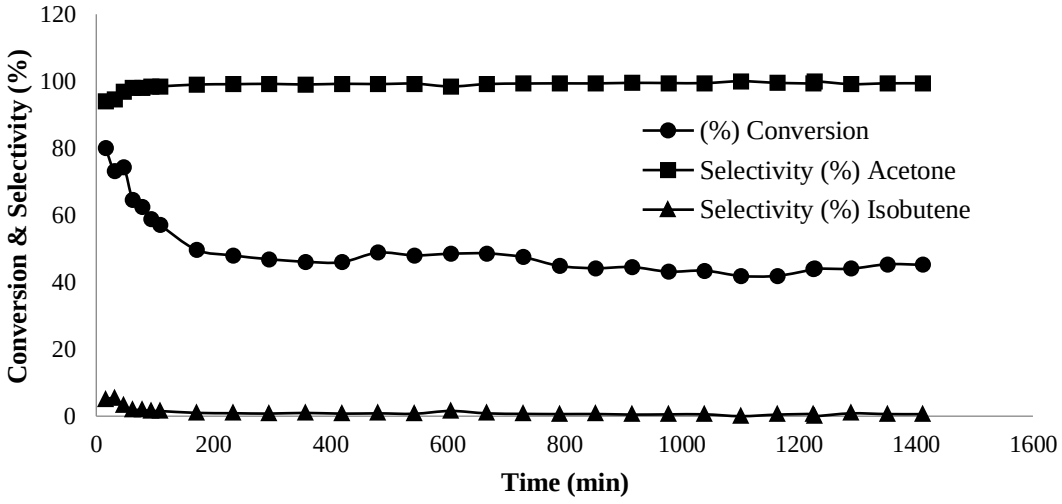

Figure 5.2. The selectivity and conversion for the 1:1 TiO_2-ZrO_2 precipitation catalyst (0.20 g, 300 ^oC, 3.35 kPa HOAc partial pressure, 20 mL min^{-1} flow rate).

The best-performing catalyst in the conversion of acetic acid to acetone was the 1:2 TiO_2-ZrO_2 catalyst with an initial conversion of 76%. The plot of selectivity and conversion for this catalyst is shown in Figure 5.3, with an average acetic acid conversion of 52% over 24 h time on stream.

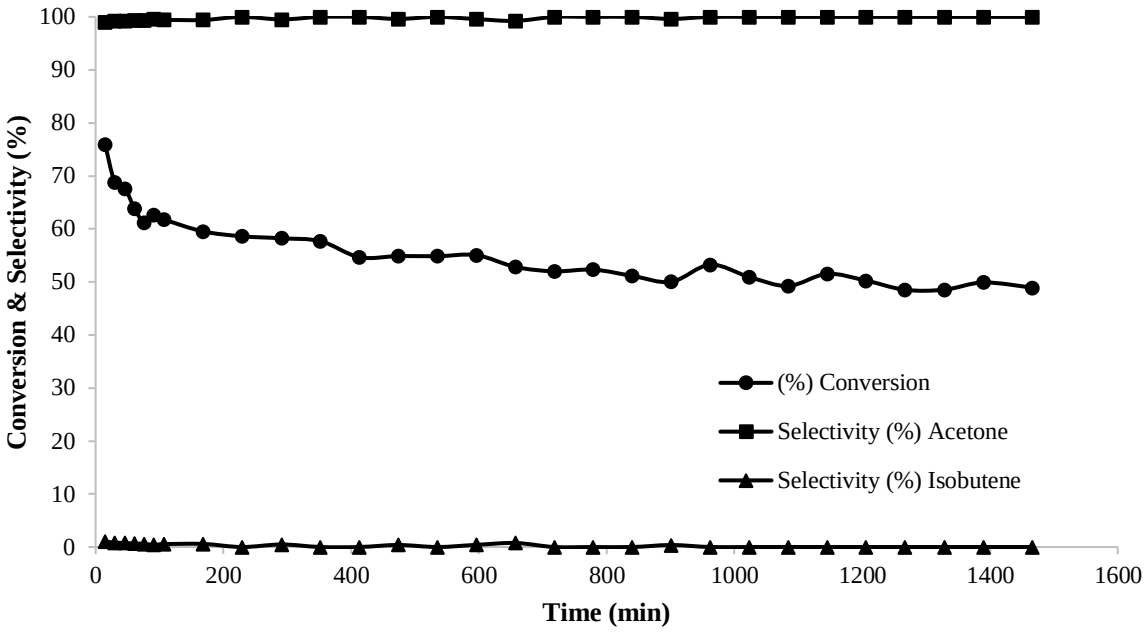

Figure 5.3. The selectivity and conversion for the 1:2 TiO_2-ZrO_2 catalyst (0.20 g, 300 ^oC, 3.35 kPa HOAc partial pressure, 20 mL min^{-1} flow rate).

Although the initial conversion was high, it began to steadily decrease (Figure 5.3). This could be explained by catalyst deactivation due to coking. The conversion reached 49% at the end of the reaction, which is still fairly high when compared to other catalysts. There was thus an overall drop of 27% over the course of the 24 h.

Increasing the Zr/Ti ratio in the mixed oxide showed a great depreciation in catalytic performance. For example, the 1:5 TiO_2-ZrO_2 (Figure 5.4) showed the lowest conversion, whereas the pure ZrO_2 showed a similar performance as the other pure metal oxide, TiO_2.

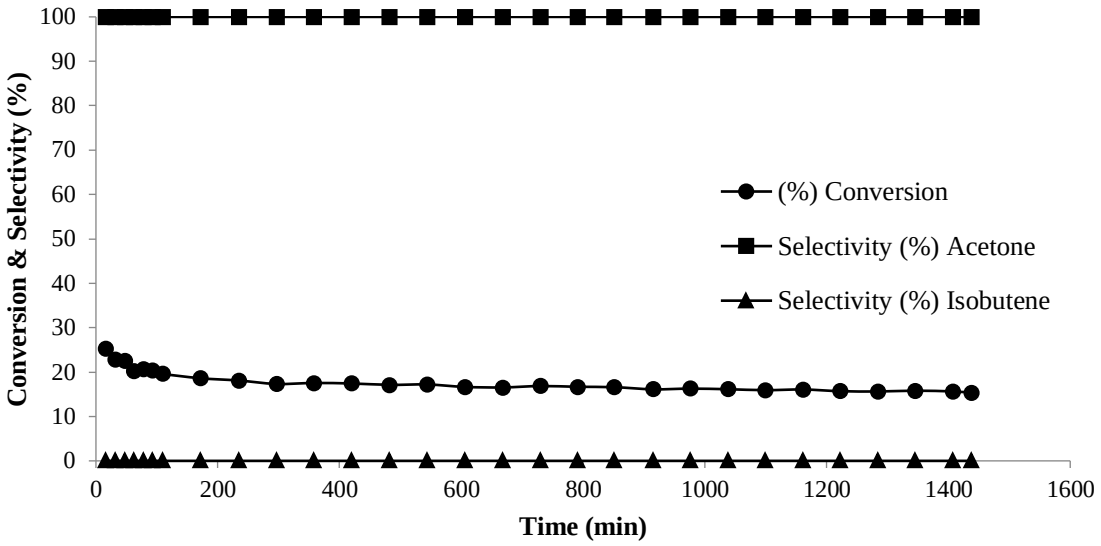

Figure 5.4. The conversion and selectivity for the 1:5 TiO_2-ZrO_2 (0.20 g, 300 ^oC, 3.35 kPa HOAc partial pressure, 20 mL min^{-1} flow rate).

As shown above, the 1:5 Ti-Zr oxide showed the lowest conversion out of all the catalysts studied with a maximum of just 23% at the first injection. Although this conversion was low, the catalyst showed little depreciation over the course of the reaction, decreasing to a minimum of 15% at the end of the 24 hours. There was thus an overall decrease of just 8% over the full course of reaction and hence less coking than in the case of 1:2 TiO_2-ZrO_2 catalyst.

The 5:1 Ti-Zr catalyst also showed poor conversion with a maximum value of just 25%. Its performance plot is depicted in Figure 5.5.

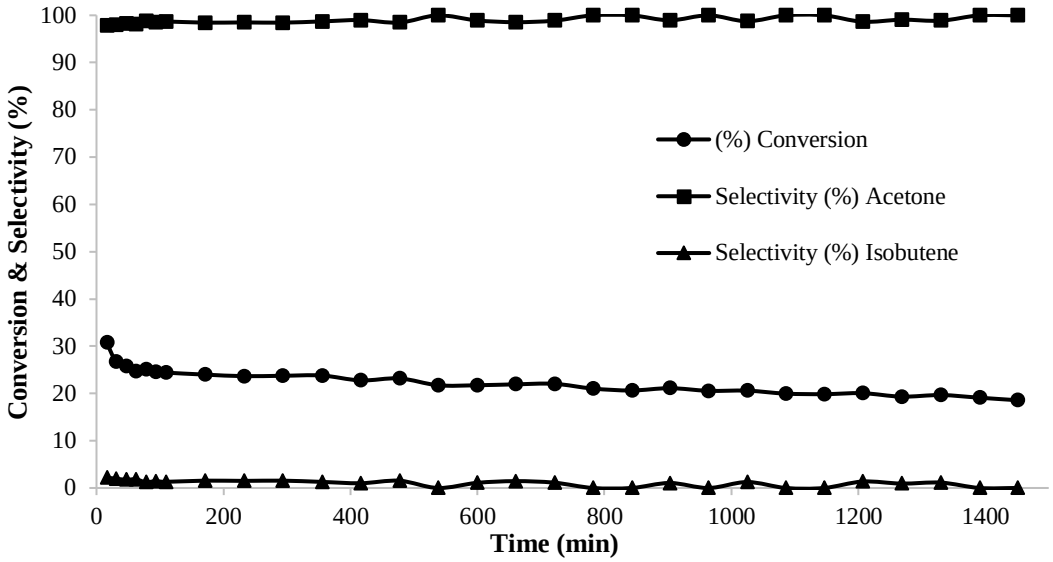

Figure 5.5. The conversion and selectivity for the 5:1 TiO_2-ZrO_2 catalyst (0.20 g, 300 ^oC, 3.35 kPa HOAc partial pressure, 20 mL min^{-1} flow rate).

Like the 1:5 Ti-Zr catalyst mentioned earlier, this catalyst also showed its maximum conversion of 31% at the beginning of the reaction. Also, similarly to the 1:5 Ti-Zr mixed oxide, this solid showed a relatively low level of depreciation of performance throughout its time on stream, reaching a minimum conversion of 19% at the last injection point. The overall decrease in conversion was thus 8%, identical to the 1:5 Ti-Zr and much lower than the 27% depreciation shown by the 1:2 Ti-Zr mixed oxide.

Another active solid was the 1:1 TiO_2-ZrO_2 catalyst, showing an average conversion of 46% and a selectivity for acetone of 99%. The time course for this catalyst is displayed in Figure 5.6.

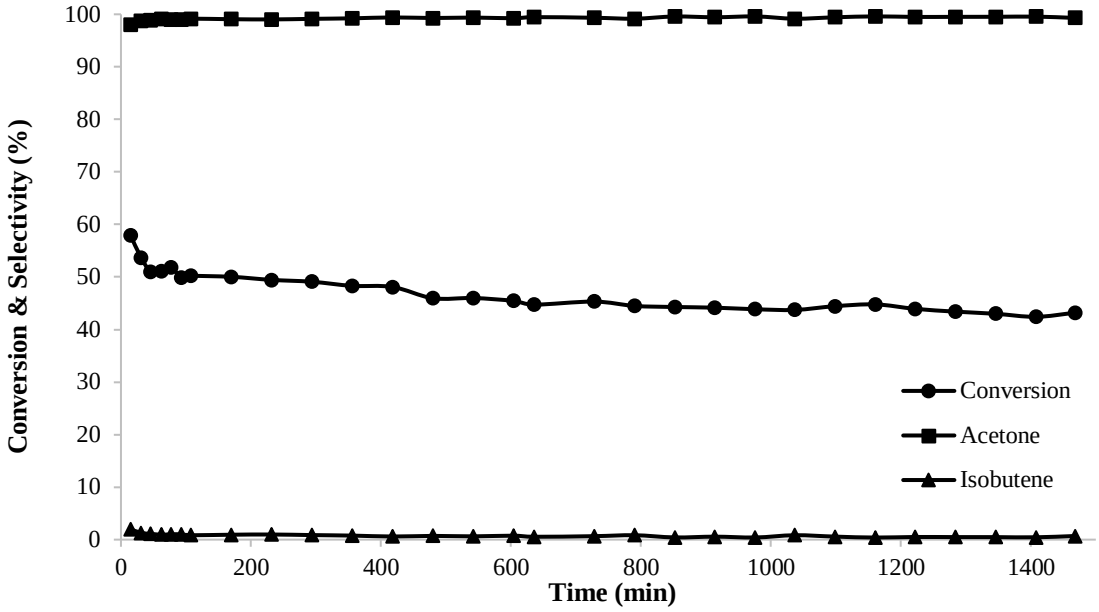

Figure 5.6. The conversion and selectivity for the 1:1 TiO_2-ZrO_2 (0.20 g, 300 ^oC, 3.35 kPa HOAc partial pressure, 20 mL min^{-1} flow rate).

The highest conversion for this mixed oxide was 58% at the first injection after 15 min on stream. The conversion to acetone then steadily decreased over the course of the reaction, reaching a minimum value of 42% after 24 h. Therefore, the overall drop in conversion was 16%, meaning it showed less coking than the best-performing 1:2 Ti-Zr mixed oxide but double that of the 1:5 and 5:1 Ti-Zr catalysts.

Overall, in terms of both conversion and selectivity, the best-performing catalyst in this series was the 1:2 TiO_2-ZrO_2 mixed oxide. However, this catalyst showed rather severe depreciation over the course of the 24 h, suggesting catalyst regeneration may be required, which could probably be done using the procedure described in Chapter 4. Hence, the 1:1 Ti-Zr catalyst maybe is a better option, since it also showed relatively high conversion and selectivity but suffered less depreciation and coking.

The results for the sol-gel and precipitation mixed oxide TiO_2-ZrO_2 catalyst are summarised in Table 5.2. A plot detailing average conversion and selectivity for sol-gel TiO_2-ZrO_2 catalysts as a function of catalyst composition is shown in Figure 5.7.

Table 5.2. The molar ratios, atomic ratios and average conversion.

TiO_2/ZrO_2 (mol/mol)	**Zr/Zr+Ti (atomic)**	**Average conversion (%)**
1:0	0	40[a]
1:0	0	49[b]
5:1	0.17	21[a]
2:1	0.33	37[a]
1:1	0.50	46[a]
1:1	0.50	46[b]
1:2	0.67	52[a]
1:5	0.83	17[a]
0:1	1	35[a]
0:1	1	73[b]

[a] Sol-gel catalysts. [b] Precipitation catalysts (for ZrO_2, see Chapter 4).

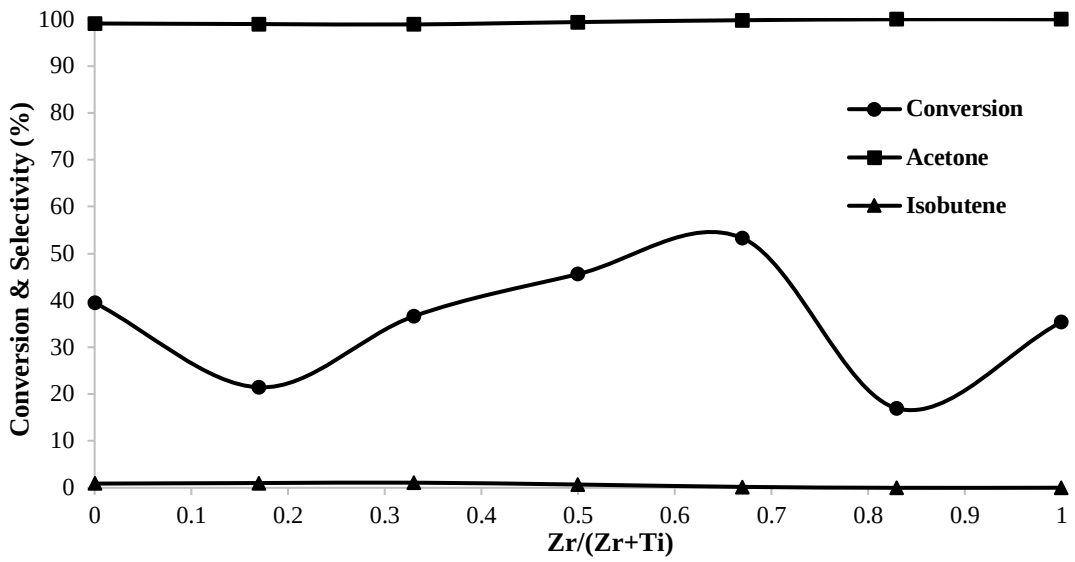

Figure 5.7. The plot of average conversion and selectivity over sol-gel TiO_2-ZrO_2 catalysts vs. Ti/Zr atomic ratio.

According to the plot above, the sol-gel mixed oxides that have a molar ratio of Ti/Zr closer to 1:1-1:2 performed better than either of those with ratios of 5:1 or 1:5 Ti-Zr or pure TiO_2 and ZrO_2. The results for the 5:1 and 1:5 Ti-Zr at the lowest conversion values were reproduced twice using different catalyst batches to obtain concordant conversion values. The 1:2 Ti-Zr mixed oxide had the highest average conversion amongst the sol-gel Ti-Zr catalysts. The graph also depicts that each solid showed excellent selectivity for acetone, the lowest being 98%. The pure sol-gel solids showed higher conversions than the 1:5 and 5:1 Ti-Zr catalysts but lower ones than the other mixed oxides, showing conversions of 35% (ZrO_2) and 40% (TiO_2), respectively. Despite being the catalyst with the highest conversion, the mixed oxide that showed the greatest signs of coking was the 1:2 TiO_2-ZrO_2 catalyst, its maximum to minimum at the first and last injection points, respectively.

From the results shown in Table 5.2, it can be seen the sol-gel pure TiO_2 and ZrO_2 catalysts are less active than the corresponding precipitation catalysts. This may be explained by the lower surface area of the former compared to the latter catalysts (Table 5.1).

5.4. Conclusion

To conclude, it has been shown that TiO_2-ZrO_2 mixed oxides, prepared by the sol-gel synthesis, are active catalysts in the ketonisation reaction of acetic acid to acetone at 300 ^oC. All the mixed oxides were characterised by BET measurements as well as powder XRD. The 1:2 Ti-Zr catalyst showed the best conversion, while the worst-performing catalyst in that respect was the 1:5 Ti-Zr mixed oxide. The parent oxides, TiO_2 and ZrO_2, prepared by sol-gel method showed relatively good conversion in comparison to the mixed oxides, showing better performance than both the 5:1 Ti-Zr and 1:5 Ti-Zr catalysts. Although all of the catalysts showed varied performance in terms of conversion, all samples gave excellent selectivity, with the lowest being 98% for the 2:1 Ti-Zr oxide. The 1:5 Ti-Zr catalyst showed the highest selectivity for acetone at 100%. However, as can be seen from Table 5.2, the sol-gel TiO_2, ZrO_2 and TiO_2-ZrO_2 catalysts have no advantages in activity and selectivity over the same catalysts prepared by the precipitation method. Moreover, mixed oxide TiO_2-ZrO_2 catalysts are considerably less active than the pure ZrO_2 prepared by precipitation method.

References

1. S. Matsuda and A. Kato, *Applied Catalysis*, 1983, **8**, 149-165.
2. P. Karaolia, I. Michael-Kordatou, E. Hapeshi, C. Drosou, Y. Bertakis, D. Christofilos, G. S. Armatas, L. Sygellou, T. Schwartz, N. P. Xekoukoulotakis and D. Fatta-Kassinos, *Applied Catalysis B: Environmental*, 2018, **224**, 810-824.
3. P. V. L. Reddy, B. Kavitha, P. A. K. Reddy and K. H. Kim, *Environmental Research*, 2017, **154**, 296-303.
4. M. Q. Sun, J. Xia, H. F. Wang, X. H. Liu, Q. N. Xia and Y. Q. Wang, *Applied Catalysis B: Environmental*, 2018, **227**, 488-498.
5. D. M. Alonso, S. G. Wettstein and J. A. Dumesic, *Green Chemistry*, 2013, **15**, 584-595.
6. K. Yan, Y. Yang, J. Chai and Y. Lu, *Applied Catalysis B: Environmental*, 2015, **179**, 292-304.
7. H. M. Tasdemir, S. Yasyerli and N. Yasyerli, *International Journal of Hydrogen Energy*, 2015, **40**, 9989-10001.
8. S. J. Pfleiderer, D. Lutzenkirchen-Hecht and R. Frahm, *Journal of Sol-Gel Science and Technollogy*, 2012, **64**, 27-35.

Chapter 6: Infrared spectroscopic study of reaction intermediates and mechanistic insights

6.1. Introduction

Infrared spectroscopy has been widely used for studying carboxylic acid adsorption on metal oxides such as TiO_2, Al_2O_3, CeO_2, SnO_2 and MgO [1, 2, 3–5]. It is well documented that carboxylic acids adsorb dissociatively on the neighbouring surface Lewis acid and base sites M-O-M to form a metal carboxylate in monodentate, bidentate chelate or bidentate bridging bonding mode, with the bidentate bridging acetate more likely to form [3–5] (Equation (1), charges omitted for simplicity). Different surface acetate species have been suggested as possible intermediates for ketonisation of carboxylic acids, including monodentate [1] and bridging bidentate [2, 6–8] acetates.

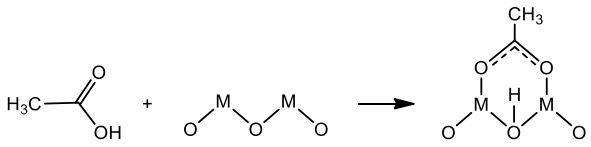

(1)

6.2. Infrared spectra of acetic acid adsorbed on metal oxides

Figure 6.1 shows the DRIFT spectra of acetic acid adsorbed on Al_2O_3, TiO_2, ZrO_2 and CeO_2, which were measured at room temperature in the absence of acetic acid in the gas phase after evacuation at 130 °C against pure oxide background. All these spectra have similar features and are in agreement with those reported previously [2, 3–5]. The small peaks in the region of 1700–1716 cm^{-1} (C=O stretching) indicate the presence of traces of physisorbed acetic acid. The peaks at 1319–1340 cm^{-1} can be assigned to C-H deformations (CH_3 bending). The bands at 1455–1559 cm^{-1} for TiO_2, ZrO_2 and CeO_2 can be attributed to symmetric and antisymmetric stretching of the OCO group of surface acetate [1, 2, 3–5], which indicate the bidentate bridging mode for acetate bonding (Equation (1)) [1, 2, 3–5]. For the non-transition metal oxide γ-Al_2O_3, the bands for OCO group exhibit a blue shift to 1475-1595 cm^{-1}, which is in agreement with data [2].

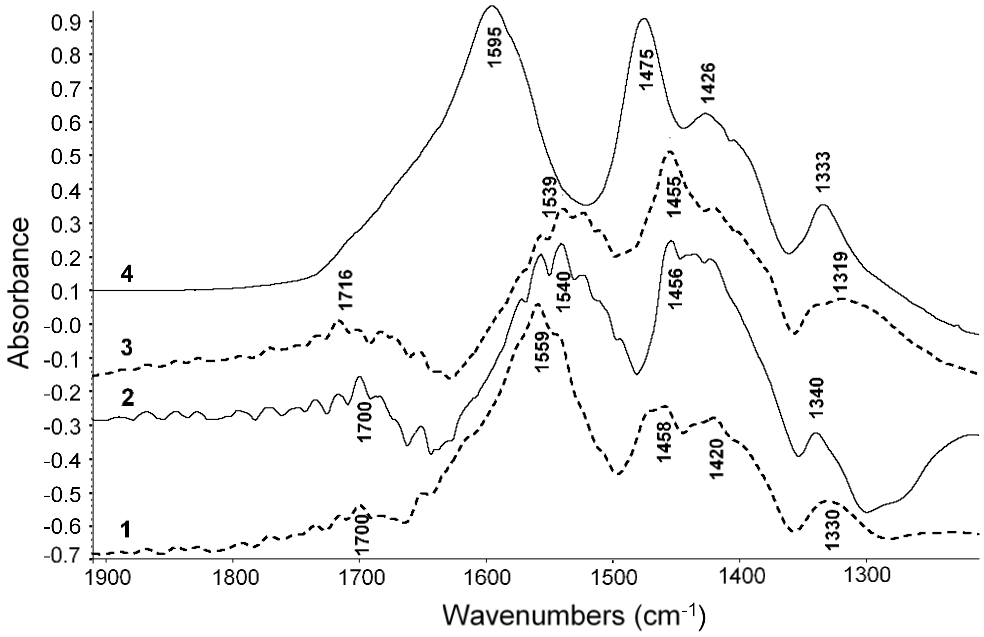

Figure 6.1. DRIFT spectra of acetic acid adsorbed on ZrO_2 (1), CeO_2 (2), TiO_2 (3) and Al_2O_3 (4) after evacuation at 130 ^oC/1 Pa.

The surface bidentate bridging acetates in the absence of acetic acid in the gas phase are known to be very stable, up to 300 °C [4] and even higher temperatures [2]. Based on DFT calculations and in-situ DRITS studies, it has been suggested that the bidentate bridging acetates are inactive, and it is the monodentate surface acetates that are the likely active intermediates in ketonisation of carboxylic acids over phase-pure TiO_2 [1]. Conversely, other DFT studies [6, 7, 9] consider the bidentate bridging acetates the active intermediates in acid ketonisation on ZrO_2.

6.3. CH_3COOH/CD_3COOD exchange at the oxide surface

Here, we looked at the behaviour of surface bidentate bridging acetates in the absence and in the presence of acetic acid in the gas phase. These conditions portray the ketonisation reaction at the oxide surfaces. Specifically, we looked at a CH_3COOH/CD_3COOD exchange at the oxide surface and the behaviour of undeuterated and deuterated surface bidentate bridging acetates d_0 and d_3 using DRIFT spectroscopy.

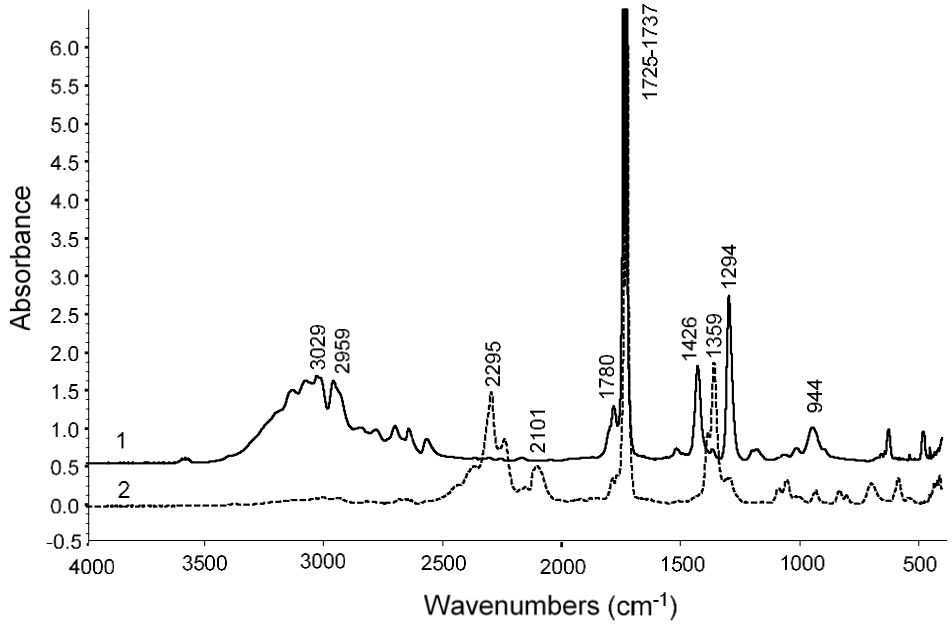

Figure 6.2. FTIR spectra of CH_3COOH (1) and CD_3COOD (2) in gas phase (ca. 1 kPa partial pressure).

Figure 6.2 shows the FTIR spectra of CH_3COOH and CD_3COOD in the gas phase. It can be seen that the vibration bands for CH_3 deformation (1426 cm^{-1}) and C-H and C-D stretching (2959 and 2101 cm^{-1}, respectively) [5] can be used to monitor the CH_3COOH/CD_3COOD exchange. The results for acid exchange on TiO_2 are presented in

Figure 6.3. It shows the DRIFT spectra of CH_3COOH (spectrum 1) and CD_3COOD (spectrum 2) adsorbed on TiO_2 to form the bidentate bridging acetate d_0 and d_3, respectively. Each acid (~1 kPa) was adsorbed at room temperature followed by evacuation at 130 °C/1 Pa for 1 h to remove the acids from the gas phase, then the spectra were recorded at room temperature against pure oxide background. Notably, spectrum 1 for the adsorbed CH_3COOH shows the CH_3 deformation band (1319 cm^{-1}) and the C-H stretch (2936 cm^{-1}), whereas spectrum 2 for the adsorbed CD_3COOD lacks these bands, but has the C-D stretch (2115 cm^{-1}) in it. Spectrum (3) represents the CH_3COOH sample (1) after exposure to CD_3COOD vapour (~1 kPa) at 130 °C for 0.5 h followed by pumping out at 130 °C/1 Pa for 1 h as above. This spectrum looks the same as spectrum 2 for the adsorbed CD_3COOD, which clearly points to an H/D exchange in the system. Moreover, the exchange occurred already at 130 °C, i.e., well below temperature threshold for the ketonisation reaction on TiO_2 (250–300 °C). This process could be repeated several times, each time showing the H/D exchange. Similar results were also obtained for Al_2O_3 (Figure 6.4), ZrO_2 (Figure 6.5) and CeO_2 (Figure 6.6), all exhibited the H/D exchange at 130 °C.

It is important that no H/D exchange was observed when CD_3COOD was adsorbed on fresh oxides. This would rule out the H/D exchange between the deuterated surface acetate and the proton sites present on the oxide surface, but only if the undeuterated Brønsted acid sites still existed after the exposure of the oxide to gaseous CD_3COOD. To prove this, the pre-adsorbed CD_3COOD on TiO_2 was treated with H_2O (~1 kPa) at 130 °C for 0.5 h followed by pumping out at 130 °C/1 Pa for 1 h. This treatment would restore the undeuterated Brønsted acid sites on the TiO_2 surface. The resulting DRIFT spectrum is shown in Figure 6.3 (spectrum 4). As seen, similar to spectrum (2) for the adsorbed CD_3COOD, it does not have the vibration band of CH_3 group at 1319 cm^{-1}. This rules out the H/D exchange between the deuterated surface acetate and the proton sites present on the oxide surface at 130 °C. It should be noted

that there is a small new unidentified peak at 1265 cm^{-1} in this spectrum, which might be indicative of some partial H/D exchange between the surface acetate-d_3 and surface proton sites. This will be addressed below in more detail. Notably, spectrum 4 lacks the carbonyl stretch at 1718 cm^{-1}, hence there is no trace of physisorbed CD_3COOD. This can be due to the water treatment of this sample and extended pumping out.

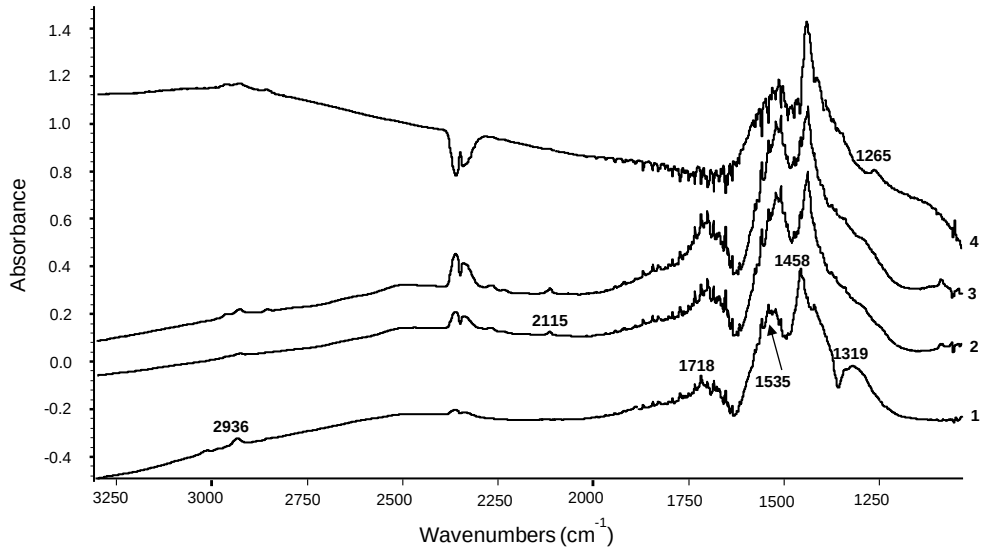

Figure 6.3. DRIFT spectra of CH_3COOH (1) and CD_3COOD (2) adsorbed on TiO_2 after evacuation at 130 ^oC/1 Pa for 1 h. Spectrum (3) represents CH_3COOH sample (1) after exposure to CD_3COOD vapour at ~1 kPa partial pressure and 130 ^oC for 0.5 h followed by evacuation at 130 ^oC/1 Pa for 1 h. Spectrum (4) represents CD_3COOD sample (2) treated with H_2O (~1 kPa) at 130 ^oC/0.5 h and evacuated at 130 ^oC/1 Pa for 1 h.

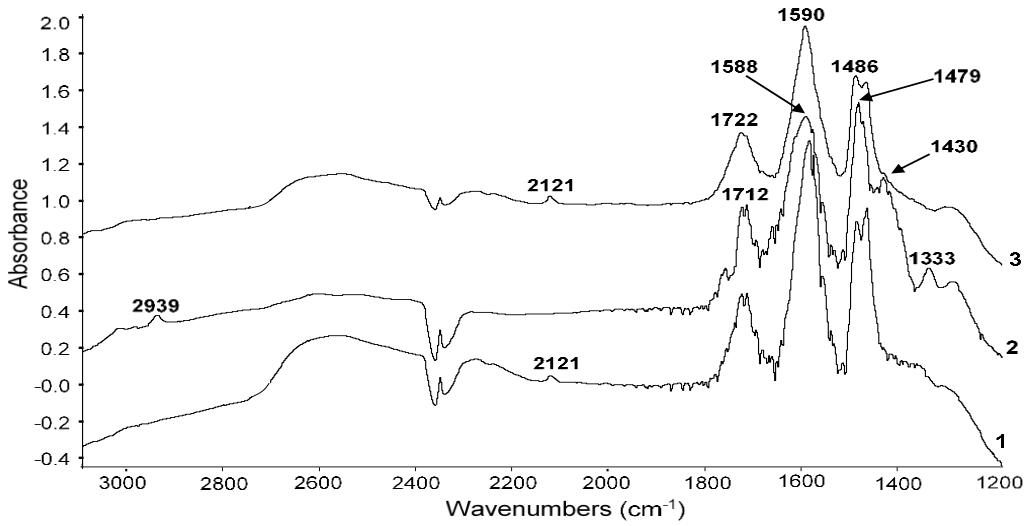

Figure 6.4. DRIFT spectra of CD_3COOD (1) and CH_3COOH (2) adsorbed on γ-Al_2O_3 (Degussa) after evacuation at 130 °C/1 Pa for 1 h. Spectrum (3) represents sample (2) after exposure to CD_3COOD vapour at ca. 1 kPa partial pressure and 130 °C for 0.5 h followed by evacuation at 130 °C/1 Pa for 1 h.

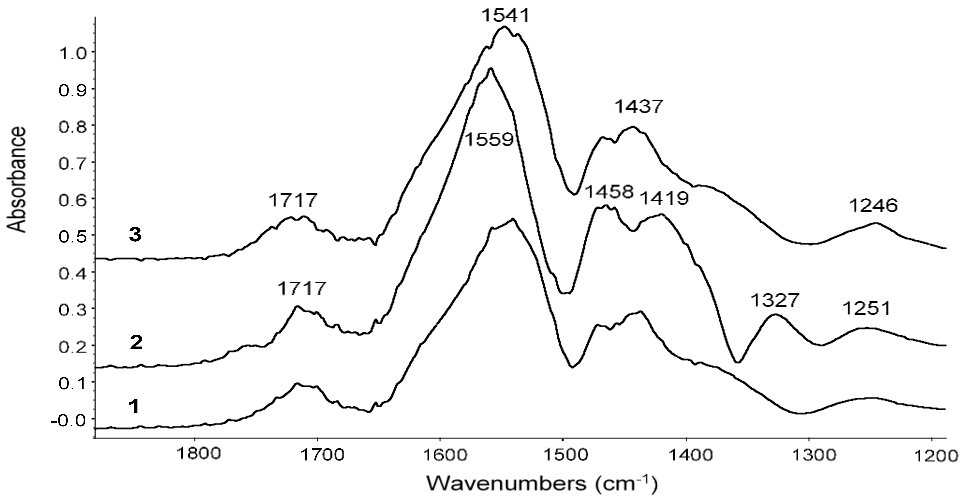

Figure 6.5. DRIFT spectra of CD_3COOD (1) and CH_3COOH (2) adsorbed on ZrO_2 after evacuation at 130 °C/1 Pa for 1 h. Spectrum (3) represents sample (2) after exposure to CD_3COOD vapour at ca. 1 kPa partial pressure and 130 °C for 0.5 h followed by evacuation at 130 °C/1 Pa for 1 h.

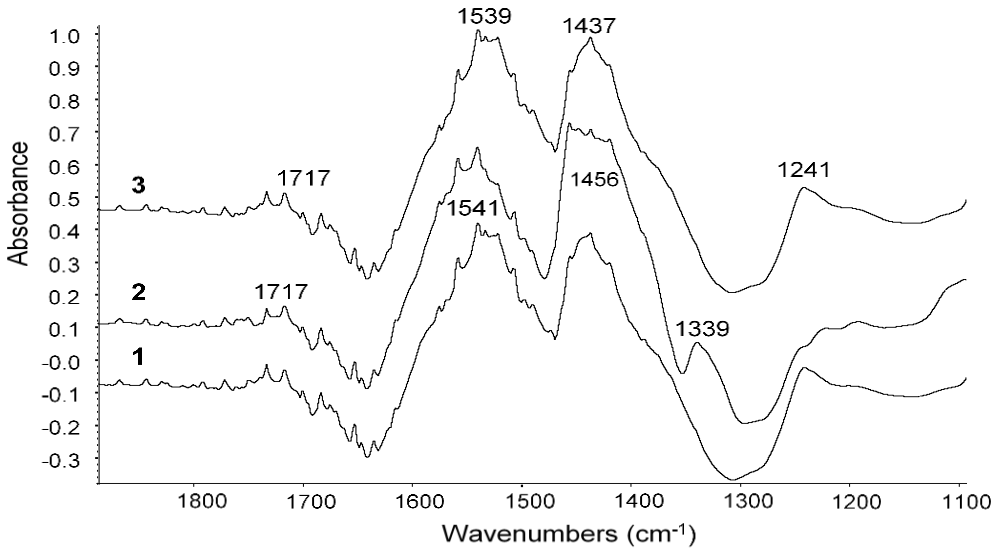

Figure 6.6. DRIFT spectra of CD_3COOD (1) and CH_3COOH (2) adsorbed on CeO_2 after evacuation at 130 °C/1 Pa for 1 h. Spectrum (3) represents sample (2) after exposure to CD_3COOD vapour at ca. 1 kPa partial pressure and 130 °C for 0.5 h followed by evacuation at 130 °C/1 Pa for 1 h.

One explanation for these results might be the H/D exchange of the bidentate surface acetate through enolate species (Equation (2)); the latter has been suggested as an intermediate in acid ketonisation [6,7]. In such a case, the H/D exchange would occur without desorption of bidentate acetate species from the oxide surface and would involve H^+ (or D^+) surface sites. This would imply that the deuterated bidentate surface acetate-d_3 would undergo H/D exchange with proton sites on the oxide surface without the addition of acetic acid-d_0. This contradicts the above experimental evidence as no such H/D exchange was observed. Moreover, DFT calculations [6,7] show that the formation of surface enolate requires a high activation energy, which would make it the rate-limiting step in the H/D exchange under the CH_3COOH/CD_3COOD acid exchange conditions at 130 °C. As a result, the H/D exchange can be expected to depend on the nature of metal oxide. This is not in agreement with experiment

either as no such dependence was observed within the time scale of acid exchange. On this bases, the H/D exchange through the surface enolate species can be ruled out at 130 °C.

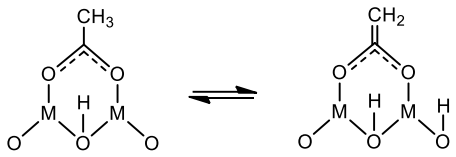

(2)

A possible mechanism for the acid exchange on oxide surface at 130 °C is represented in Scheme 6.1. This mechanism involves desorption of bidentate bridging surface acetates from the oxide surface aided by acetic acid from the gas phase. Here, the bidentate surface acetate A formed initially interacts with the co-adsorbed CD_3COOD to form intermediate B, which would lead to acid exchange to give the deuterated acetate C and release CH_3COOD into the gas phase (possibly together with CH_3COOH due to H/D exchange of CH_3COOD with the surface proton sites). Further kinetic studies could reveal the effect of metal oxide nature on the rate of CH_3COOH/CD_3COOD exchange.

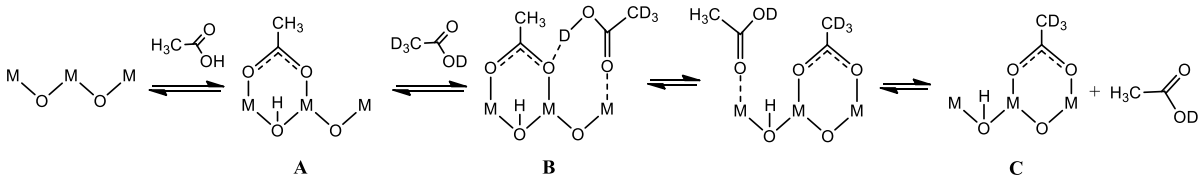

Scheme 6.1. CH_3COOH/CD_3COOD exchange on oxide surface at 130 °C.

Now the question is can the H/D exchange between the surface bidentate acetate A and the oxide Brønsted acid sites occur at higher temperatures typical of those for acid ketonisation? To prove this, the pre-adsorbed CD_3COOD on TiO_2 was again treated with H_2O

(∼1 kPa) as above, but this time at 250 °C to restore the undeuterated surface Brønsted acid sites. The resulting DRIFT spectrum is presented in Figure 6.7 (spectrum 2). It clearly shows the band for CH_3 vibrations, blue-shifted at these conditions to 1340 cm^{-1}, indicating H/D exchange between the bidentate bridging acetate-d_3 and Brønsted acid sites on TiO_2 surface. Increasing the temperature to 270 °C further enhanced the H/D exchange, as can be seen from the increased intensity of this band (spectrum 3). Even without any water treatment, heating the TiO_2-adsorbed CD_3COOD at 270 °C caused some H/D exchange, as seen from spectrum 4 in Figure 6.7. This means that the relatively weak proton sites on TiO_2 surface were not fully deuterated by the adsorbed CD_3COOD. Similar results were also obtained for ZrO_2 (Figure 6.8), which has higher ketonisation activity (Table 4.4) and higher Brønsted acid site density compared to TiO_2 (Table 4.1). In Figure 6.8, spectra 1–3 demonstrate facile CH_3COOH/CD_3COOD exchange on ZrO_2 at 130 °C as in the case of TiO_2 (Figure 6.3). At 250 °C, without water treatment, the adsorbed CD_3COOD did not show any H/D exchange with the surface proton sites possibly due to their deuteration by the CD_3COOD, as seen from the absence of CH_3 vibration band at ∼1330 cm^{-1} in DRIFT spectrum 4. However, this band clearly showed after the pre-adsorbed CD_3COOD was treated with H_2O (∼1 kPa) at 250 °C to restore the undeuterated Brønsted acid sites on ZrO_2 surface, thus supporting the H/D exchange between the bidentate bridging acetate and the surface Brønsted acid sites. The observed H/D exchange can be attributed to the surface enolate species, which have been inferred as the intermediates in acid ketonisation from DFT calculations [6,7]. Therefore, these results provide an important mechanistic insight, giving experimental evidence for the intermediacy of enolate species in ketonisation of carboxylic acids. A plausible reaction pathway for the H/D exchange is represented in Scheme 6.2.

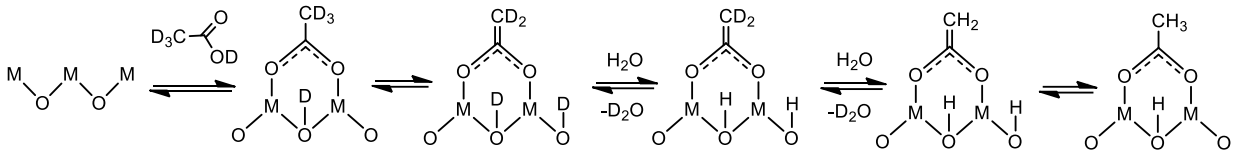

Scheme 6.2. H/D exchange between bidentate bridging acetate and Brønsted acid sites on oxide surface.

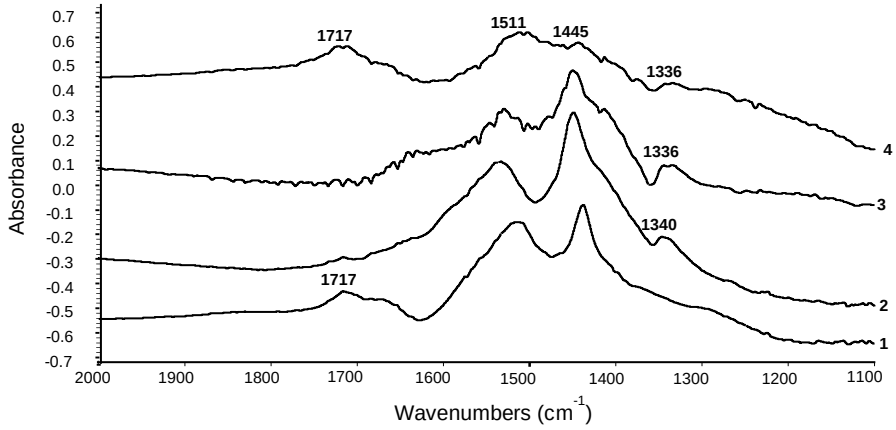

Figure 6.7. DRIFT spectra of CD_3COOD adsorbed on TiO_2: (1) CD_3COOD evacuated at 250 ^oC/1 Pa for 1 h, (2), CD_3COOD sample (1) treated with H_2O (~1 kPa) at 250 ^oC for 0.5 h and evacuated at 250 ^oC/1 Pa for 1 h, (3) the same as (2) but treated with H_2O and evacuated at 270 ^oC, (4) CD_3COOD evacuated at 270 ^oC/1 Pa for 1 h in the absence of H_2O.

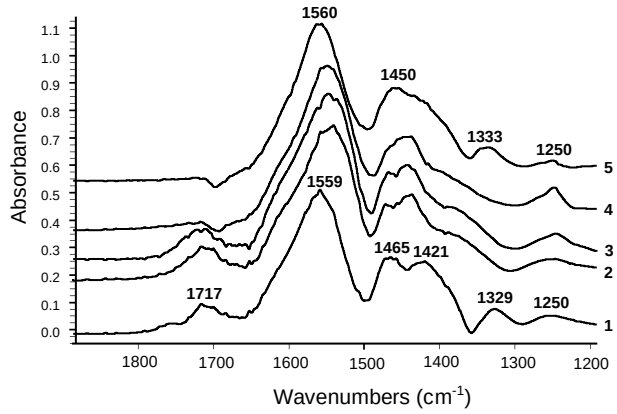

Figure 6.8. DRIFT spectra of CH_3COOH (1) and CD_3COOD (2) adsorbed on ZrO_2 after evacuation at 130 ^oC/1 Pa for 1 h. Spectrum (3) represents CH_3COOH sample (1) after exposure to CD_3COOD vapour at ~1 kPa partial pressure and 130 ^oC for 0.5 h followed by evacuation at 130 ^oC/1 Pa for 1 h. (4) represents CD_3COOD evacuated at 250 ^oC/1 Pa for 1 h. (5) represents CD_3COOD sample (4) treated with H_2O (~1 kPa) at 250 ^oC/0.5 h and evacuated at 250 ^oC/1 Pa for 1 h.

6.4. Ketonisation mechanism

Several mechanisms have been proposed for acid ketonisation reaction including (i) decomposition of a metal carboxylate, (ii) via an acid anhydride intermediate, (iii) via a ketene intermediate route and (iv) via a β-ketoacid intermediate (for a review, see [9,10]). More recent theoretical calculations and experimental data favour the β-ketoacid intermediate route with the rate-limiting step of C-C bond formation [1, 6-11]. Nevertheless, exact reaction mechanism and the requirements for catalytically active sites are still controversial [1,9]. From DFT analysis, different surface carboxylate species such as monodentate acetate [1] and bidentate bridging acetate [6,7] have been suggested as active intermediates in this reaction. Also different mechanisms of C-C bond formation have been proposed. These include the C-C

coupling (i) between a surface carboxylate and ketene [9,10], (ii) between enolate species and co-adsorbed acid [1], (iii) between enolate species and bidentate bridging carboxylate [9,11], (iv) between enolate species and acylium intermediate [6,7] and (v) via a concerted pathway [6]. The C-C coupling involving the enolate and a surface carboxylate or acylium species is currently considered to be the most plausible reaction mechanism [1,6,7,9].

In this work, we made two mechanistically significant observations. First, we found facile exchange between the bidentate bridging acetate and co-adsorbed acetic acid on the oxide surface under mild conditions well below ketonisation temperatures. This result demonstrates the lability of the surface bidentate bridging acetate species in the ketonisation system. This shows that prior to C-C bond formation various types of surface acetate species are equilibrated in the ketonisation system, which makes them kinetically indistinguishable. Secondly, we observed proton exchange between the bidentate bridging acetates and the Brønsted acid sites on oxide surfaces at typical ketonisation temperatures, which supports the intermediacy of enolate species in ketonisation of carboxylic acids. On this basis, the rate-limiting step of ketonisation reaction involving the C-C coupling to form the β-ketoacid intermediate can be represented by interaction between the enolate and a surface acetate species, for example bidentate bridging acetate, as shown in Scheme 6.3 [9,11]. The latter species, however, is kinetically indistinguishable from other possible surface acetates, e.g., monodentate acetate [1], existing in equilibrium with the bidentate bridging acetate.

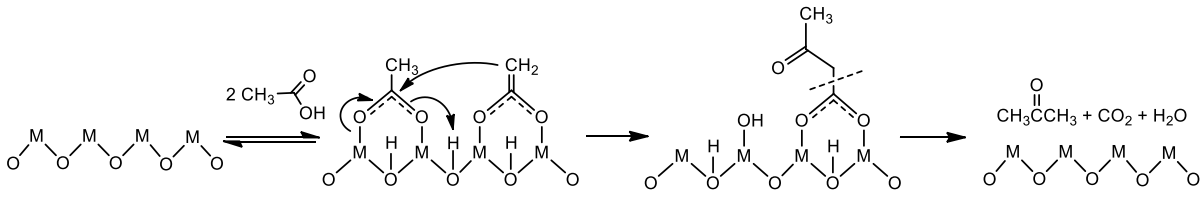

Scheme 6.3. Interaction between enolate and bidentate bridging acetate as an example of C-C coupling to form the β-ketoacid intermediate in ketonisation of acetic acid.

It would be highly desirable to be able to correlate the catalytic activity of oxides to a specific physicochemical property measured on the fresh oxides. There is a concern, however, that such properties of the fresh oxides may not be representative of the properties under reaction conditions, i.e., in the presence of CO_2 and water by-products formed in the course of acid ketonisation. In particular, this concerns the acid-base properties and the surface structure of oxide materials. Nevertheless, our study demonstrates a correlation between the reactivity of oxides in the ketonisation of acetic acid and their mild basicity existing in the ketonisation system in the presence of CO_2. On the other hand, no such correlation with the acid properties of oxide was observed. This is not unexpected because several reaction steps preceding the rate-limiting step of C-C coupling, namely the formation of surface acetate and enolate species, involve interaction with the catalyst base sites (Scheme 6.3). Our DRIFTS work provided interesting insights into the reaction mechanism. Further kinetic studies of the H/D exchange complemented by in-situ catalyst characterisation in these systems could give better mechanistic understanding and reactivity differentiation across oxide catalysts.

6.5. Conclusions

Two mechanistically significant observations were made from our DRIFTS studies. First, facile exchange was found between the bidentate bridging acetate and co-adsorbed acetic acid on the oxide surfaces under mild conditions well below ketonisation temperatures, which demonstrates the lability of the surface bidentate bridging acetate species in the ketonisation system. This shows that various types of surface acetate species are equilibrated in the ketonisation system, which makes them kinetically indistinguishable. Secondly, we observed proton exchange between the bidentate bridging acetates and the Brønsted acid sites on oxide surfaces at typical ketonisation temperatures, which supports the intermediacy of enolate species in ketonisation of carboxylic acids.

References

1. S. Wang and E. Iglesia, *Journal of Catalysis*, 2017, **345**, 183–206.
2. M. A. Hasan, M. I. Zaki and L. Pasupulety, *Applied Catalysis A: General*, 2003, **243**, 81–92.
3. C. Martin, I. Martin and V. Rives, *Journal of Molecular Catalysis*, 1992, **73**, 51–63.
4. Z.-F. Pei and V. Ponec, *Applied Surface Science*, 1996, **103**, 171–182.
5. N. M. D. Brown, R.B. Floyd and D.G. Walmsley, *Journal of the Chemical Society, Faraday Transactions*, 1979, **275**, 17–31.
6. A. Pulido, B. Oliver-Tomas, M. Renz, M. Boronat and A. Corma, *ChemSusChem*, 2013, **6**, 141–151.
7. S. Tosoni and G. Pacchioni, *Journal of Catalysis*, 2016, **344**, 465–473.
8. T. N. Pham, D. Shi and D.E. Resasco, *Journal of Catalysis*, 2014, **314**, 149–158.
9. G. Pacchioni, *ACS Catalysis*, 2014, **4**, 2874–2888.
10. T. N. Pham, T. Sooknoi, S.P. Crossley and D.E. Resasco, *ACS Catalysis*, 2013, **3**, 2456–2673.
11. T. N. Pham, D. Shi and D.E. Resasco, *Catalysis Today*, 2014, **57**, 706–714.

Chapter 7: General conclusions and future outlook

Carboxylic acids are readily available from renewable natural resources and can be used for the production of value-added chemicals and carbon-neutral bio-fuels [1,2]. For fuel applications, carboxylic acids require an increase in their caloric value. This can be achieved by reduction in their oxygen content, i.e. by deoxygenation. Therefore, much current research is focussed on the deoxygenation (usually hydrodeoxygenation) of carboxylic acids, primarily using heterogeneous oxide catalysis [3-7].

Ketonisation (Equation (1)) converts two molecules of a carboxylic acid into a ketone, carbon dioxide and water [8,9]. It makes a new C-C bond and removes three oxygen atoms. In contrast to catalytic hydrodeoxygenation, no hydrogen is required for the ketonisation of carboxylic acids, which is an important advantage of the ketonisation chemistry.

$$2\ CH_3COOH \rightarrow (CH_3)_2CO + CO_2 + H_2O \quad (1)$$

Ketonisation has long been employed as a clean method for the synthesis of ketones ([8,9] and references therein). Currently, this reaction attracts significant interest for the upgrading of biomass-derived oxygenates. Specifically, ketonisation is considered to be a promising method for the upgrading of bio-oil produced by fast pyrolysis of biomass, which, among other oxygenated compounds, contains lower C_1-C_4 carboxylic acids, which make the oil unstable and corrosive. Ketonisation can eliminate the adverse effects of carboxylic acids by converting them to non-corrosive ketone products with higher caloric value. The ketones thus produced can be further subjected to aldol condensation to increase the carbon chain length to the gasoline/diesel/kerosine range [1,2,9].

Ketonisation of carboxylic acids has been extensively studied both in gas phase and liquid phase ([8,9] and references therein). In the gas phase, the reaction is catalysed by many metal oxides in the temperature range of 200-500 ^oC [8-19]. The best catalytic activity have amphoteric oxides such as CeO_2, MnO_2, ZrO_2, TiO_2, etc. [8,9, 17]. Despite numerous research

efforts, reaction mechanism and the nature of catalytically active sites and intermediates is still under debate [8,9,16-19]. In addition, catalyst deactivation remains a serious problem in the commercialisation of catalytic ketonisation of carboxylic acids. Therefore, the understanding of reaction mechanism and the causes of catalyst deactivation as well as the improvement of catalyst stability remain a challenge in the acid ketonisation [9].

In this work, we have studied the performance of four typical metal oxide catalysts, namely γ-Al_2O_3, TiO_2, ZrO_2 and CeO_2, in the ketonisation of acetic acid to acetone (Equation (1)). Our primary focus was on their activity and stability to deactivation. We also aimed to provide new insights into ketonisation mechanism and site requirements on oxide surfaces through kinetic studies, characterisation of catalyst acid and base sites and, in particular, IR spectroscopic investigation of reaction intermediates.

The ketonisation of acetic acid over oxide catalysts was studied in the gas phase using a continuous flow fixed-bed microreactor in the temperature range of 180-350 ^oC and ambient pressure (Chapter 4). The reaction gives acetone as the primary reaction product with ≥ 99% selectivity. Catalyst activity was found to increase in the order Al_2O_3 << TiO_2 < ZrO_2 < CeO_2, with specific reaction rates (10^5 mol $m^{-2}h^{-1}$) of 0.047, 1.1, 1.7 and 3.4, respectively, at 260 ^oC. These catalysts suffered from deactivation, which increased in the order TiO_2 < ZrO_2 << CeO_2, in parallel with the amount of coke formed. TiO_2 (commercial Degussa P25 catalyst) and ZrO_2 exhibited the best ketonisation performance regarding the catalyst activity and long-term stability. The Degussa TiO_2 catalyst showed practically no deactivation. The other oxides, CeO_2 and ZrO_2, which suffered from deactivation, could be regenerated by air calcination to regain their activity.

Given the very good ketonisation performance of the TiO_2 and ZrO_2 pure oxides, it was interesting to test the performance of mixed oxide Ti-Zr catalysts in this reaction well (Chapter

5). The mixed oxide TiO_2-ZrO_2 catalysts were prepared by two methods, namely by (i) the sol-gel synthesis via hydrolysis and condensation of a mixture of titanium propoxide $Ti(OC_3H_7)_4$ and zirconium propoxide $Zr(OC_3H_7)_4$ in propanol and (ii) precipitation methods (Chapter 2). All the mixed oxides were characterised by BET measurements as well as powder XRD. It was shown that TiO_2-ZrO_2 mixed oxides, prepared by the sol-gel synthesis, are active catalysts in the ketonisation reaction of acetic acid to acetone at 300 ^oC. The 1:2 Ti-Zr catalyst showed the best acetic acid conversion, which exceeded the conversion over the pure TiO_2 and ZrO_2 oxides prepared by sol-gel method. Although all of the catalysts showed varied performance in terms of conversion, all samples gave excellent selectivity to acetone of 98-100%. Overall, however, the sol-gel TiO_2, ZrO_2 and TiO_2-ZrO_2 catalysts had no advantages in activity and selectivity over the same catalysts prepared by the precipitation method. Moreover, mixed oxide TiO_2-ZrO_2 catalysts were considerably less active than the pure ZrO_2 prepared by precipitation method.

In this study, we also attempted to obtain new insights into ketonisation mechanism and site requirements on oxide surfaces. Thus, our study demonstrates a correlation between the reactivity of oxides in the ketonisation of acetic acid and their mild basicity existing in the ketonisation system in the presence of CO_2. On the other hand, no such correlation with the acid properties of oxide was observed. This is not unexpected because several reaction steps preceding the rate-limiting step of C-C coupling, namely the formation of surface acetate and enolate species, involve interaction with the catalyst base sites (Scheme 6.3).

Two mechanistically significant observations were made from our DRIFTS studies. First, facile exchange was found between the bidentate bridging acetate and co-adsorbed acetic acid on the oxide surfaces under mild conditions (130 ^oC) well below ketonisation temperatures. This demonstrates the lability of the surface bidentate bridging acetate species in the ketonisation system. This result shows that various types of surface acetate species are

equilibrated in the ketonisation system, which makes them kinetically indistinguishable. Secondly, at higher temperatures typical for acid ketonisation, in the absence of gas-phase acetic acid, we found that the adsorbed bidentate bridging acetate-d_3 species underwent H/D exchange with proton sites on oxide surfaces. This, for the first time, provides experimental evidence supporting the intermediacy of enolate species in ketonisation of carboxylic acids. Previously, the intermediacy of these species has been deduced from theoretical (DFT) calculations.

In the future, it would be highly desirable to be able to correlate the catalytic activity of oxides to a specific physicochemical property measured on the fresh oxides. There is a concern, however, that such properties of the fresh oxides may not be representative of the properties under reaction conditions, i.e., in the presence of CO_2 and water by-products formed in the course of acid ketonisation. In particular, this concerns the acid-base properties and the surface structure of oxide materials. Nevertheless, our study demonstrates a correlation between the reactivity of oxides in the ketonisation of acetic acid and their mild basicity existing in the ketonisation system in the presence of CO_2. Our DRIFTS work provided interesting insights into the reaction mechanism. Further kinetic studies of the H/D exchange complemented by in-situ catalyst characterisation in these systems could give better mechanistic understanding and reactivity differentiation across various oxide catalysts.

References

1. A. Corma, S. Iborra and A. Velty, *Chemical Reviews*, 2007, **107**, 2411–2502.
2. E. L. Kunkes, D.A. Simonetti, R.M. West, J.C. Serrano-Ruiz, C.A. Gaertner and J.A. Dumesic, *Science*, 2008, **322**, 417–421.
3. M. Snare, I. Kubickova, P. Maki-Arvela, K. Eranen and D.Yu Murzin, *Industrial & Engineering Chemistry Research*, 2006, **45**, 5708–5715.
4. H. Bernas, K. Eranen, I. Simakova, A.-R. Leino, K. Kordas, J. Myllyoja, P. Maki-Arvela, T. Salmi and D.Yu Murzin, *Fuel*, 2010, **89**, 2033–2039.
5. J.G. Immer, M.J. Kelly and H.H. Lamb, *Applied Catalysis A: General*, 2010, **375**, 134–139.
6. P. T. Do, M. Chiappero, L.L. Lobban and D. Resasco, *Catalysis Letters*, 2009, **130**, 9–18.
7. M. Arend, T. Nonnen, W.F. Hoelderich, J. Fischer and J. Groos, *Applied Catalysis A: General*, 2011, **399**, 198–204.
8. M. Renz, *European Journal of Organic Chemistry*, 2005, 979–988.
9. T. N. Pham, T. Sooknoi, S.P. Crossley and D.E. Resasco, *ACS Catalysis*, 2013, **3**, 2456–2673.
10. T. Yokoyama and N. Yamagata, *Applied Catalysis A: General*, 2001, **221**, 227–239.
11. O. Nagashima, S. Sato, R. Takahashi and T. Sodesawa, *Journal of Molecular Catalysis A* 2005, **227**, 231–239.
12. M. Glinski, J. Kijenski and A. Jakubowski, *Applied Catalysis A: General*, 1995, **128**, 209–217.
13. C. A. Gaertner, J.C. Serrano-Ruiz, D.J. Braden and J.A. Dumesic, *Journal of Catalysis*, 2009, **266**, 71–78.

14. H. Bayahia, E. Kozhevnikova and I. Kozhevnikov, *Chemical Communication*, 2013, **49**, 3842–3844.

15. H. Bayahia, E.F. Kozhevnikova and I.V. Kozhevnikov, *Applied Catalysis B: Environmental*, 2015, **165**, 253–259.

16. S. Wang and E. Iglesia, *Journal of Catalysis*, 2017, **345**, 183–206.

17. M. A. Hasan, M.I. Zaki and L. Pasupulety, *Applied Catalysis A: General*, 2003, **243**, 81–92.

18. A. Pulido, B. Oliver-Tomas, M. Renz, M. Boronat and A. Corma, *ChemSusChem*, 2013, **6**, 141–151.

19. S. Tosoni and G. Pacchioni, *Journal of Catalysis*, 2016, **344**, 465–473.